

LOCAL TSUNAMIS AND EARTHQUAKE SOURCE PARAMETERS

ERIC L. GEIST

*U.S. Geological Survey
345 Middlefield Road
Menlo Park, CA 94025*

1. INTRODUCTION

A persistent problem in estimating the severity of local tsunamis generated by earthquakes is explaining the great event-to-event variability of tsunami run-up heights relative to the magnitude of the earthquake. Undoubtedly, there is always variability in run-up that is dependent on local bathymetry. However, many earthquakes in recent years have produced unexpectedly high local run-up heights, given the magnitude of the earthquake, suggesting a complex relationship between local tsunami run-up and the source processes of the earthquake. By contrast, the average tsunami amplitude run-up measured far from the earthquake seems to be more simply related to an accurate estimate of the size of the earthquake represented by its moment magnitude (Abe, 1979; Kajjura, 1981; Okal, 1988; Pelayo and Wiens, 1992; Okal, 1993).

The purpose of this study is to establish the relationship between earthquake source parameters and the generation, propagation, and run-up of local tsunamis as summarized in Fig. 1. In general terms, displacement of the seafloor during earthquake rupture is modeled using elastic dislocation theory (left panel, Fig. 1) for which the displacement field is dependent on the slip distribution ($D_i(x)$), fault geometry (Σ, ν_j), and elastic response and properties of the medium (U_m^{ij} calculated from the elastic Green's tensor, Rybicki, 1986). The process of tsunami propagation generally is the result of an exchange between gravitational energy and horizontal kinetic energy in the water column (Okal, 1988). Specifically, nonlinear long-wave theory governs the propagation and run-up of tsunamis (middle and right panels, Fig. 1). Separation of tsunami wave propagation from dynamic seismic displacements away from the source (Comer, 1984; Okal, 1988) permits one to consider only long-wave propagation in the ocean, subject only to quasi-initial conditions given by the coseismic displacements at the source. Temporal dependence of coseismic displacement ($u_z(x, t)$) can be incorporated into the propagation calculations, using a spatially independent rise time (τ_r) and rupture front (Γ) propagation defined by rupture velocity (ν_r), rupture length (L), and rupture direction

	<u>Generation</u>	<u>Propagation</u>	<u>Broadside Runup</u>
Representative Equations	$u_m = \iint_{\Sigma} D_{ij} U_m^{ij} d\Sigma$	$\frac{\partial(\eta+h)}{\partial t} + \nabla \cdot \{v(\eta+h)\} = 0$ $\frac{\partial v}{\partial t} + (v \cdot \nabla)v + g \nabla \eta = 0$ $h(x, t) = h_0(x) - u_1(x, t)$	$(\sigma \phi_\sigma)_\sigma - \sigma \phi_\lambda = 0$ $v = \frac{\phi(\sigma, \lambda)}{\sigma}$ $x = \cot \beta \left(\frac{\phi_\lambda}{4} - \frac{\sigma^2}{16} - \frac{v^2}{2} \right)$ $\eta = \frac{\phi_\lambda}{4} - \frac{v^2}{2}$ $t = \cot \beta \left(\frac{\lambda}{2} - v \right)$
	Displacement for an arbitrary Somigliana dislocation (Rybicki, 1986)	Shallow wave equations	Carrier and Greenspan (1958) transformation
General Input	$D_j(x)$ Slip distribution	u_1 Vertical displacement	$\eta_0(x)$ Initial waveform
	Σ Rupture area	τ_r Rise time	β Beach slope
	c_{ijkl} Modulus tensor	$\Gamma(t)$ Propagation of rupture front	
	v_j Surface normal		

FIG. 1. Governing equations and general input for calculating the generation, propagation, and broadside run-up of local tsunamis derived from earthquakes. See Section 2 for a description of each process.

(middle panel, Fig. 1). In calculating broadside run-up, the Carrier and Greenspan (1958) transformations of the shallow-water wave equations describe the evolution of tsunamis during run-up in such a way that the shoreline is fixed in (σ, λ) coordinates at $\sigma = 0$ (right panel, Fig. 1).

Because the physics that describes tsunamis from generation through run-up is complex, a parametric study is devised to examine the relative importance of individual earthquake source parameters on local tsunamis. This is not meant to imply separability among source parameters. For example, fracture mechanics studies have long established (as in the early study by Starr, 1928) that the distribution of slip for a static crack is functionally dependent on the dimensions of the crack. Results from the present study do, however, enable the dissection of complex and anomalous earthquakes in terms of explaining the observed local run-up. As noted by Tadepalli and Synolakis (1994a), analyzing run-up from the parameterization of source motions is preferable to studies using assumed tsunami waveforms.

Early studies on how earthquake source parameters affect tsunamis dealt primarily with verifying tsunami amplitudes with seismologically-derived fault parameters (Aida, 1969, 1978, 1983; Ando, 1975). By testing

different fault models and by using a numerical approximation to the linear long-wave equations, the effect that certain source parameters, such as fault length, width, and dip, had on the tsunami was determined (e.g., Yamashita and Sato, 1974; Kajiura, 1981). Later studies related source parameters directly to the amplitude of far-field tsunamis using normal-mode theory—a common technique in earthquake seismology (Ward, 1980; Okal, 1982). More recently, analysis of the source parameters of recent tsunamigenic earthquakes have indicated that details of the earthquake source, namely, nonuniform distribution of slip along the fault plane, have a significant effect on local tsunami run-up (Satake, 1994a; Piatanesi *et al.*, 1996).

A common observation from tsunami simulation studies was that the predicted offshore tsunami amplitude was substantially less than the measured run-up, often by a factor of approximately 2–3 (Shuto, 1991). Much of the problem in linking observed tsunami run-up to calculated earthquake source parameters has been trying to implement a realistic run-up model. Recent advances have been made in describing the run-up associated with nonbreaking waves from hydrodynamic theory, verified by laboratory results (e.g., Briggs *et al.*, 1995). In addition, numerical methods have been developed to address realistic bathymetric and shoreline conditions. However, the run-up from breaking tsunamis has continued to be difficult to estimate because of energy dissipation from turbulent flow (Sato, 1996). It is emphasized in this study that the accuracy of determining run-up on shore is also directly dependent on the source parameters of the earthquake, which provide the initial conditions used for the hydrodynamic models. Without accurate source parameters and coseismic displacement calculations, the best hydrodynamic model is prone to yielding erroneous results. Recent advances in earthquake mechanics in addition to observation of tsunamigenic earthquakes provided by the installation of the long-period worldwide seismic network give us the opportunity to determine not only how the static source parameters affect tsunami excitation, but also the relative importance of the spatial and temporal variations in source parameters on tsunami generation.

This type of study is analogous to near-field ground motion studies from seismic waves, with some basic differences: (1) the propagation velocity for tsunamis is much lower than for seismic waves, suggesting (but remaining to be proven) that the time history of rupture is of secondary importance for tsunami calculations compared to spatial variations in source parameters; (2) the propagation velocity for tsunamis is easily determined from the bathymetry, removing the problematic contribution of earth structure persistent in ground motion studies; (3) “site effects” for tsunami run-up are largely geometrically defined (near-shore bathymetric slope) rather

than based on near-site physical properties (bottom friction does, however, affect tsunami run-up).

This chapter is organized as follows: Sections 2 through 4 provide introductory material important for understanding the relationship between earthquake source parameters and local tsunamis. Section 2 briefly outlines approaches for synthesizing the tsunami waveform and estimating run-up. The general difference in the effect that source parameters have on far-field tsunamis compared to local tsunamis is described in Section 3. Following this, a brief discussion on the tectonic setting of major tsunami-genic earthquakes is given in Section 4. The main objective of the chapter is addressed in Sections 5, 6, and 7, where static source parameters and spatial and temporal variations in source parameters, respectively, are systematically described in relation to the generation and propagation of local tsunamis. Results from these sections are used to infer local effects of "tsunami earthquakes" in Section 8. Tsunami earthquakes are earthquakes that generate anomalously large tsunamis relative to the surface-wave magnitude of the earthquake as originally described by Kanamori (1972). To synthesize the findings from the study, the tsunami generated from the 1992 Nicaragua tsunami earthquake is examined using source parameters from seismic waveform inversions. Finally, Section 10 summarizes the main results from this study.

2. TSUNAMI THEORY

The shallow-water wave equations are most often used to describe tsunami propagation and run-up. The manner in which these equations are invoked, however, differ greatly for the two problems (Fig. 1, middle and right panels). Factors such as propagation distance and complexity of the run-up problem influence the choice of technique used to describe and model the tsunami. Progress continues to be made both in the field of nonlinear propagation and in tsunami evolution during run-up. The different approaches to describe tsunami generation, propagation, and run-up are described in this section.

Many tsunami studies follow a forward modeling approach, in which the tsunami is computed for a given set of source parameters. Objectives of forward modeling are to understand past tsunamis in relation to the causative earthquake and, in some cases, to estimate future tsunamis that might occur (Ando, 1975; Ng *et al.*, 1990; Whitmore, 1993; Geist and Yoshioka, 1996). Another interesting and highly useful application, developed largely by Satake (1987, 1989), follows an inverse modeling approach. This technique is used to invert tsunami waveform data recorded at distant

tide gauges for the source parameters of earthquakes that are not amenable to conventional seismologic analysis. Depending on the amount of data and the accuracy of the bathymetry, resolution of heterogeneous fault motion can be obtained. In the next section, two general approaches for synthesizing tsunami waveforms are discussed: normal-mode and gravity-wave theories.

2.1. General Approaches

2.1.1. Normal-Mode Theory

The normal-mode approach, introduced by Ward (1980), views tsunamis as long-period, free oscillations of a self-gravitating earth, with an outermost layer of water representing a constant-depth ocean (in the spherically symmetric case). Whereas displacements in the solid earth are dependent on both spheroidal and torsional modes of spherical harmonics, only spheroidal modes are necessary to describe tsunamis, because the shear stress vanishes at the ocean floor. The real part of the tsunami displacement field ($\mathbf{u}(\mathbf{r}, t)$) resulting from a point source can be constructed by summing the normal modes of the spherical harmonics (Ward, 1980):

$$\mathbf{u}(\mathbf{r}, t) = \sum_n a_n(t) \mathbf{U}_n(\mathbf{r}),$$

where $a_n(t)$ are the excitation coefficients and $\mathbf{U}_n(\mathbf{r})$ is condensed notation for the normal-mode eigenfunctions. This technique is similar to the one used to describe the displacements of Rayleigh waves (Aki and Richards, 1980), except for different boundary conditions and the fact that only one branch of modes exist for tsunamis, as demonstrated by Okal (1982). Ward (1982) expands this technique to synthesize tsunamis arising from line sources.

The advantages of the normal-mode approach are that (1) it explicitly incorporates coupling of motion between the solid earth and the ocean, (2) it is computationally efficient to reconstruct far-field tsunamis, and (3) effects from source parameters can readily be analyzed through the computation of excitation coefficients. Fault heterogeneity and variations in local bathymetry are less amenable using this approach, which is why gravity-wave theory is typically used for inversion schemes (e.g., Satake and Kanamori, 1991) and for the parametric analysis presented here. However, important results relating source parameters to tsunamis from the normal-mode approach will be referred to throughout this study. Another type of normal-mode analysis, different from the analysis of coupled displacements across the ocean–solid earth interface, involves the calcula-

tion of tsunami waveforms within a closed or semi-closed basin (Satake and Shimazaki, 1987; 1988).

2.1.2. Gravity-Wave Theory

The more conventional method to describe tsunamis is the gravity-wave approach. Here the hydrodynamic equations for long-period gravity waves are used, subject to initial conditions defined by the earthquake source. Displacement of the ocean surface mimics the vertical component of seafloor displacement if the lateral dimensions of the rupture zone are three to four times the water depth (Kajiura, 1963; 1981). Because for significant tsunamis this is most often the case, a two-step procedure is normally used, in which (1) the coseismic vertical displacement of the seafloor is calculated from elastic dislocation theory using the source parameters of the earthquake and (2) propagation of the resulting ocean wave is computed from hydrodynamic theory. For cases in which the bathymetric slope is very steep over the rupture area, it may also be necessary to calculate the coseismic horizontal displacement field (Tanioka and Satake, 1996a; Johnson and Satake, 1997). As previously indicated, calculation of tsunami run-up and inundation often involves separate techniques than are used to describe propagation in the open ocean. Although coupling of propagating seismic and tsunami waves at the ocean-solid earth boundary may be thought significant, equivalence of the normal-mode and gravity-wave techniques is demonstrated by Okal (1982, 1988) and by Comer (1984). The reason that tsunami wave propagation can be considered separately from seismic waves at distances away from the source is the large ratio of dynamic vertical displacements at the ocean surface to vertical displacements at the ocean floor (Okal, 1988).

The gravity-wave approach can also be described as the convolution of linear filters, as in conventional waveform modeling in seismology. In this way, the recorded displacement ($u(t)$) from a point source is the convolution of three basic filters (Lay and Wallace, 1995):

$$u(t) = s(t)*g(t)*i(t),$$

where $s(t)$ is the source filter, $g(t)$ is the propagation filter, and $i(t)$ is the instrument response, which in the case of tsunamis is the tide gauge or bottom pressure sensor. For the case of determining run-up, a separate filter would be included to account for the effects of run-up $r(t)$, and $i(t)$ would not be included:

$$u(t) = s(t)*g(t)*r(t).$$

For a finite source representation, Satake and Kanamori (1991) discretize the fault plane, resulting in the following system of equations:

$$A_{ij}(t)x_j = b_i(t).$$

Here, $b_i(t)$ is the observation at station i , x_j is the slip on the j th sector of the fault, and A_{ij} are the computed Green's functions from standard elastostatic and hydrodynamic theories (the instrument response is not explicitly included in this case). From this, the heterogeneous distribution of slip can be determined (see, however, related cautionary studies regarding the inversion of seismograms by Hartzell and Langer, 1993, and Das and Suhadolc, 1996). It should be noted that the Green's function representation for tsunamis is considerably simpler, albeit computationally more intensive, than for ground motion time histories, given the homogeneity of the propagation medium and that propagation paths can be accurately determined from the known bathymetry of the ocean basins. To determine fully the entire far-field tsunami wavefield, one must also include partial reflection both from bathymetric features and from coastlines, and include the computation of edge waves (discussed in Section 2.3).

2.2. Coseismic Surface Deformation

The first step in the gravity-wave formalism is to determine the static (and later, transient) vertical displacement of the seafloor. It is in this first step that earthquake source parameters relate directly to tsunami generation. The displacement field is determined from linear elastic dislocation theory. Because for the purpose of synthesizing the tsunamis we need only the coseismic surface displacement arising from earthquake rupture, we will not discuss in detail components of internal deformation or post-seismic viscoelastic effects. First, the static deformation from a point source double-couple is reviewed. Second, the surface deformation from a fault with finite dimensions is discussed. Last, numerical techniques for surface deformation arising from dislocation within an inhomogeneous earth are introduced.

2.2.1. Static Displacement for a Point Source

The governing elastostatic equilibrium equation for an isotropic and homogeneous solid is

$$(\lambda + \mu)\nabla(\nabla \cdot \mathbf{u}) + \mu\nabla^2\mathbf{u} + \rho\mathbf{f} = 0,$$

derived from the general Navier equation (Malvern, 1969; Rybicki, 1986), in which the acceleration term, $\partial^2\mathbf{u}/\partial t^2$, is zero. In the elastostatic

equation, ρ is the density, λ, μ are the Lamé constants, \mathbf{u} is the vector displacement field, and \mathbf{f} is the body force per unit mass.

A review of the derivation of the displacement field for a double-couple point source by Lay and Wallace (1995) first involves determining the displacement from a single force. By linear superposition, the displacement for a single-force couple and then a double couple is obtained. Alternatively, the static displacement field can be determined by taking the limit ($t \rightarrow \infty$) in the elastodynamic equations for seismic wave motion (p. 84, Aki and Richards, 1980). The form given by Lay and Wallace (1995) for the static displacement from a double-couple system of forces is (in polar coordinates r, θ, ϕ):

$$\begin{aligned} u_r &= \frac{M}{4\pi\mu r^2} \left(1 + \frac{\Gamma}{2}\right) \sin^2\theta \sin 2\phi \\ u_\theta &= \frac{M}{4\pi\mu r^2} \left(\frac{1}{2} + \frac{\Gamma}{2}\right) \sin 2\theta \sin 2\phi \\ u_\phi &= \frac{M}{4\pi\mu r^2} (1 + \Gamma) \sin \theta \cos 2\phi, \end{aligned}$$

where

$$\Gamma = \frac{\lambda + \mu}{\lambda + 2\mu}$$

and M is the moment of the force couple.

2.2.2. Static Displacement for a Finite Source

The displacement field for a finite source can be obtained by superposition of point source double-couple solutions, as discussed by Chinnery (1961). Many researchers have derived expressions for surface and internal static displacement for a finite source. A review of these derivations is given by Okada (1985). In the same paper, Okada (1985) presents analytical expressions for surface displacement and deformation, owing not only to slip within the dislocation plane but also to tensile slip, in which the Burgers vector is normal to the dislocation plane. Displacement calculations for this type of rupture would be useful, for example, in simulating a tsunami generated by sudden dike injection. The closed-form expressions for vertical surface displacement due to slip along a rectangular fault are lengthy—the reader is referred to Okada (1985) and the Appendix to this chapter for these expressions.

The expressions derived by Okada (1985) are for an isotropic, homogeneous half-space. Other researchers have derived the displacements associated with faulting in a horizontally layered elastic medium (most recently, Savage, 1987; Ma and Kuszniir, 1992, 1994; Pollitz, 1996; see Ma and Kuszniir, 1994, for a comprehensive background of research) and in a laterally inhomogeneous medium (McHugh and Johnston, 1977; Rybicki, 1978; Niewiadomski and Rybicki, 1984). The effect of contrasts in shear modulus between horizontal layers is especially significant (Savage, 1987; Ma and Kuszniir, 1994; Pollitz, 1996). Also, analytical expressions for the displacement field resulting from nonuniform slip along vertical faults is presented in Wang and Wu (1983) and Singh *et al.* (1994).

2.2.3. Numerical Techniques

The previously described analytical expressions are invaluable toward understanding the effects that source parameters, inhomogeneity, and non-uniform slip have on the static displacement field. Still, to model realistic conditions of geometrically complex faults, complex slip distributions, and elastic layers of variable thickness accurately, numerical methods are needed.

The two commonly used methods are boundary element and finite element methods. A boundary element method developed to study static stress changes incorporates the analytical expressions for internal deformation by Okada (1992) into boundary elements described by Crouch and Starfield (1983) (see Bilham and King, 1989, and Stein *et al.*, 1992, for description). Although this method is designed for determining static stress changes in relation to spatial aftershock distributions and earthquake triggering, the static displacement field from complex faulting in a homogeneous medium can also be determined.

Three-dimensional finite element models for studying the displacement field and stress changes associated with earthquake slip have been developed by Hashimoto (1982), Yoshioka *et al.* (1989), Dmowska *et al.* (1996), and others. Geist and Yoshioka (1996) use the model developed by Yoshioka *et al.* (1989) to study the type of tsunamis that might be generated along both planar and nonplanar faults, using an inhomogeneous elastic structure for the Cascadia margin of western North America. Dislocation is introduced into this model using the split-node technique developed by Melosh and Raefsky (1981). Using this method, slip along the fault can be explicitly incorporated in the model. Similarly, stress-drop conditions can be used to specify rupture as in the so-called slippery-node technique developed by Melosh and Williams (1989). The fault zone can also be represented by a narrow but continuous layer of elements, as in the

study by Dmowska *et al.* (1996). In that study, differences in elastic moduli for the fault layer elements are used to specify the region that undergoes coseismic slip (asperities in their model) separate from surrounding fault layer elements in which no coseismic change in shear stress is imposed. Faulting represented by shear strain localization along a slip surface using continuous functions is amenable to adaptive mesh refinement (Zienkiewicz and Taylor, 1991).

2.3. Tsunami Propagation

From what is observed along the shoreline (i.e., tide gauge records, run-up, and inundation), the effects of the earthquake source on the tsunami will necessarily be modified during propagation. Even for local tsunamis, directivity, radial spreading, and attenuation importantly affect the tsunami as it reaches shore. A thorough review of tsunami propagation theory would be quite lengthy (see Kajiura, 1963; Carrier, 1971; and Mei, 1983, for a more complete discussion); we present a summary of some of the important points.

2.3.1. Shallow-Water Wave Equations

Because tsunamis are very long gravity waves (i.e., many tens to hundreds of kilometers), propagation is conventionally described using depth-averaged, hydrostatic, shallow-water wave equations:

$$\frac{\partial(\eta + h)}{\partial t} + \nabla \cdot [\mathbf{v}(\eta + h)] = 0 \quad \text{Continuity equation}$$

$$\frac{\partial \mathbf{v}}{\partial t} + (\mathbf{v} \cdot \nabla) \mathbf{v} + g \nabla \eta = 0, \quad \text{Momentum equation}$$

where $\mathbf{v} = v_i$, ($i = 1, 2$) are the depth-averaged components of horizontal velocity, η and h are the water surface elevation and water depth relative to a reference state, respectively, and g is the gravitational acceleration. Note that to consider finite source process times, the $\partial h / \partial t$ term in the continuity equation cannot be ignored.

The preceding form of the shallow-water wave equations assumes a static pressure distribution. More general shallow-water wave equations that include additional nonlinear terms, for example, due to vertical acceleration, have been derived in relation to tsunami propagation (Carrier, 1966; Peregrine, 1967; Wu, 1981; Liu and Earickson, 1983; Mei, 1983). A measure of the magnitude of these nonlinear effects relative to linear effects is given by the Ursell number ($Ur \equiv \eta_0 l^2 / h^3$), where η_0 is the

maximum wave amplitude and l is the characteristic wavelength (Hammack, 1973; Wu, 1981). Soon after the tsunami leaves the source region, $U_r \ll 1$, indicating that the linear form of the shallow-water wave equations adequately describes propagation. As the tsunami continues to propagate, U_r increases as a function of $t^{1/3}$ as nonlinear effects (i.e., amplitude dispersion in addition to frequency dispersion for $U_r \ll 1$) become more influential (Kajiura, 1970; Hammack, 1973). Shibata (1983) indicates that not including the effects of dispersion overestimates the wave height for local propagation near continental margins. Mei (1983) also indicates that the effects of dispersion may be important for tsunamis generated near the edges of continental shelves, although in general the cases in which dispersive theory is necessary may be limited (Shuto, 1991).

Two other effects that have been shown to be important are the generation of edge waves and partial reflection during propagation. Of particular importance is constructive interference of edge waves with the nontrapped modes of the tsunami to produce higher-than-expected secondary wave arrivals and run-up (Carrier, 1966). Edge waves are coastal trapped waves that occur in distinct modes, characterized by an exponential amplitude decay away from shore (Fuller and Mysak, 1977; LeBlond and Mysak, 1978; Mei, 1983; Carrier, 1995) and have been likened to Love waves in seismology (Sezawa and Kanai, 1939). The possibility that edge waves are excited by tsunamis is discussed by a number of authors (e.g., Fuller and Mysak, 1977; LeBlond and Mysak, 1978; Carrier, 1995). Fuller and Mysak (1977) further indicate that the amplitude of trapped edge waves excited by a tsunami is approximately 70% of the incident amplitude and that edge waves slowly attenuate from scattering along irregular coastlines.

Direct observation of edge waves excited by a tsunamigenic earthquake was made by González *et al.* (1995a, b) for the 1992 Cape Mendocino earthquake. Numerical modeling of the tsunami by González *et al.* (1995a, b) indicates that local tsunamis excite the gravest-mode ($n = 0$) edge waves, similar to edge waves excited by storms (LeBlond and Mysak, 1978). In terms of propagation velocity, Ishii and Abe (1980) demonstrate a dependence of group velocity and phase velocity on the slope angle of the continental shelf. The fact that the group velocity for edge waves is significantly slower than for non-trapped modes may partly explain the observation that the largest-amplitude arrival of a tsunami is commonly not the leading wave (Carrier, 1966), emphasizing the importance of understanding tsunami-generated edge waves for local tsunami hazards (González *et al.*, 1995a, b).

Reflection from bathymetric variations can also result in significant modification of the tsunami during propagation. Whereas accurate compu-

tation of tsunami reflection from coastlines is difficult because of the dynamics associated with run-up, reflection concurrent with propagation is a tractable problem addressed in previous studies. When tsunamis are reflected along the continental shelf, an attendant change in the waveform and a decrease in amplitude occurs (Peregrine, 1967; Wu, 1981; Carrier and Noiseux, 1983; Liu *et al.*, 1991). Abe and Ishii (1980) examine the reflection and transmission of a tsunami across a bathymetric ramp representative of continental slopes. They find that the reflection coefficient is dependent on a number of factors, including incidence angle, angle of slope, and spectrum of the incident wave. These changes occur from distortion due to the dynamics of reflection, exclusive of frictional dissipation during propagation (Carrier and Noiseux, 1983). The combined influence of trapped modes and oblique reflection results in a lengthy and complex tsunami coda.

In certain circumstances, other effects may be significant for tsunami propagation, including Coriolis effects, viscous and diffusive effects, and bottom friction. As explained by Peregrine (1967) and Kowalik and Whitmore (1991), viscous boundary layer effects and friction at the sea-floor do not significantly affect tsunami propagation in the open ocean. Stoneley (1964) also demonstrates that dissipation of energy from bottom friction is of primary concern near the shoreline, although dissipating effects may also occur near the source area. In comparing tsunamis predicted with and without the effect of bottom friction, Satake (1995) shows that bottom friction near the coast affects the later phases of the tsunami more than it does the first arrival.

2.3.2. Linear Long-Wave Equations

Linearizing the standard shallow-water wave equations results in the following set of equations:

$$\frac{\partial(\eta + h)}{\partial t} + \nabla \cdot (h\mathbf{v}) = 0 \quad \text{Continuity equation}$$

$$\frac{\partial \mathbf{v}}{\partial t} + g\nabla\eta = 0, \quad \text{Momentum equation}$$

which are valid for $\eta/h \ll 1$. Practically, the linear long-wave equations can represent local tsunami propagation for water depth greater than approximately 50 m (Nagano *et al.*, 1991; Shuto, 1991). The linear long-wave equations are commonly used for tsunami propagation in deep water and for the inversion schemes of Satake and Kanamori (1991).

2.3.3. Radiation, Directivity, and Decay

To translate the effects that source parameters have on tsunamis as they propagate toward shore, it is useful to understand the basic properties of radiation patterns, directivity, and amplitude decay of tsunamis. The characteristic radiation pattern associated with tsunamis is considerably different than for surface seismic waves. As discussed by Yamashita and Sato (1974) and Okal (1988), the point-source radiation pattern for both seismic and tsunami waves is, in general, dependent on frequency, depth, and variations in shear modulus. With this in mind, the tsunami radiation pattern at long wavelengths for a thrust mechanism is less lobate and more isotropic than the comparable radiation pattern for Rayleigh waves (Okal, 1988). The effect of source finiteness on the radiation pattern is dependent on the wavelength of the tsunami and the distance from the source. In general, a beaming effect is apparent for wavelengths less than the fault length (Kajiura, 1970; Yamashita and Sato, 1974; Ward, 1982). A profound example of this beaming effect is given for the 1964 Alaskan earthquake tsunami by Ben-Menahem and Rosenman (1972), who show that much of the tsunami energy was directed toward California and Chile rather than being azimuthally distributed throughout the Pacific basin. In the near field, additional lobes exist due to the source finiteness (Ben-Menahem and Rosenman, 1972; Ward, 1982). Directivity effects due to rupture propagation and whether rupture occurs in low-rigidity sediment (Okal, 1988) can also be significant. Finally, directivity of the tsunami will be altered greatly by focusing and defocusing, owing to refraction of the tsunami from bathymetric variations. Therefore, it is frequently more useful for local tsunamis to study the time history of propagation rather than to describe the source directivity (Aida, 1969; Kajiura 1981; Geist and Yoshioka, 1996).

The amplitude decay of the leading wave of a tsunami is dependent on the sense of seafloor displacement generating the tsunami. For a constant water depth and celerity ($C = (gh)^{1/2}$), in one horizontal dimension, the amplitude of the leading wave decays as a function of $t^{-1/3}$ for a positive, one-sided displacement of the seafloor (termed a *monopole* source) (Wu, 1981; Mei, 1983). In contrast, the leading wave decays faster for adjacent positive and negative displacement (termed a *dipole* source) and is a function of $t^{-2/3}$. For propagation in two horizontal dimensions, radial spreading also contributes to amplitude decay such that the effective decay is $t^{-5/6}$ for a monopole source and $t^{-4/3}$ for a dipole source (Wu, 1981; Mei, 1983). In terms of realistic earthquake mechanisms, monopole sources for seafloor displacement are rare: earthquake slip along a dip-slip fault results in a dipole source, whereas slip along a strike-slip fault results in a

quadrupole source. Within and near the source region, the decay functions are more complex than presented here; they are discussed in Section 3.

In general terms, amplification due to shoaling near the coastline is governed by Green's Law, in which η_{\max} is proportional to $h^{-1/4}$ (Mei, 1983). From theoretical and laboratory results, Synolakis (1991) and Synolakis and Skjelbreia (1993) demonstrate the validity of Green's Law for solitary waves propagating over combined bathymetry (variable slope), including the effects of reflection. Other scaling relations for shoaling tsunamis include reduction in the effective wavelength and phase velocity, proportional to $h^{1/2}$ (Wu, 1981). For both far-field and local tsunamis, complex three-dimensional variations in the bathymetry result in focusing and defocusing of tsunamis, which are not as easily quantified.

2.3.4. Numerical Methods

For simple source configurations, analytic expressions for tsunami propagation can be obtained (Carrier, 1966, 1971; Kajiura, 1970). In addition, Comer (1984) presents analytic expressions for tsunami propagation in relation to an arbitrary point source for constant ocean depth. For complex seafloor displacement patterns and realistic bathymetry, numerical methods are most often used. The most common methods are various finite difference schemes. Because grid size is critical to the stability of finite difference methods, variable grid sizes have been used to encompass both open-ocean propagation and near-shore propagation (e.g., Satake, 1985; Kowalik and Whitmore, 1991; Mader and Curtis, 1991; Whitmore, 1993). For regional studies, finite element methods have also been used (e.g., Peraire *et al.*, 1986; Greenberg *et al.*, 1993; Myers and Baptista, 1995; Tinti and Piatanesi, 1996). Many of these models are adapted to analyze tsunamis from generalized tidal circulation models based on the shallow-water wave equations.

2.4. Tsunami Run-up

Despite the accuracy at which tsunami propagation can be modeled, observed run-up values often differ from computed tsunami wave heights by a factor of 2 or more (Shuto, 1991; Satake, 1994a). The reason for this discrepancy is related primarily to the dynamics of run-up. The consistency between the observed run-up and calculated offshore wave height has led to the use of an empirical amplification factor to relate modeled tsunamis to run-up values. The amplification factor for wave heights computed at a depth of 50–200 m is usually between 2 and 3, although the factor can

range between approximately 1 and 20 depending on local bathymetric conditions (Shuto, 1991; Satake, 1994a).

Early theoretical work on determining maximum run-up analytically was related to standing periodic waves (Keller and Keller, 1964; Shuto, 1972). The ratio of the maximum run-up height above mean sea level (R) to the height of the incident tsunami is given by

$$\frac{R}{H} = [J_0^2(U) + J_1^2(U)]^{-1/2},$$

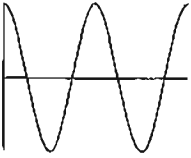
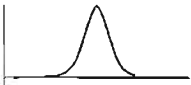
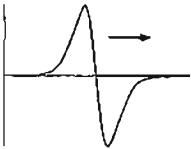
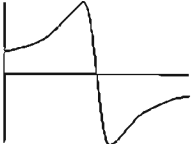
where J_0 and J_1 are the zeroth-order and first-order Bessel functions, respectively, and

$$U = \frac{4\pi h}{L \cot \beta},$$

where h is the water depth prior to run-up, L is the dominant wavelength, and β is the beach slope (Goto and Shuto, 1983; Togashi, 1983). Although the run-up of standing monochromatic waves appears to have limited applicability with respect to tsunami run-up, Synolakis (1987, 1991) indicates that the run-up for traveling waves can be obtained by linear superposition. It is important to emphasize, however, that using a dominant wavelength for tsunamis that are better characterized by solitary, cnoidal, or similar pulse waveforms may lead to inaccurate results (Synolakis *et al.*, 1987). Synolakis (1987, 1991) shows that the maximum run-up is identical using either the linear theory or the nonlinear theory advanced by Carrier and Greenspan (1958). To determine the full evolution of a tsunami during run-up, however, the nonlinear theory is necessary.

Run-up laws similar to the preceding one have been derived for a variety of waveforms that are thought to represent tsunamis best (Table 1). In particular, N-waves encompass a wide range of dipole waveforms and can be used to estimate the run-up of local tsunamis for a constant beach slope (Tadepalli and Synolakis, 1994b). These studies emphasize the fact that aspects of the tsunami waveform other than maximum amplitude (specifically, leading wave steepness and polarity) have a controlling influence on run-up. The inclusion of bottom friction necessitates the use of numerical methods to determine run-up. Bottom friction has the effect of attenuating wave height and run-up (Chu and Abe, 1983; Satake, 1995). Because bottom friction is thought to be considerably less seaward of the shoreline than onshore (Chu and Abe, 1983), its effects on the tsunami before run-up are of secondary importance in relation to source effects (Goto and Shuto, 1983; Myers and Baptista, 1995). Nagano *et al.* (1991) suggest that, especially in bays, energy dissipation by scouring may be important.

TABLE I THEORETICAL RUNUP LAWS FOR DIFFERENT WAVEFORMS^a

Waveform	Graph	Run-up law	Reference
Sinusoidal wave		$\frac{R}{H} = [J_0^2(U) + J_1^2(U)]^{-1/2}$ $U = \frac{4\pi d}{L} \cot \beta^{(b)}$	Keller and Keller (1964); Shuto (1972)
Cnoidal wave		see reference	Synolakis et al. (1988)
Solitary wave		$R = 2.831 \sqrt{\cot \beta} H^{5/4(c)}$	Synolakis (1987)
N-wave		$R = 3.86 \sqrt{\cot \beta} H^{5/4(c, d)}$	Tadepalli and Synolakis (1994a)
Lorentz wave		$\frac{R}{H} = P_+ \sqrt{(d \cot \beta)/L} \quad (e)$ $P_+ = \pi \sqrt{2} \cos^{5/2}(2\theta/5)$	Pelinovsky and Mazova (1992)

^a For each case, R , H , d , and β are the maximum runup, initial wave height, initial water depth, and slope angle, respectively. See references for specific applications and limiting conditions.

^b U notation from Togashi (1983) (see text). L is wavelength. J_0 and J_1 are the zeroth-order and first-order Bessel functions, respectively.

^c Spatial parameters nondimensionalized with respect to the initial water depth (d).

^d Valid for isosceles N-wave. See reference for generalized N-wave runup law.

^e See reference for specific parameters and conditions.

Run-up laws such as those listed in Table 1 are valid only for waves that do not break during run-up. (Pelinovsky and Mazova, 1992, estimate that approximately 75% of tsunamis apparently do not break during run-up.) Synolakis and Skjelbreia (1993) study the behavior of solitary waves before and after breaking. They find that near the point of breaking, solitary wave evolution deviates from Green's Law to a regime of rapid amplification followed by rapid decay immediately after breaking. Because of the characteristic turbulent flow, run-up from breaking waves is difficult to estimate, although research is progressing in this field (Yeh, 1991; Liu *et al.*, 1991; Antunes do Carmo and Seabra-Santos, 1996; Sato, 1996).

3. LOCAL VERSUS FAR-FIELD TSUNAMIS

The manner in which source parameters affect tsunamis is highly dependent on the propagation distance. Namely, a distinction is made between local tsunamis and far-field tsunamis. Although the distinction between the two types of tsunamis is based on propagation distance, it may be more practical to distinguish local and far-field tsunamis by the direction of propagation from the source: immediately landward and basinward, for local and far-field tsunamis, respectively. The reason for the distinction is not so much the hydrodynamic effects during propagation (once generated, the leading tsunami waveform is remarkably stable), but rather the characterization of the source parameters of the earthquake. For far-field tsunamis, a line-source or even point-source representation using static source parameters is adequate to describe the run-up height averaged over large distances. In contrast and as will be demonstrated, local tsunamis often require a full source representation of the rupture area as well as consideration of spatial and temporal changes in the source parameters of the earthquake. In this section we discuss how, in general, source parameters affect far-field tsunamis differently from local tsunamis, where the source region is very near the site of run-up.

3.1. Source Parameters Affecting Far-Field Tsunamis

As mentioned in the introduction, the average amplitude of a far-field tsunami is dependent primarily on the size of the scalar seismic moment (M_0). (At the same time, of course, details of the seismic source can be extracted by the collective inversion of far-field tide gauge records, as in Satake, 1987.) Pelayo and Wiens (1992) establish the following empirical relationship between average tsunami run-up (\bar{R}) and moment magnitude

(M_w), where Δ is angular distance and k is a proportionality factor:

$$\log[\bar{R}(\Delta)] = 1.5M_w + 16.1 + \log[k(\Delta)]$$

This relationship was determined by applying a geometrical spreading factor of $\sqrt{\sin \Delta}$ (see also Okal, 1988) to the average tsunami run-up measured at Hawaii for 36 far-field, tsunamigenic earthquakes. Here, a slope of 1.5 for the line relating the logarithm of equalized run-up height to M_w is proposed, in contrast to a slope of 1.0 proposed by Abe (1979).

From the normal-mode approach, Ward (1980) estimates that only 4% of the energy in tsunami modes is stored elastically in the solid earth and, as such, only very large earthquakes ($M_0 \geq 4 \times 10^{28}$ dyne-cm) tend to generate destructive, far-field tsunamis (Okal, 1988). As explained by Okal (1988), depth is not a controlling factor for far-field tsunami magnitude, primarily because, although seafloor displacement decreases with focal depth, the area over which seafloor displacement occurs increases with depth, resulting in only a slight overall reduction in the volume of water displaced with increasing depth. By way of an example, the 1977 Tonga event ($M_w = 8.1$, Talandier and Okal, 1979; Silver and Jordan, 1983) had a hypocentral depth of 100 km and produced a sizable tsunami relative to the moment magnitude of the earthquake. As calculated by Okal (1988), an event shallower by an order of magnitude (10 km) but with the same geometric source parameters as the 1977 Tonga event produces a tsunami only four times larger than the 100-km-depth event. It should be noted, however, that the spectral characteristics of the two tsunami waves were determined to be quite different (Okal, 1988). The focal mechanism of a tsunamigenic event also has a secondary influence on the far-field magnitude of the tsunami (Okal, 1988), although in most cases, for a given seismic moment strike-slip mechanisms are deficient in generating tsunamis in comparison to dip-slip mechanisms, in part because the ratio of maximum vertical surface displacement to slip is less for strike-slip mechanisms (Kajiura, 1981; see also Ward, 1980). For dip-slip events shallower than 15 km depth, dip of the fault plane becomes increasingly important. As mentioned previously, other source parameters can also affect the far-field radiation pattern of tsunamis.

3.2. Coseismic Displacement near a Coastline

Local tsunami run-up near or over the earthquake rupture area is particularly complex because of coseismic displacement of both the seafloor and coastline and its effects on propagation and run-up. For most major thrust events along the interplate boundary of subduction zones, the

submerged part of the vertical displacement profile is commonly positive (uplift) whereas all or part of the negative displacement may occur landward of the shoreline (Fig. 2a, b). In the case shown in Fig. 2a, coastline subsidence exacerbates the effect of tsunami inundation from an interplate event. These effects are essentially observed for the 1960 Chilean earthquake (Linde and Silver, 1989) and for the 1964 Alaskan earthquake (Hwang and Divoky, 1970). Whether or not coastline uplift or subsidence occurs or what part of the seafloor displacement profile is submerged depends on the position of the interplate rupture area relative to the coastline (Fig. 2). Earthquakes in other environments, such as back-arc thrust events, will have different effects. For example, during the 1993 Hokkaido Nansei-Oki earthquake, Okushiri Island west of Hokkaido subsided entirely (Satake and Tanioka, 1995).

3.3. Wave Evolution over the Source Area

Another complication in calculating local tsunamis is the variability of the tsunami waveform during propagation through the source area. For example, the evolution of a tsunami resulting from slip along a shallow-dipping thrust fault (slip = 3 m, $\delta = 10^\circ$) is modeled using the nonlinear, dispersive wave propagation theory of Liu and Earickson (1983) (Fig. 3). During the first minute, the phase velocity (dashed lines, left-hand side, Fig. 3) is slower than what would be expected from the long-wave velocity (\sqrt{gh}) for the Airy phase of the tsunami (Kajiura, 1963; Stoneley, 1964). Similarly, the maximum depth-averaged velocity during the first minute is lower than for the tsunami propagating far from the source area. Within the rise time of the earthquake (slightly exaggerated for illustration purposes compared to the rise time of typical earthquakes) there is a concomitant increase in the amplitude of the tsunami. The decrease in amplitude following generation is due to splitting of the tsunami into the left- and right-propagating waves (right-hand side, Fig. 3). The amplitude of the oppositely propagating tsunamis is modified during propagation through the source area. This is particularly evident for the peak phase of the right-propagating tsunami in Fig. 3 as it passes over the region of seafloor subsidence. A near-source reduction in the amplitude of the phase that passes through the source region is also noted by Kajiura (1970). Far from the source, the maximum amplitude of the oppositely propagating tsunamis is slightly different (perhaps as a result of using a finite rise time), but asymptotically approaches half the maximum amplitude of the initial displacement, as would be expected for the two-dimensional case. For the experiment shown in Fig. 3, the rise time of the earthquake is less than the

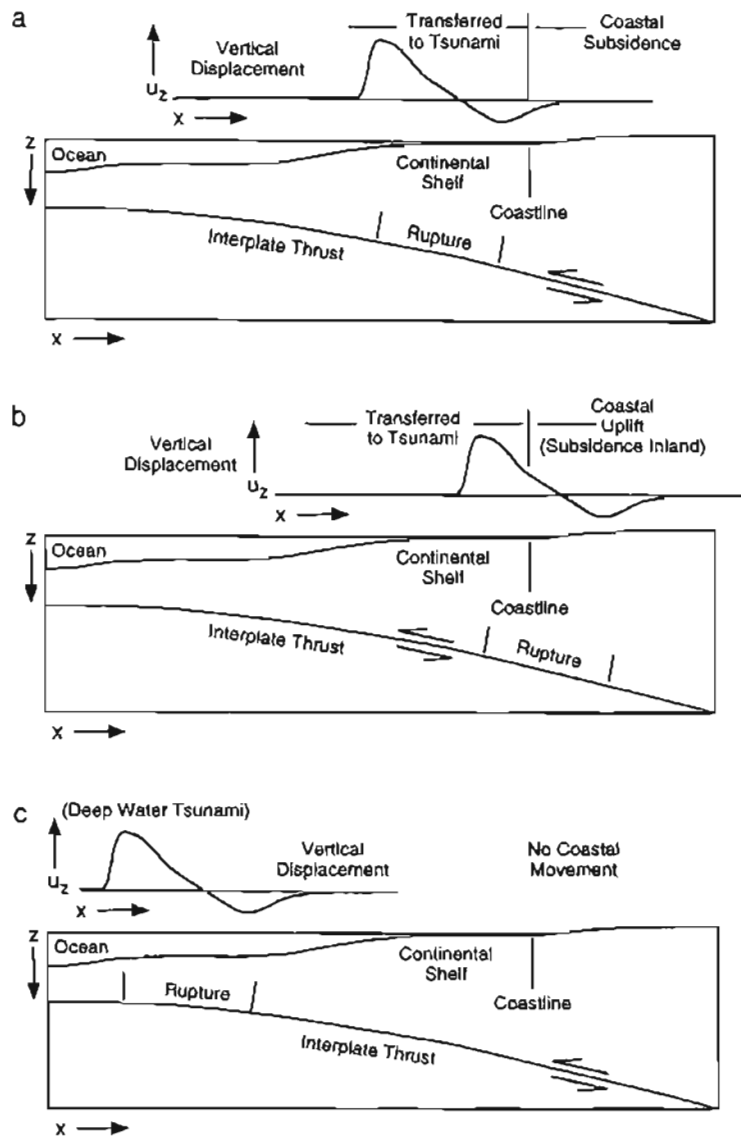


FIG. 2. Schematic diagram of the effect of relative position between rupture zone and coastline. Vertical displacement resulting from thrust fault dislocation shown above; cross-section of continental margin shown below. (Scale of vertical displacement is greatly exaggerated with respect to the scale of the cross-section.) (a) Rupture zone adjacent to coastline on the seaward side. Coseismic coastal subsidence occurs. (b) Rupture zone located farther landward than (a). Coseismic coastal uplift occurs. Only part of the vertical displacement field is transferred to the tsunami. (c) Rupture zone beneath the continental slope. No coastal movement occurs in this case. A deep-water tsunami is generated that is subsequently amplified during propagation across the continental margin.

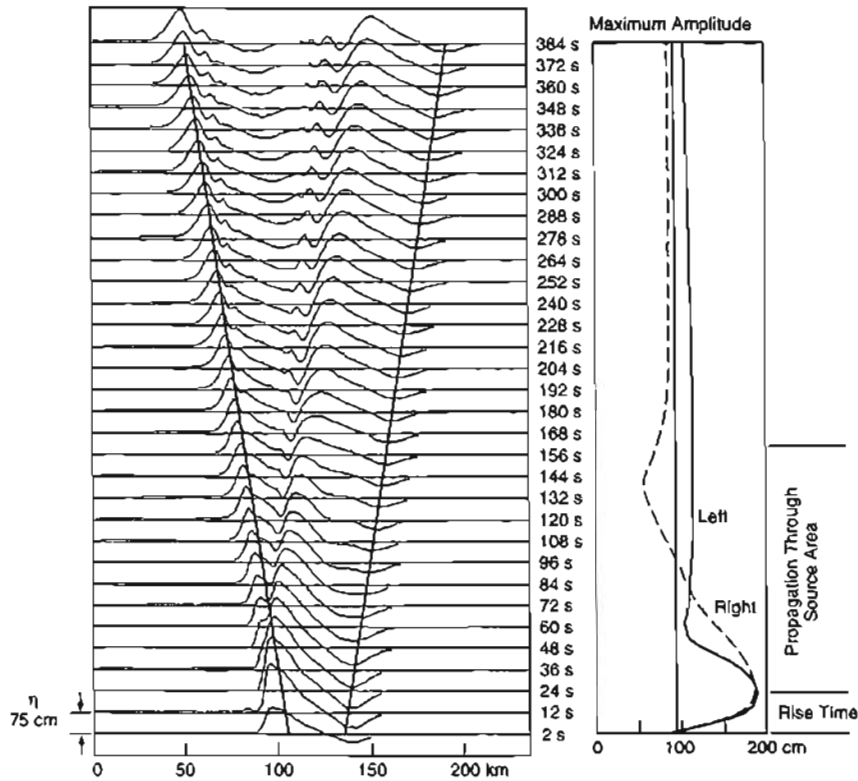


FIG. 3. Evolution of tsunami during propagation through the source region for constant water depth ($h = 2.2$ km). *Left*: Tsunami waveform at 12-s time intervals. Slope of lines inversely proportional to expected long-wave phase velocity. Note lag in phase velocity during tsunami generation. *Right*: Maximum amplitude of left- and right-propagating tsunamis. (For typical landward-dipping faults associated with subduction zones, the left-propagating tsunami would be basinward and the right-propagating tsunami would be landward.) Thin centerline represents half of maximum amplitude.

characteristic period of tsunami propagation (Ando, 1982). However, for earthquakes with long deformation times, different effects are observed, as discussed in Section 6.1.

In three-dimensions, Momoi (1964), Kajiura (1970), and Liu and Earickson (1983) indicate that a single-sided displacement generates large wave amplitudes of opposite sign in the source region. For more realistic dipole-type displacements, the opposite displacement phases tend to cancel this effect, though the exact three-dimensional behavior of the tsunami in the source region is quite complex. In addition, the effects on phase velocity and amplitude observed in Fig. 3 are for constant water depth.

Certainly, variations in the local bathymetry will modify the evolution of the tsunami waveform from what is shown here. In summary, although tsunamis generated in deep water (Fig. 2c) will be amplified to a greater extent than continental-shelf tsunamis, the effects of coastal subsidence (Fig. 2a) and near-source wave evolution may lead to larger run-ups than expected from considering only Green's Law.

4. TECTONIC SETTING OF TSUNAMIGENIC EARTHQUAKES

Subduction zones are the setting for most significant tsunamigenic earthquakes. In comparison to spreading ridges and transform faults, subduction zones are characterized by a greater abundance of large earthquakes (Pacheco and Sykes, 1992). In this section, the type of faulting observed along subduction zone margins is discussed as well as what controls rupture along the interplate thrust.

4.1. Types of Subduction Zone Faulting

The location and different types of faults observed along subduction margins are indicated in Fig. 4. Because most of the relative motion between two tectonic plates at a subduction zone is accommodated at the

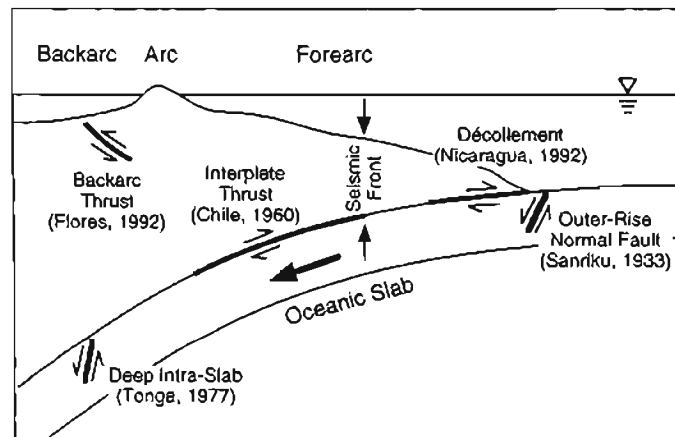


FIG. 4. Schematic representation of the characteristic faults within a subduction zone that have historically generated tsunamis. An example of an event that generated a large local tsunami is listed for each fault type.

interplate thrust, this fault generates most of the largest tsunamigenic earthquakes. Great earthquakes ($M \sim 9$) along interplate thrusts (e.g., 1952 Kamchatka, 1957 Aleutian, 1960 Chile, and 1964 Alaska earthquakes) are responsible for most of the damaging far-field tsunamis in this century (Furumoto, 1991). The ambient level of seismicity for a subduction zone, including activity on the interplate thrust, is often delineated by a seismic front near the trench (Yoshii, 1979; Byrne *et al.*, 1988). Very shallow earthquakes can occur, albeit very infrequently, up-dip from the seismic front along the interplate thrust (or the décollement within the overriding accretionary wedge). These enigmatic events are particularly important in tsunami hazard studies, because they are most often classified as tsunami earthquakes, defined by anomalously high tsunami excitation and a substantial difference between M_s and M_w (Kanamori, 1972; discussed further in Section 8). In recent years tsunami earthquakes have produced unexpectedly large local tsunamis, primarily because of the higher amounts of slip associated with these earthquakes. Examples of tsunami earthquakes include the 1896 Sanriku, 1946 Aleutian, 1960 Peru, 1963 Kurile, 1992 Nicaragua, and 1994 Java earthquakes.

In addition to the interplate thrust, strain is also distributed within either plate of a subduction zone, resulting in intraplate faulting. Back-arc thrust events have produced destructive tsunamis in recent years, such as the 1983 Japan Sea, 1992 Flores, and 1993 Hokkaido Nansei-Oki earthquakes. Because many back-arc regions encompass semi-closed ocean basins, it is important to address free oscillations arising from back-arc tsunamis (Satake and Shimazaki, 1988). Finally, earthquakes rupturing within the oceanic slab can generate sizable tsunamis, both in the outer-rise region (e.g., 1933 Sanriku, 1977 Sumba, and 1990 Mariana earthquakes) and at great depths within the subducted part of the slab (e.g., 1977 Tonga and 1994 Kurile earthquakes). Mechanisms for intraslab earthquakes are often complex and are not consistently of a particular mechanism.

4.2. Nature of Rupture along the Interplate Thrust

Observationally, the spatial distribution of moment release, and therefore the distribution of slip, for interplate thrust earthquakes is remarkably heterogeneous (Thatcher, 1990). For the majority of earthquake sequences studied by Thatcher (1990), zones of concentrated moment release occur roughly in the same location for successive subduction zone earthquakes, and the epicenter of the earthquake is located within or near these high-moment-release zones. (A notable exception is the 1974 M_w 8.0 Peru earthquake, in which the hypocenter occurred in a region of relatively low

slip: Beck and Ruff, 1989; Hartzell and Langer, 1993.) In contrast, other rupture characteristics, such as rupture dimensions and average slip and moment, may vary considerably between successive cycles (see also Swenson and Beck, 1996; Mendoza, 1993). The zones of concentrated moment release are often interpreted as high-shear-strength regions of the fault and, as such, termed asperities (Kanamori, 1981; for examples, see Beck and Christensen, 1991; Dmowska and Lovison, 1988; Ruff, 1992; Mendoza, 1993). However, there are also cases in which the zones of high moment release do not remain spatially fixed (Thatcher, 1990; Boyd *et al.*, 1995; Tanioka *et al.*, 1996), indicating that the stationary asperity interpretation of regions of high moment release may not be globally applicable. As an alternative to the regionally-fixed asperity model, Fukao and Furumoto (1985) and Kikuchi and Fukao (1987) suggest a self-similar model in which the length scale of variations in the moment distribution increases with the growth of rupture. Cochard and Madariaga (1996) also indicate that observed spatial variations in slip for an event may be explained by the complex dynamics of earthquake rupture, without necessarily invoking lateral strength heterogeneities (see also Ben-Zion and Rice, 1995; Rice and Ben-Zion, 1996).

The asperity interpretation of regions of high seismic moment release can also be viewed on a tectonic scale in the context of slip stability (Scholz, 1990; Boatwright and Cocco, 1996). The stability of the interplate thrust of the subduction zone falls within a *stability field*, defined as being either stable, conditionally stable, or unstable. Here, the *unstable* regions would correspond to asperities, *conditionally stable* regions to regions that may slip due to slip in neighboring unstable regions, and *stable regions* to regions where stable sliding occurs. At any particular location along the fault plane, the position in the stability field is dependent on the state of stress (specifically, shear stress and the effective normal stress along the fault) and on material properties, including fault zone composition, permeability, and roughness along the fault (Scholz, 1990; Pacheco *et al.*, 1993). In particular, Boatwright and Cocco (1996) identify asperities with strong velocity-weakening frictional behavior.

Variations in the frictional behavior along the interplate thrust of a subduction zone can be related to the overall coefficient of *seismic coupling*, defined as the ratio of the long-term seismic slip rate to the tectonic slip rate (Pacheco *et al.*, 1993). Using the concept of stability fields, the seismic coupling coefficient is related to the area of the fault plane that is in the unstable portion of the stability field (Lay *et al.*, 1982; Ruff and Kanamori, 1983). Although factors such as slab dip and age of the oceanic lithosphere initially were thought to correlate with seismic coupling, further analysis by Pacheco *et al.* (1993) indicates poor correla-

tion with these variables. Instead, Pacheco *et al.* (1993) suggest that topographic roughness of the interplate fault and frictional behavior of the fault zone related to material properties and permeability may control the pattern of stability fields and overall seismic coupling. In general, the type and amount of material subducted (i.e., sediments or lack thereof, sheared seamounts) certainly play an important role in the stability of subduction segments, along with the amount of fluids in the fault zone. Current research focused on determining the parameters that control stability fields and determining whether or not stability fields are stationary between successive earthquakes is critical towards eventually predicting where the areas of highest moment release and slip may be located for impending earthquakes.

5. EFFECT OF STATIC SOURCE PARAMETERS ON TSUNAMIS

Although earthquake rupture is a complex process, various approximations can be made, depending on the wavelength and period of the observation. Conceptually, earthquake rupture is initiated at the hypocenter and propagates outward in the plane of the fault (Fig. 5). Within the rupture area, a variable amount of slip occurs (i.e., consistent with a Somigliana dislocation). Both the area of rupture and the slip vector field are spatially and temporally variable, as indicated in Fig. 5 (Lay and Wallace, 1995). After rupture ceases, the final value for the source param-

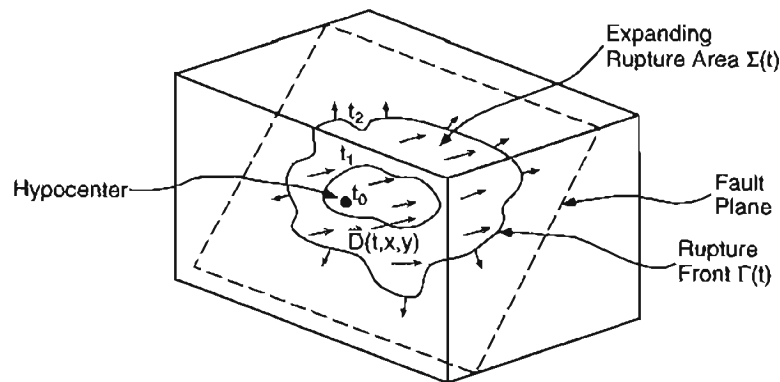


FIG. 5. General case of a spatially and temporally variable displacement field (interior vector field) associated with an expanding rupture front (peripheral vector field). (Lay and Wallace, 1995; reproduced with permission from *Modern Global Seismology*, © 1995 Academic Press)

eters is referred to as the *static* value. It is important to realize, however, that the time history of a particular source parameter during rupture may not be simple, as is often realized with stress drop (Fig. 6) (Yamashita, 1976; Dmowska and Rice, 1986). The lowest-order approximation is the equivalent body force representation of rupture as a point-source approximation involving a double-couple model (Fig. 7 right panel, Lay and Wallace, 1995). In more general terms, the point-source representation can be modeled by the complete seismic moment tensor. Under a moment tensor description, Ward (1982) notes that two of the six moment tensor ($M_{rr}, M_{r\theta}$) components dominate far-field tsunami excitation for large events. Also, the scalar seismic moment is related to the average source parameters by the following relationship:

$$M_0 = \mu \bar{D} A,$$

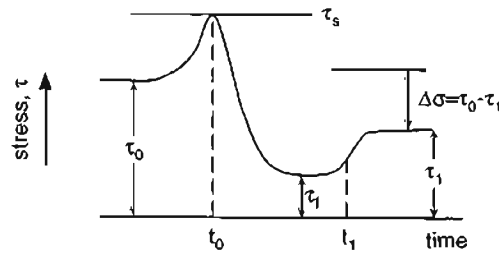


FIG. 6. Diagram of shear stress evolution at a point along the fault during rupture. τ_0 , τ_1 , τ_f , and τ_s are the initial, final, failure, and dynamic stress, respectively. $\Delta\sigma$ is the static stress drop. (Lay and Wallace, 1995, after Yamashita, 1976; reproduced with permission from *Modern Global Seismology*, © 1995 Academic Press)

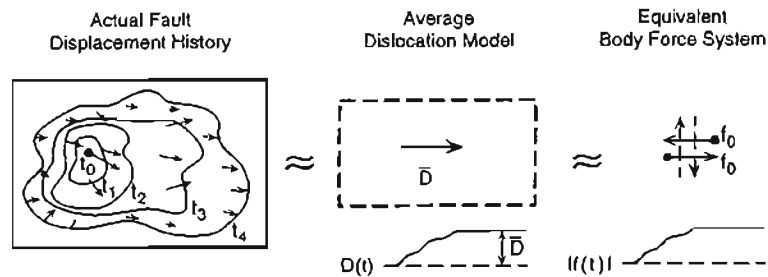


FIG. 7. Two levels of approximation (middle and right panels) to the generalized vector displacement field (left panel). (Lay and Wallace, 1995; reproduced with permission from *Modern Global Seismology*, © 1995 Academic Press)

where μ is the shear modulus, \bar{D} is the average slip, and A is the area of rupture. The moment magnitude scale introduced by Kanamori (1977) is related to the scalar seismic moment by the following relationship:

$$M_w = \frac{2}{3} \log M_0 - 10.73.$$

Intermediate between a point source and full source representation, an average (Volterra) dislocation model (Fig. 7 middle panel) is often used for seismic wavelengths greater than the fault dimensions. Because the temporal resolution of seismic observations is often less than the rupture duration (i.e., the seismic propagation velocities α, β are greater than the rupture velocity v_r), the time history of the spatially averaged source parameters (A, \bar{D}, v_r , rake, and rupture azimuth) can be determined from seismic observations.

Complementary to temporal resolution of rupture from seismic observations, tsunami data can yield spatial resolution of the rupture process (Satake, 1987). Because the propagation velocity is much lower for tsunamis than for seismic waves, different phases relating to the rupture process will be spatially separated on tide gauge records (Satake, 1987). Conversely, the observation of large spatial variation in source parameters from near-source seismic modeling of earthquakes (Beroza, 1995) therefore suggests that local tsunami run-up is importantly affected by spatial heterogeneity in source processes. In this section, how the average static source parameters of an earthquake affect tsunami generation is demonstrated. Section 5.1 discusses how tsunamis are affected by the geometry of the rupture zone. In sections 5.2 and 5.3 the effect that the static parameters of rupture (slip magnitude and direction) have on tsunamis is investigated. Finally, in sections 5.4 and 5.5 the effect that physical parameters and secondary faulting, respectively, have on tsunamis is addressed. Where applicable, the factors that control each source parameter from earthquake mechanics are first discussed, followed by how the source parameter affects the local tsunami. In particular, how variations in source parameters affect local tsunami run-up is established following the versatile N-wave run-up model recently formulated by Tadepalli and Synolakis (1994a). The two sections that follow discuss how spatial variations (Section 6) and temporal variations for slow earthquakes (Section 7) affect local tsunamis, progressing closer to a full source representation (Fig. 5).

Consider the geometry shown in Fig. 8, where the depth (z_1) is defined as the depth to the top of the rupture zone. The resulting seafloor displacement profile can be described by the amplitudes of the local extrema ($u_{z(\max)}$ and $u_{z(\min 1)}, u_{z(\min 2)}$, respectively) and distances that the local minima occur from the central maximum, defined as X_1 and X_2 . In

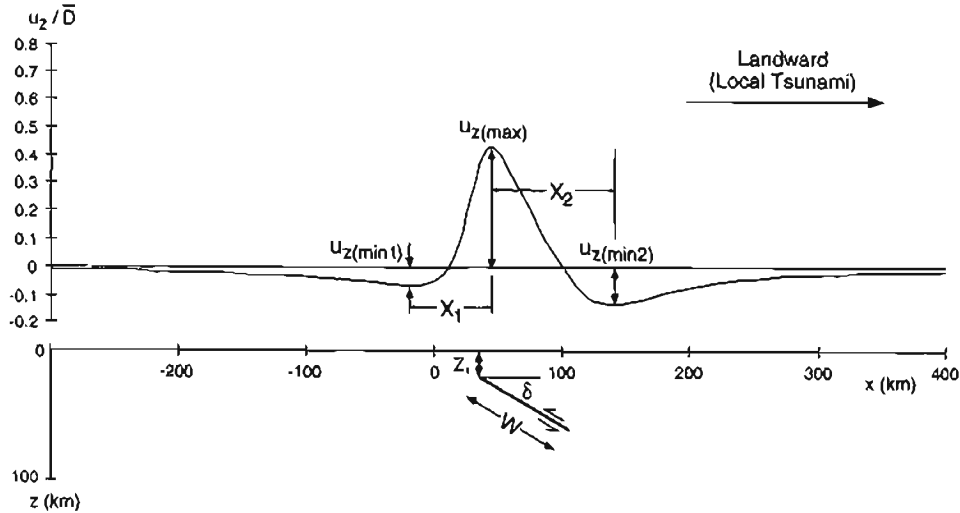


FIG. 8. Geometric source parameters in the $x-z$ plane and nomenclature describing vertical displacement of the seafloor and the initial tsunami waveform. Geometric source parameters include: z_1 , top of rupture zone; W , width of the fault zone; and δ dip of the fault.

this way, the effect that earthquake source parameters have on seafloor displacement can be related to the phenomenology of N-wave run-up described by Tadepalli and Synolakis (1994a). To do this, I am implicitly working under the following two conditions: (1) Only broadside run-up is being examined in which the point of run-up is alongside the source region. The component of the tsunami wavefield that involves the computation of edge waves is neglected (Carrier, 1995). (2) For comparative purposes the simple case of constant slope applicable to run-up laws is assumed, recognizing that the exact transformation is specific to the regional bathymetry. (It should be noted that run-up laws can be applied to a composite bathymetry approximated by sloping segments; S. Tadepalli, personal communication, 1996). In addition, the approximation of a tsunami waveform with N-waves ignores the trailing trough for typical landward-dipping faults of subduction zones ($u_{z(\min 1)}$, Fig. 8). However, by obtaining a best fit with the leading slope and leading extrema amplitude ($u_{z(\max)}$ and $u_{z(\min 2)}$, Fig. 8), the essential elements of the dynamics of run-up are captured (Togashi, 1983; Tadepalli and Synolakis, 1994a). The generalized N-wave form is

$$\eta(x)|_{t=0} = (\varepsilon H)(x - X_a) \operatorname{sech}^2[\gamma_s(x - X_b)], \quad (1)$$

where $\gamma_s = \sqrt{\frac{3}{4}H}$ controls the effective wavelength, $X_b - X_o$ controls the relative amplitude between the leading depression and the central peak, and εH controls the absolute amplitude. The maximum run-up normalized with respect to a reference depth is given by

$$R = 2.831 \varepsilon \sqrt{\cot \beta} H^{5/4} [|X_o - X_b - 0.366/\gamma_s| + 0.618/\gamma_s]. \quad (2)$$

Because both R and H are nondimensionalized with respect to a reference water depth (h_0), Green's law $\hat{R} \propto h_0^{-1/4}$ is evident in the foregoing run-up law. The relationship between maximum run-up and the other parameters specified for the seafloor displacement profile are indicated in Fig. 9. Specifying the wave steepness as $\tan^{-1}(H_0/X_2)$, where H_0 is a reference wave height, the maximum run-up is approximately linearly proportional to wave steepness, except for very broad waves. The interesting dynamics of N-waves is illustrated in Fig. 9b. Here, note that the maximum run-up is dependent on the amplitude of the central peak relative to the leading depression (equivalent to $u_{z(\max)}/u_{z(\min 2)}$ if the reduction in amplitude for both phases is the same when the tsunami leaves the source region). For the specific case of isosceles N-waves, in which the central peak and leading depression amplitudes are equal, Tadepalli and Synolakis (1994a) demonstrate that the maximum run-up is greater than that for solitary waves, according to the ratio

$$\frac{R|_{N\text{-wave}}}{R|_{\text{solitary wave}}} = 1.364.$$

5.1. Fault Geometry

5.1.1. Source Depth

Onset of rupture is constrained by frictional stability transitions, as discussed by Scholz (1989; 1990). The upper stability transition, which defines the minimum depth for earthquake initiation, is controlled by the level of normal stress on the fault and the velocity-strengthening behavior of fault gouge at shallow levels (Marone and Scholz, 1988). In addition, lithologic changes may affect the upper stability transition (e.g., consolidation of fault gouge, Scholz, 1990). It is important to note that although the bulk mechanical properties of accretionary wedge rocks may indicate a regime where brittle failure would not occur, it is the mechanical properties (specifically, pore pressure) of the shear zone within such a regime that dictates the occurrence of unstable slip (Zhang *et al.*, 1993). The lower

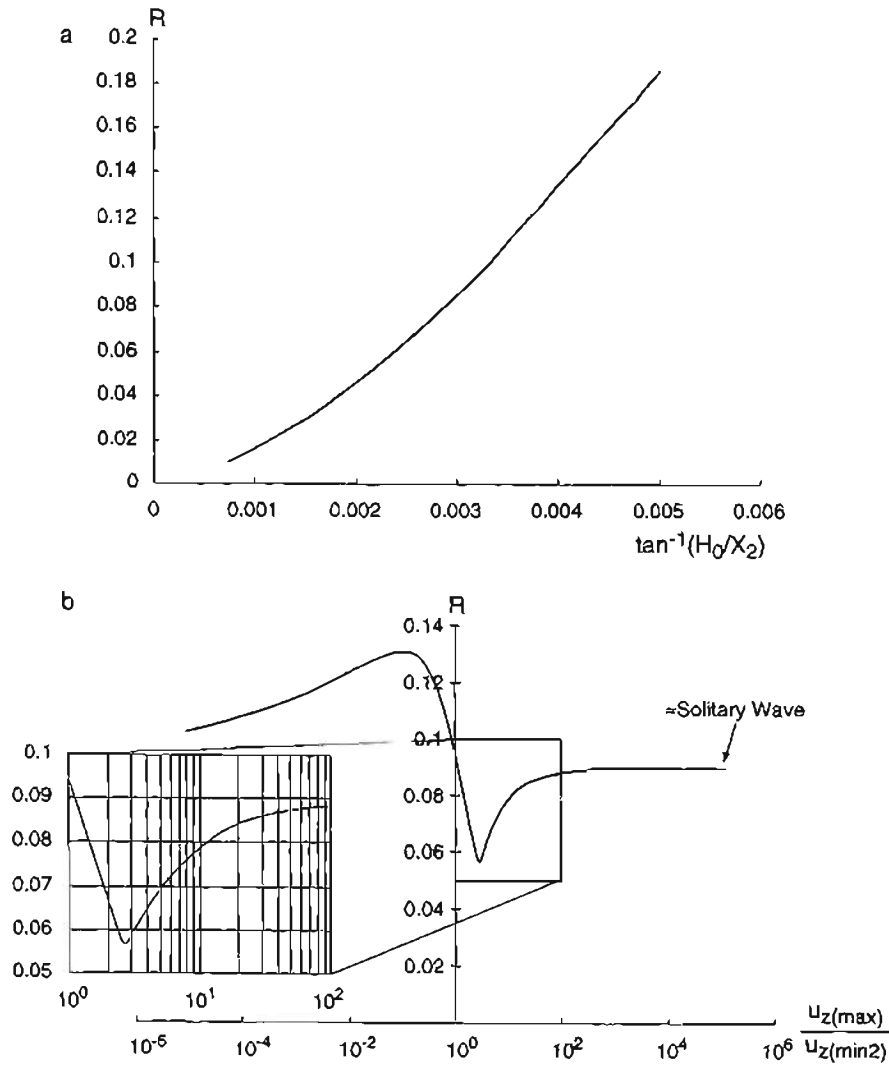


FIG. 9. Variation of maximum non-dimensional run-up (R) based on the N-wave run-up law of Tadepalli and Synolakis (1994a) with respect to the following parameters: (a) wave steepness as measured by $\tan^{-1}(H_0/X_2)$, where H_0 is the wave height from the leading depression to the central peak (held constant at 0.04); (b) amplitude ratio between the central peak and the leading depression (H in Eq. (1) held constant to approximate constant leading wave steepness).

stability transition, which defines the maximum depth of earthquake nucleation (i.e., the base of the seismogenic zone), is controlled by the onset of the brittle-plastic transition at depth. The brittle-plastic transition itself is determined by the rock type and temperature. Typically, 300°C is taken as the temperature coincident with lower stability transition (see analysis by Tse and Rice, 1986). Large earthquakes typically initiate near the lower stability transition, where the magnitude of frictional instability is greatest (Das and Scholz, 1983).

The primary effect of increasing the depth of rupture, here defined as the depth to the top of the rupture zone z_1 , is a decrease in the amplitude of the seafloor displacement and resulting initial tsunami waveform (Fig. 10b). In Fig. 10 and the figures that follow, other source parameters are held constant at values typical for interplate subduction zone earthquakes (Table 2). Kajiura (1981) also notes that the decrease in tsunami

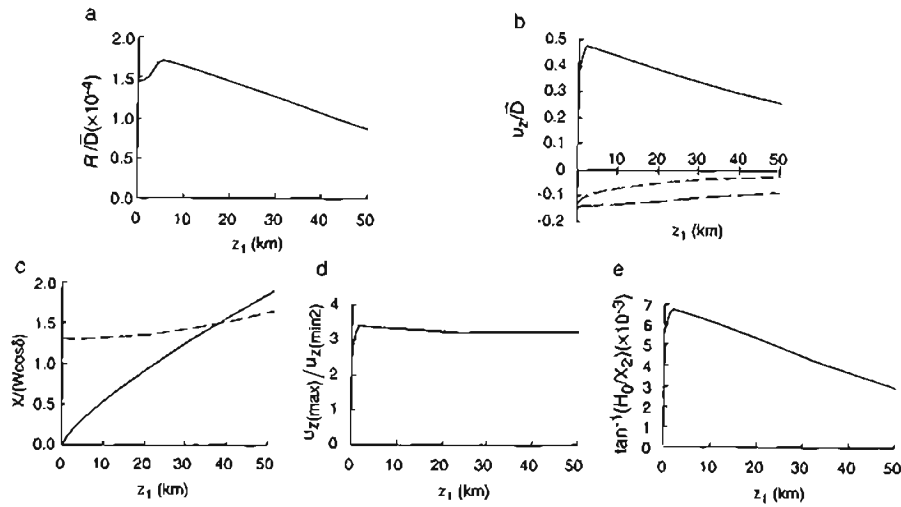


FIG. 10. Effect of varying the depth to the top of the rupture zone (z_1) on local run-up and characteristic parameters of the initial waveform (see Fig. 8). Other geometric source parameters held constant: $\delta = 30^\circ$, $W = 80$ km, $L = 200$ km. (a) Normalized maximum run-up calculated from an N-wave approximation to the initial tsunami waveforms. For this figure and others that follow, a beach slope angle (β) of 10° and a reference water depth of 2 km are used to illustrate the relative effect of source depth on run-up. Absolute maximum run-up is dependent on the particular bathymetric parameters and a breaking criterion specified by Tadepalli and Synolakis (1994a). (b) Amplitude of local extrema normalized by the average amount of slip during rupture. Solid line is $u_{z(max)}$; short-dashed line is $u_{z(min 1)}$; long-dashed line is $u_{z(min 2)}$. (c) Distance from central maximum to local minima, normalized by surface-projected width. Solid line is X_1 , dashed line is X_2 . (d) Ratio of amplitude of central maximum to leading minimum. (e) Leading wave steepness.

TABLE 2. CRITICAL TSUNAMI SOURCE PARAMETERS FOR LARGE, SHALLOW SUBDUCTION ZONE EARTHQUAKES FOR WHICH SLIP VALUES HAVE BEEN DETERMINED^a

Region	Date	M_0 (10^{20} N - M)	M_w	Average slip (m)	Maximum slip (m)	Length (km)	Width (km)	Reference
Alaska	11/10/38	20.	8.2	1.1	3.3	300	150	Johnson and Satake (1994)
Ecuador	5/14/42	7	7.9	1.2	8.5	200	90	Swenson and Beck
Tonankai	12/7/44	20	8.2	0.8	1.6	270	180	Satake (1993)
Nankaido	12/20/46	39.	8.4	1.3	2.4	360	180	Satake (1993)
Aleutian	3/9/57	88.	8.6	1.7	7.0	1100	150	Johnson and Satake (1993)
Colombia	1/19/58	5.2	7.8	2.3		100	60	Kanamori and Given (1981)
Chile	5/22/60	2700.	9.6	20.3	54.0	920	300	Linde and Silver (1989)
Alaska	3/28/64	630.	9.2	8.6	18.0	500	300	Johnson <i>et al.</i> (1996)
Rat Islands	2/4/65	140.	8.7	7.5	12.0	600	60	Beck and Christensen (1991)
New Hebrides	8/11/65	3.	7.6	1.5		100	50	Ebel (1980)
Middle America	8/23/65	1.7	7.5	0.7		105	47	Chael and Stewart (1982)
Peru	10/17/66	2.	7.5	2.6		140	80	Abe (1972)
Kyushu	4/1/68	1.8	7.5	1.6		56	32	Shono <i>et al.</i> (1976)
Honshu	5/16/68	28.	8.3	4.1		150	100	Kanamori (1971)
Kurile	8/11/69	22.	8.2	2.9		180	85	Abe (1973)
Solomon Islands	7/14/71	12.	8.0	1.3		200	70	Lay and Kanamori (1980)
Hokkaido	6/17/73	6.7	7.9	1.6		100	60	Shimazaki (1974)
Peru	10/3/74	15.	8.1	3.0	7.0	240	40	Beck and Ruff (1989)
Mindanao	8/16/76	19.	8.2	3.0		160	80	Stewart and Cohn (1979)
Middle America	3/14/79	1.5	7.4	0.6 ^b	1.2	80	80	Mendoza (1995)
Colombia	12/12/79	29.	8.3	2.7	5.8	230	100	Beck and Ruff (1984)
Middle America	10/25/81	0.7	7.2	0.6 ^b	3.6	50	60	Mendoza (1993)
Chile	3/3/85	15	8.1	1.6 ^b	2.9	200	120	Mendoza <i>et al.</i> (1994)
Middle America	9/19/85	15.	8.1	1.4 ^b	6.5	180	150	Mendoza and Hartzell (1989)
Middle America	9/21/85	1.4	7.4	0.7 ^b	2.0	70	70	Mendoza (1993)
Andreanof	5/7/86	13.	8.0	1.8	4.5 ^c	220	65	Hwang and Kanamori (1986)

^a Updated from compilation by Lay *et al.* (1982). Does not include tsunami earthquakes (Table 3).

^b Calculated assuming $\mu = 4 \times 10^{10}$ Pa.

^c Furumoto (1991).

energy with depth is greater for smaller rupture dimensions. In addition, the surface displacement profile is broader with increasing depth, such that the leading wave steepness decreases (Fig. 10c,e). The combined influence of decreasing extrema amplitude and leading wave steepness with source depth results in a concomitant decrease in normalized maximum run-up (Fig. 10a). The ratio between the central peak and the leading depression remains approximately constant with increasing depth. All of the parameters shown in Fig. 10 indicate that the coseismic displacement field is different if the rupture extends the surface, such that a local maximum of tsunami amplitude exists if one were to examine only variations in depth. Yamashita and Sato (1974) and Kajiura (1981), also noting an "optimal focal depth" for tsunami generation, indicate that for large fault dimensions or large dip angles, the optimal depth is essentially at the surface. It is also important to consider, however, dramatic changes in slip that accompany surface rupture, indicated by fault mechanic models (Section 8.3), in addition to the depth dependence of vertical displacement derived here and by Yamashita and Sato (1974) and Kajiura (1981).

5.1.2. Width and Length

Whereas the onset of rupture is limited by the upper and lower stability transitions, for large earthquakes the rupture zone may dynamically transgress the stability transitions and extend to the free surface (i.e., the seafloor for tsunamigenic events) or to the lower limit of the brittle-plastic transition (Scholz, 1989). This maximum width is termed the width of the "schizosphere" by Scholz (1990). A distinction between large and small earthquakes is made by Scholz (1990) based on the width of the rupture zone in comparison to the thickness of the schizosphere (z_s). Small earthquakes are those in which the length and width dimensions of rupture are comparable and $W \leq z_s/\sin \delta$. In contrast, for large earthquakes the width of rupture will "saturate" at $W = z_s/\sin \delta$, and the length of rupture can increase for larger earthquakes, with an attendant increase in the aspect ratio of the rupture zone.

The cessation of rupture, which determines the final dimensions of the rupture zone (specifically, the length of rupture for large earthquakes that rupture the entire schizosphere), can be affected dynamically or by the geometry and material properties of the fault zone. Heaton (1990) proposed a self-healing model in which slip and velocity-dependent friction is assumed, with the effect that a self-healing slip pulse is generated during rupture. Alternatively, rupture can be arrested by both strength barriers and relaxation barriers (Lay and Wallace, 1995). Barriers are defined as regions along the fault plate resistant to dynamic slip (Das and Aki, 1977;

Das and Scholz, 1981). Both strength barriers and relaxation barriers can be caused by both geometric and material heterogeneity along the fault zone. Boatwright and Cocco (1996) note that the driving stress for dynamic rupture decreases with distance and that rupture into a velocity-strengthening or slightly velocity-weakening regime leads to rupture arrest. Such frictional regimes can therefore act as barriers. Also, however, barriers can arise from residual changes in the initial static stress field from the last earthquake cycle. For example, relaxation barriers can result from regions of high slip during the last coseismic phase (e.g., Mendoza, 1993) or aseismic creep during the preceding interseismic phase (Lay and Wallace, 1995). Finally, rupture length can also be affected by the complex interaction between adjacent asperities (Ruff, 1992) or earthquake quanta (Rydelek and Sacks, 1996).

To examine the effect that the rupture dimensions have on tsunami generation, we examine two cases: (1) the length and width of the rupture zone are equal and range from 10 to 200 km; and (2) the length and width of the rupture zone are equal from 10 to 80 km, beyond which the width of the rupture zone remains fixed at 80 km as the rupture zone increases in length from 80 to 200 km. The latter case is intended to represent rupture of the entire schizosphere 10 km below the surface (i.e., z_1 remains constant at 10 km). For each case, the surface profile is calculated in the center of the rupture zone at $y = L/2$. Little difference in the amplitude of the extrema is noted for these two cases (Fig. 11b). As one might expect, if W is limited to 80 km, X_2 will also be limited (Fig. 11c). Accordingly, this limits the decrease in leading wave steepness with increasing rupture length (Fig. 11e). The amplitude of the vertical displacement of the seafloor increases substantially with increasing rupture dimension for rupture zones less than 50 km in dimension (Fig. 11b).

The relationship between source dimensions and normalized run-up (Fig. 11a) is more complex than for the case of source depth (Fig. 10a). The origin of this complexity is the competing influence of (1) increasing extrema amplitude with rupture dimension (Fig. 11b) and (2) decreasing leading wave steepness with increasing rupture dimension (Fig. 11e). The result is that a local maximum of run-up with respect to rupture dimension is apparent in Fig. 11a. For small ruptures, the relationship between rupture dimensions and the characteristic parameters of the initial tsunami waveform appears to change at a point where the rupture dimension is approximately equal to the source depth (z_1). For large ruptures, fixing the fault width is equivalent to increasing the aspect ratio (L/W) with increasing L . Yamashita and Sato (1974) also note an increase in tsunami amplitude with increasing aspect ratio (L/W). Not included in the foregoing analysis, however, is the fact the slip most likely scales with the

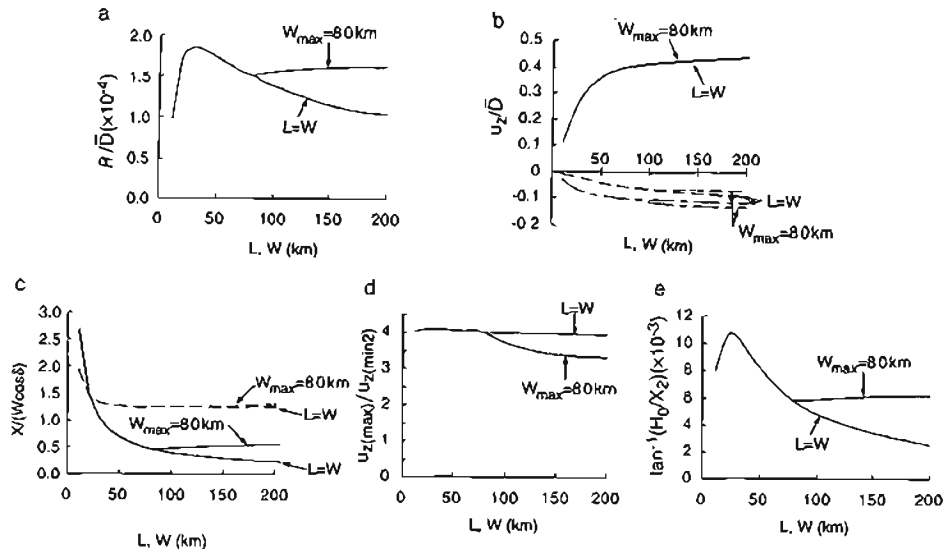


FIG. 11. Effect of varying the dimensions of the rupture zone on local run-up and characteristic parameters of the initial waveform (see Fig. 8). Two cases are considered: (1) both width and length increase from 10 to 200 km, and (2) width increase limited to a maximum of 80 km, whereas length increases from 10 to 200 km. Other geometric source parameters held constant: $\delta = 30^\circ$, $z_1 = 10$ km. (a) Normalized maximum run-up calculated from an N-wave approximation to the initial tsunami waveforms. Run-up parameters described in Fig. 10a. (b) Amplitude of local extrema normalized with respect to the average amount of slip during rupture. Solid line is $u_{z(\max)}$; short-dashed line is $u_{z(\min 1)}$; long-dashed line is $u_{z(\min 2)}$. (c) Distance from central maximum to local minima normalized by surface-projected width. Solid line is X_1 , dashed line is X_2 . (d) Ratio of amplitude of central maximum to leading minimum. (e) Leading wave steepness.

dimensions of the rupture zone, thereby increasing the amplitude and run-up of the generated tsunami (discussed in Section 5-2).

For small rupture zones with dimensions less than approximately three times the water depth, the assumption that the vertical seafloor displacement and the initial tsunami waveform are identical is probably not valid (Kajiura, 1963; 1981). For these small ruptures, the long-wave assumption for propagation also becomes invalid (Satake, 1987). Because the tsunamis generated from such small ruptures are likely to be insignificant, the effect of the validity of these assumptions is not pursued here. An additional phenomenon with decreasing the width of the fault zone, shown by Carrier (1971), is that frequency dispersion becomes increasingly important during propagation. It should be emphasized that for a fixed location along the shoreline that is not across from the rupture area (i.e., nonbroadside run-up), the relationship between run-up and source parameters is more

complex (Carrier, 1995) and is especially dependent on the closest distance between the run-up location and the rupture area (thus, the length of the rupture zone).

5.1.3. Dip

Unlike the preceding parameters, the dip of the fault is a permanent feature of the fault and can be determined from focal mechanism solutions, well-defined locations of aftershocks, and controlled seismic reflection and refraction experiments. The interplate thrust of subduction zones dips on average $25^\circ \pm 9^\circ$ at seismogenic depths and approximately $20^\circ \pm 8^\circ$ closer to the trench (Jarrard, 1986). The effect of fault dip on parameters describing the surface displacement profile is shown in Fig. 12. Interestingly, as also noted by Kajiura (1981), there is a maximum in the amplitude of the central peak phase at about $\delta = 50^\circ$ (Fig. 12b). Note also that the amplitude of the leading depression decreases to zero with increasing dip, increasing the ratio of extrema amplitudes to infinity (Fig. 12d). Because of

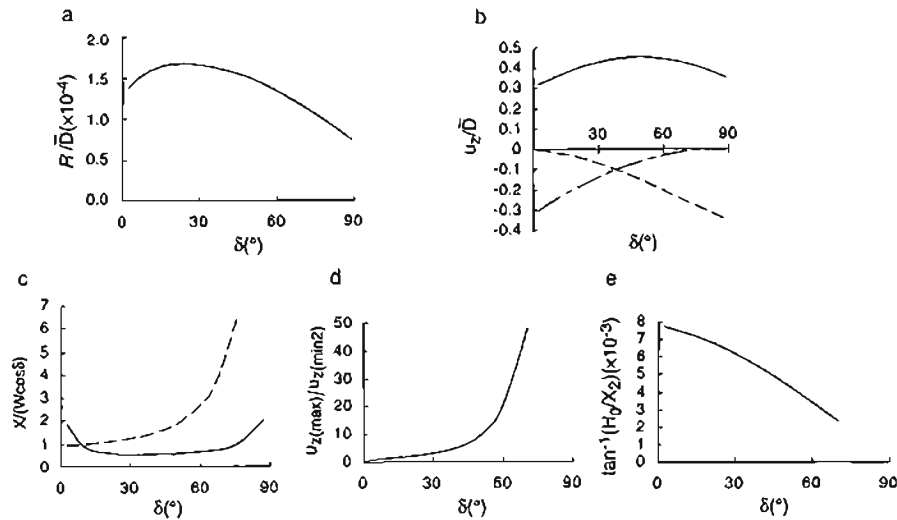


FIG. 12. Effect of varying the dip of the fault on local run-up and characteristic parameters of the initial waveform (see Fig. 8). Other geometric source parameters held constant: $z_1 = 10$ km, $W = 80$ km, $L = 200$ km. (a) Normalized maximum run-up calculated from an N-wave approximation to the initial tsunami waveforms. Run-up parameters described in Fig. 10a. (b) Amplitude of local extrema normalized with respect to the average amount of slip during rupture. Solid line is $u_{z(max)}$; short-dashed line is $u_{z(min1)}$; long-dashed line is $u_{z(min2)}$. (c) Distance from central maximum to local minima normalized by surface-projected width. Solid line is X_1 , dashed line is X_2 . (d) Ratio of amplitude of central maximum to leading minimum. (e) Leading wave steepness.

this, $\tan^{-1}(H_0/X_2)$ becomes a poor measure of leading wave steepness at high dip angles. The trend, though, is a reduction in the leading wave steepness with increasing dip (Fig. 12d), perhaps contrary to intuition. As with the effect associated with rupture dimensions (Fig. 11a), the competing influence of increasing extrema amplitude at low dips and decreasing leading wave steepness results in a normalized run-up maximum with respect to dip (Fig. 12a) skewed toward lower dip angles than one would surmise from Fig. 12b. Coincidentally, the optimal dip angles associated with maximum run-up (20° – 30°) are approximately the same as the average dip of interplate thrusts cataloged by Jarrard (1986).

5.2. Fault Slip

In determining the effect that fault slip has on local tsunamis, we first examine how average slip affects tsunami amplitude. Thus, for the purpose of discussion in this section, constant fault slip (i.e., Volterra dislocation) is assumed (as represented in the middle panel of Fig. 7). As a precaution, note that nonuniform slip distributions significantly change the tsunami waveform, as discussed in Sections 6.1 and 8.3 and in Geist and Dmowska (in prep.).

5.2.1. Slip Laws

Simple models describing the amount of earthquake slip at a point along a fault can be formulated if either the initial or the final stress is assumed to be constant over many earthquake cycles, as described by Shimazaki and Nakata (1980). If both stress limits are constant over time, earthquakes would occur periodically with a fixed amount of slip. If only the final (minimum) stress is constant, then slip (but not the time interval between earthquakes) can be predicted, resulting in a slip-predictable model. Conversely, a time-predictable model is one in which the time interval (but not the amount of slip) can be predicted and assumes that the failure (maximum) stress is constant for each earthquake cycle. Another way of envisioning earthquake recurrence and slip is the characteristic earthquake model, in which the distribution of slip and rupture length is consistent from cycle to cycle (Schwartz and Coppersmith, 1984; Wesnousky, 1994). Unfortunately, analysis of multiple earthquake cycles along circum-Pacific subduction zones by Thatcher (1990) indicates that average slip may be irregular, probably as a result of a heterogeneous and transient stress field, and may not follow strictly any of the ideal models just described.

Another approach is to use empirically derived scaling laws to estimate the average slip given other source parameters of the rupture. Two scaling laws currently offered for large earthquakes are the L-model, in which slip scales with the length of the rupture (Scholz, 1982, 1994; Cowie and Scholz, 1992a, b), and the W-model, in which slip scales with the width of the rupture (Romanowicz and Rundle, 1993; Okal and Romanowicz, 1994). Although it is beyond the scope of this chapter to assess critically the validity of these models, theoretical studies (e.g., Das, 1988; Yin and Rogers, 1996) suggest a hybrid scaling law in which slip increases with length (and width for $W_c < z_s/\sin \delta$) up to a crossover length that is many times W_c . Beyond this crossover length, slip asymptotically approaches a constant value termed by Das (1988) as the static two-dimensional ($L = \infty$) value.

Lay *et al.*'s (1982) catalog of average slip values and source dimensions of subduction zone earthquakes is updated (Table 2), using results from recently published papers. For these subduction zone events, there is poor correlation (correlation coefficient < 0.5) between average slip and either the length or the width of the fault zone. The poor correlation between slip and the dimensions of the rupture zone is also noted by Wells and Coppersmith (1994) for non-subduction zone, reverse-slip events. Because W_c is effectively dependent on the thermal structure of the subduction zone, the crossover length for the hybrid scaling law varies among subduction zones. This may explain the great variability for a global dataset in scaling between rupture dimension and slip. Scholz (1982) and Wells and Coppersmith (1994) note that the correlation between slip and length of the rupture zone is significantly better for strike-slip events.

Other factors that affect the overall slip along a fault include an inverse dependence on the shear modulus (μ) and whether or not rupture propagates to the surface. For the former factor, μ is dependent on the rock type surrounding the fault zone and specifically on whether or not sediment deposited on the down-going plate is being subducted or accreted (Kanamori and Kikuchi, 1993). For the latter factor, mean slip is approximately twice that for imbedded rupture (Knopoff, 1958; Boore and Dunbar, 1977; Shimazaki, 1986), providing an explanation for the higher mean slip associated with shallow tsunami earthquakes.

5.2.2. Effect on Tsunami Generation

Holding all other parameters constant, the amplitude of seafloor displacement is linearly proportional to the magnitude of slip. Furthermore, the phase characteristics of the initial tsunami waveform are unaffected with respect to changes in average slip. One can notice for the N -wave

run-up law (equation 5.1-2) that the relationship between the amplitude of the incident wave and maximum run-up is not a linear one ($R \propto H^{5/4}$). (Here, remember that $u_{z(\max)} \neq H$ in that the initial tsunami amplitude is reduced by approximately half as it leaves the source region.) The same proportionality is applicable for solitary waves (Synolakis, 1987). For monochromatic waves and other pulse perturbations (Table 1), the relationship between maximum run-up and incident wave amplitude is linear (Goto and Shuto, 1983; Togashi, 1983; Pelinovsky and Mazova, 1992). Recall too that run-up laws are limited to nonbreaking waves. Laboratory studies by Synolakis (1987) indicate a separate run-up regime for breaking waves that also conform to an approximately linear relationship between run-up and incident wave amplitude. This study indicates that the constant of proportionality is different for nonbreaking and breaking wave regimes.

Results so far confirm that, for local tsunamis, only earthquakes greater than a certain magnitude can generate a significant local tsunami. Such an inference has also been established for far-field tsunamis under normal-mode theory (Ward, 1980; Okal, 1988). Two relationships combine to explain the ineffectiveness of small earthquakes in generating local tsunamis: (1) for smaller earthquakes that do not rupture the entire schizosphere, slip scales with the characteristic dimension of the rupture zone; and (2) independent of slip, variation of the length or width of the rupture zone has a large effect on tsunami generation and run-up for rupture dimensions less than 50 km (Fig. 11a, b). Earthquakes less than magnitude 6 do not, with few exceptions, generate significant tsunamis, either locally or at far-field distances (see catalog of Lockridge and Smith, 1984).

5.3. Slip Direction

5.3.1. Mechanical Constraints

The rake angle (Fig. 13) of the slip vector for compressional tectonic regimes (either subduction zones or transpressional strike-slip margins) is dependent on the orientation of relative plate convergence and the dip angle of the fault. The rake angle shown in Fig. 13 is measured from the strike direction in the plane of the fault. The rake angle (λ) is related to the horizontal convergence direction (θ) and the dip of the fault (δ) by the following relationship (Michael, 1990):

$$\lambda = \tan^{-1} \left[\frac{\tan(\theta)}{\cos(\delta)} \right].$$

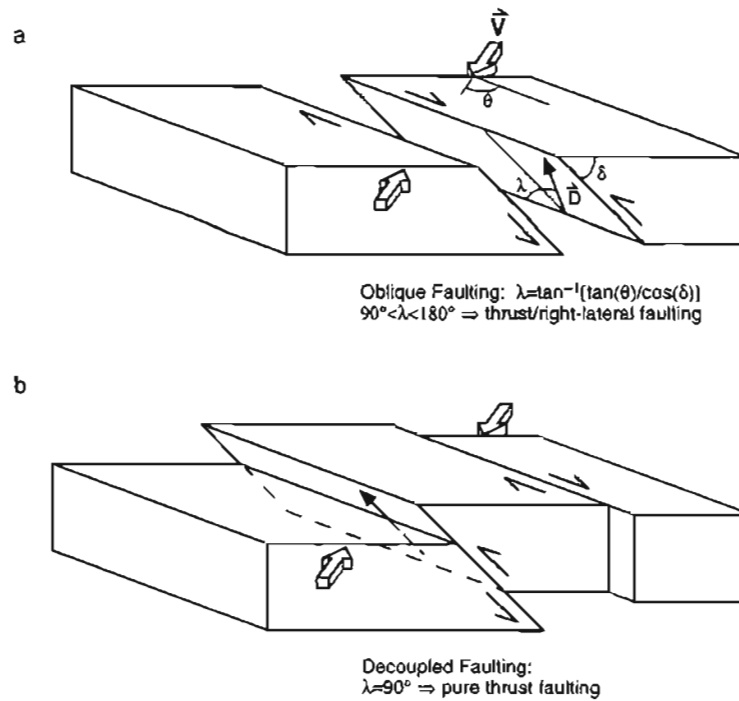


FIG. 13. Geometry of faulting in an oblique compressional regime. \bar{D} and \bar{V} represent the dislocation and relative plate convergence vectors, respectively. Two end-member cases: (a) oblique faulting—single event accommodates both strike-slip and dip-slip components of motion; (b) decoupled faulting—oblique motion accommodated by separate dip-slip and strike-slip events. Based on energy minimization arguments (Michael, 1990), the conditions for either oblique or decoupled faulting are dependent on the obliquity of relative plate motion (θ) and dip of the thrust fault (δ) (Fig. 14). Analysis of slip vectors from subduction thrust events indicate that for obliquity greater than a critical value (θ_{crit}), an intermediate state (partially decoupled faulting) occurs in which $90^\circ > \lambda > \tan^{-1}(\tan \theta / \cos \delta)$ (McCaffrey, 1992).

Except for the unique case in which the convergence direction is exactly normal to the plate boundary fault, two end-member cases for oblique compressional motion are possible: (1) oblique motion on a single fault (termed *oblique faulting*); or (2) two separate faults that accommodate the normal and parallel components of motion separately (termed *decoupled faulting*). The study by Michael (1990) examines the conditions by which either of these cases may occur. Based on arguments relating to the minimization of the conversion of potential energy to kinetic energy (earthquakes), a “crossover” dip (δ_c) exists in which for $\delta < \delta_c$ decoupled

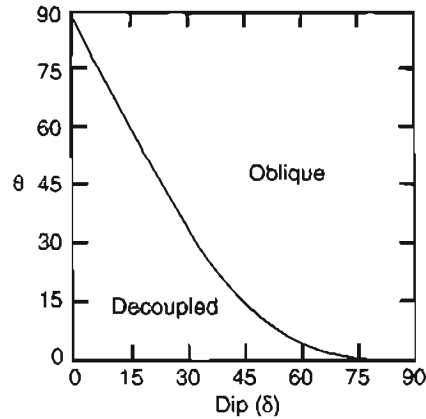


FIG. 14. Discrimination between decoupled and oblique faulting for $0^\circ \leq \delta$, $\theta \leq 90^\circ$ based on energy constraints (Michael, 1990). δ and θ as defined in Fig. 13. (Michael, 1990; reproduced from *Geophys. Res. Lett.*, American Geophysical Union)

faulting is more energy efficient and for $\delta > \delta_c$ oblique faulting is more energy efficient (Fig. 14). Michael (1990) also notes that the energy release for either oblique or decoupled faulting is very high as δ approaches 90° .

Complications to this formalism are introduced by variations in the strength (normal stress and coefficient of friction) between faults of a decoupled system (Jones and Wesnousky, 1992; McCaffrey, 1992) and cases in which distributed deformation rather than isolated faulting accommodates the margin-parallel component of oblique faulting (Geist and Scholl, 1992; McCaffrey, 1993). Compilations of slip vectors from interplate thrust earthquakes along oblique subduction zones indicate that complete decoupling is uncommon and that partial decoupling occurs only when the obliquity of relative plate convergence is greater than a critical value (θ_{crit} on the specific subduction zone, McCaffrey, 1992). For highly oblique transform systems (e.g., the San Andreas fault), complete decoupling is possible (e.g., the 1983 Coalinga earthquake, Michael, 1990).

5.3.2. Effect on Tsunami Generation

The effect that geometric parameters have on the seafloor displacement was examined in Section 5.1. These effects are for dip-slip dislocation along a fault. The vertical displacement field of an oblique slip event is the sum of the displacement fields derived from the dip-slip and strike-slip components (Fig. 15). The effect that the strike-slip component of disloca-

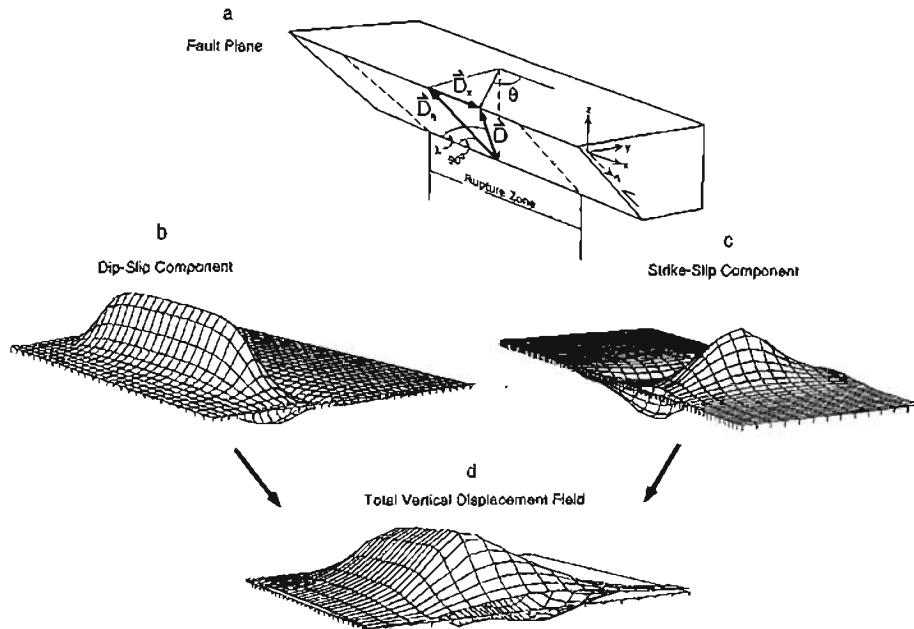


FIG. 15. Vertical surface displacement from oblique slip on a dipping fault. (a) Oblique slip is examined in terms of dip-slip \bar{D}_n and strike-slip components \bar{D}_x . Average slip acting on the entire area of the rupture zone (dashed lines) is considered for this example. (b) Vertical displacement caused by the dip-slip component. (c) Vertical displacement caused by the strike-slip component. (d) Total vertical displacement from oblique slip [sum of displacement fields shown in (b) and (c)].

tion has on the vertical displacement field is examined for a rectangular rupture zone using the analytical expressions derived by Okada (1985). Along-strike variation in the vertical displacement field is illustrated in Fig. 16 for different fault aspect ratios (L/W) and dips (δ). In general, the magnitude of the vertical displacement normalized with respect to slip components (i.e., u_z/\bar{D}_i , where $i = (n, x)$, Fig. 15) is less for the strike-slip component than for the dip slip component (see also Kajiura, 1981). Increasing the aspect ratio of the rupture zone results in increased separation between the uplift and subsidence phases of along-strike vertical displacement (Fig. 16a). As the fault dip decreases, the vertical displacement related to the strike-slip component of slip (\bar{D}_x) increases (Fig. 16b). Recall, however, that the conversion of potential to kinetic energy also increases for decreased fault dip, favoring conditions for decoupled faulting (Fig. 14; Michael, 1990). Kajiura (1981) examines changes in the integrated vertical displacement field from the combined influence of rake and dip angle, resulting in a continuous variation map of

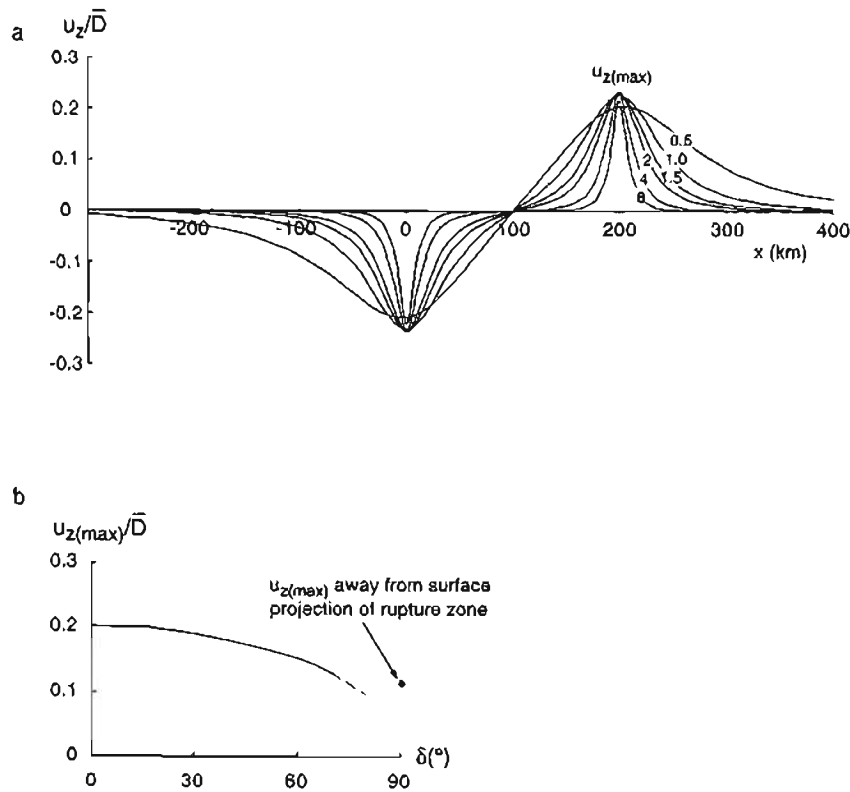


FIG. 16. Vertical seafloor displacement caused by strike-slip motion along a dipping fault. (a) Normalized vertical displacement along a strike-parallel profile centered over the rupture zone. Annotated curves represent different rupture zone aspect ratios in which the length of the rupture zone is held constant ($L = 200$ km). For each case, the depth to the up-dip extent of the rupture zone and the dip are held constant ($z_1 = -5$ km, $\delta = 30^\circ$, respectively). (b) Variation of the maximum normalized vertical displacement with respect to fault dip (δ). Aspect ratio and depth to the center of the rupture zone held constant ($L/W = 200$ km/50 km, $z_{cent} = -30$ km, respectively). For approximately $70^\circ < \delta \leq 90^\circ$, the regions of maximum vertical displacement are located outside of the surface projection of the rupture zone.

the end-member effects shown in both Figs. 12b and 16b. Of note, Kajiura (1981) shows that the increase in vertical displacement as λ increases from 0° to 90° is much greater for vertical faults than for horizontal faults.

5.3.3. Effect on Tsunami Propagation

Importantly, with respect to the length of shoreline inundated by a local tsunami, the vertical displacement resulting from the strike-slip component of oblique slip generates what I term as secondary wavefronts. Whether

the secondary wavefronts refract toward shore or toward the open ocean is dependent on the orientation of the Mode III rupture fronts relative to the bathymetric gradient. If an ideally linear rupture front is oriented counterclockwise from the bathymetric gradient, the secondary waves will be refracted toward shore. Conversely, if the linear rupture front is oriented clockwise from the bathymetric gradient, the secondary waves will refract away from the local shoreline. In nature, rupture fronts are often uneven and bathymetric gradients are laterally variable, resulting in refraction of the secondary wavefronts in both directions.

Refraction of highly oblique secondary waves can result in focusing of the tsunami during shoaling in addition to the Green's law amplification ($h^{-1/4}$) described previously. Consider the simple situation of a planar sloping beach profile and the incident angle of the wave ray (normal to the wavefront) α_0 (Fig. 17a). The ray paths from the toe of the slope to the shoreline are circular arcs in which the radius equals $\Delta x / \sin \alpha_0$ (Mei, 1983). Fig. 17b shows different ray paths for different incident angles. The shoreline-parallel distance (Δy) of the refracted ray path from the toe of the slope to the shoreline increases with α_0 . If we further consider a circular displacement (in the $x - y$ plane) of the seafloor (as in Momi, 1964) at the toe of the slope, the ray paths would initially be equidirectional, resulting in a circular radiation pattern. As a result of refraction, the tsunami at the shoreline would be focused within the $(\pm \pi/4)$ region about the x axis (Fig. 17c). Conversely, a circular displacement at the shoreline would result in defocusing of the tsunami away from the x -axis. The actual tsunami radiation pattern from an oblique slip event is complex, tending toward a four-lobe pattern with increasing obliquity (Ben-Menahem and Rosenman, 1972; Ward, 1982). In general, though, the effective radiation pattern at the shoreline is focused toward an axis coincident with the bathymetric gradient in comparison to the radiation pattern at the source. This effect is incorporated by Abe (1973) by using a refraction coefficient determined from a refraction diagram. As noted by Kajiura (1981), if the depth variations over one wavelength are not small, a simplified analysis such as this may not be valid. In addition, refraction-related focusing may subsequently be attenuated by effects such as diffraction, scattering, and wave trapping. For this reason, numerical techniques to simulate the propagation of oblique local tsunamis, as in Geist and Yoshioka (1996), are preferred (Kajiura, 1981).

5.4. Physical Properties

In the expressions for surface displacement due to faulting of a homogeneous half-space (Okada, 1985), the third term on the right-hand side of

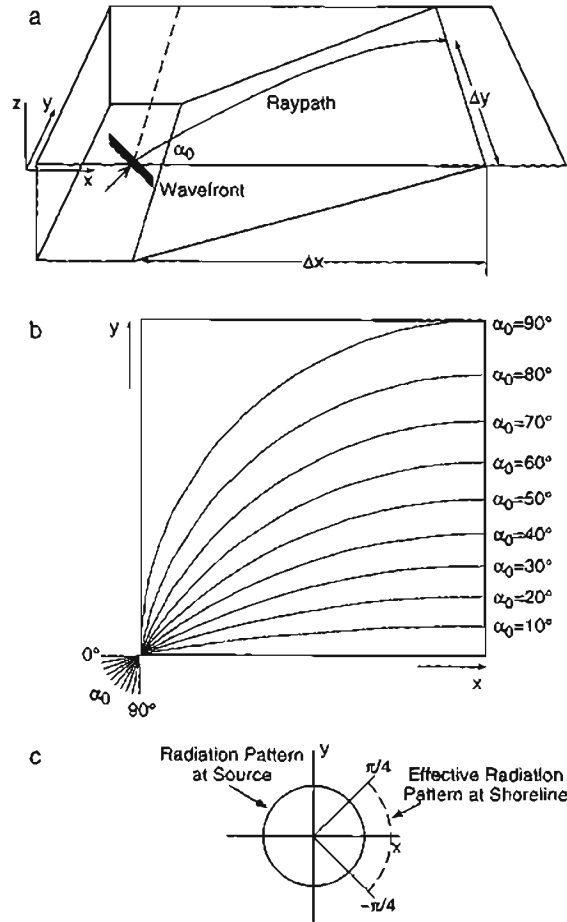


FIG. 17. Refraction of obliquely incident waves, such as secondary wavefronts generated by oblique slip events. (a) Simple example of refraction across a planar sloping water bottom. Incident angle (α_0) measured from the x axis. (b) Resulting circular ray paths for different incident angles, as described by Mei (1983). (c) For an equidirectional (circular) seafloor displacement at the toe of the slope, a shoreward-propagating tsunami is focused to within $\pm \pi/4$. Without considering edge waves and scattering, direct waves are not propagated in the range of source-target directions (θ) $\pi/4 < \|\theta\| < \pi/2$ under ideal conditions described in (a).

Eqs. (4) and (6) (in the Appendix to this chapter) involves the physical properties of the medium. Namely, the coefficient for this term is

$$\frac{\mu}{\lambda + \mu} \quad \text{or} \quad 1 - 2\nu,$$

where μ and λ are the Lamé constants (μ is the shear modulus) and ν is Poisson's ratio. Thus, for a homogeneous half-space, static surface displacement depends only on ν and not on μ (though slip itself is inversely related to μ). The term involving the physical parameters in the expressions for surface displacement is minor in comparison to the other two terms of Eqs. (4) and (6). For water-saturated sediment, ν can vary between 0.1 and 0.4, depending on saturation, porosity, and confining pressure (Gregory, 1976; O'Connell and Budiansky, 1977; Castagna *et al.*, 1985). With these values as extremes, the maximum seafloor displacement varies by approximately $\pm 10\%$ (Fig. 18). The ν -related variation is greatest for fault dips $\delta \approx 45^\circ$ and is zero for $\delta = 0^\circ, 90^\circ$ (Fig. 18; also noted by Okada, 1985).

Although surface displacement is independent of μ for a homogeneous half-space, previous researchers (most recently, Savage, 1987, and Ma and Kuszniir 1992, 1994) have noted that vertical inhomogeneity with respect to μ has a significant effect on the displacement field. Layering distinguished by variable μ is particularly relevant for subduction zones in which a lithologic interface between oceanic crust and accreted sediment often is coincident or in close proximity to the interplate thrust. The large increase in μ from the accretionary wedge to the oceanic crust, in general, results

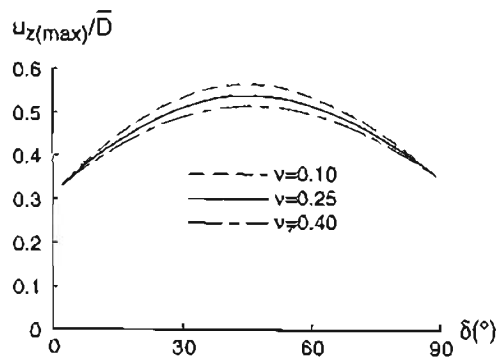


FIG. 18. Effect of varying Poisson's ratio (ν) on the maximum seafloor displacement with respect to fault dip. Calculations based on Okada's (1985) expressions for a homogeneous half-space.

in attenuation of seafloor displacement (Ma and Kuszniir, 1994). For a two-layer example, using numerical techniques developed by Hashimoto (1982) and Yoshioka *et al.* (1989), if μ_1/μ_2 decreases from 0.55 to 0.14 (corresponding to a decrease of μ_1 from $4.0 \times 10^{10} \text{ N m}^{-2}$ to $1.0 \times 10^{10} \text{ N m}^{-2}$ for water-saturated rocks, where $\mu_2 = 7.2 \times 10^{10} \text{ N m}^{-2}$), then the vertical displacement decreases for the planar-fault geometry considered in Fig. 19a; however, subsidence for the nonplanar-fault example (Fig. 19b) increases, indicating that the change related to modulus inhomogeneity is somewhat related to fault geometry (a similar pattern of displacement changes is noted by Ma and Kuszniir, 1994, for a dip-slip point source). A decrease in μ with depth can be envisioned for subduction zones in which sediment is subducted beneath a region of the accretionary wedge with higher values of μ . As such, the vertical negative contrast in μ may result in positive changes in seafloor displacement, although the magnitude of the changes is related to the thickness of the subducted sediment layer.

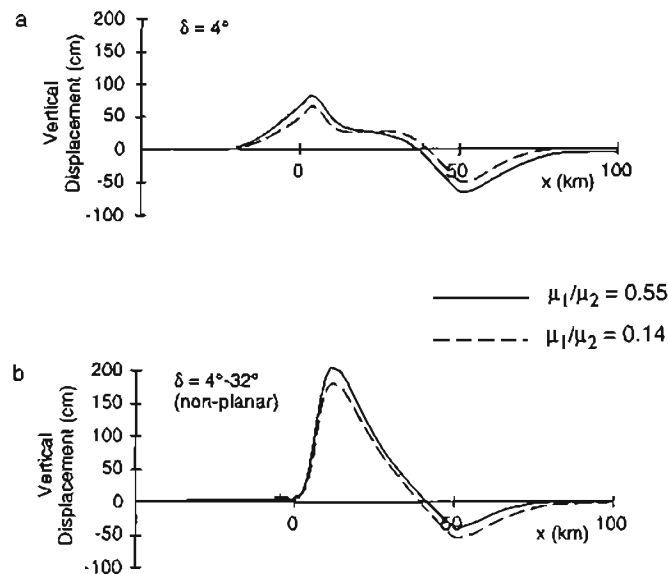


FIG. 19. Effect of inhomogeneous structure characteristic of subduction zone on seafloor displacement profiles (Yoshioka *et al.*, 1989; Geist and Yoshioka, 1996). The contrast in shear modulus between the accretionary wedge (layer 1) and the subducting oceanic crust (layer 2) is considered for two cases: $\mu_1 = 4.0 \times 10^{10} \text{ N m}^{-2}$ (solid line) and $\mu_1 = 1.0 \times 10^{10} \text{ N m}^{-2}$ (dashed line). For each case, $\mu_2 = 7.2 \times 10^{10} \text{ N m}^{-2}$ (Yoshioka *et al.*, 1989). (a) Dislocation along dicollement (constant dip; Fault B, Geist and Yoshioka, 1996). (b) Dislocation along seaward-vergent splay from dicollement (steepening toward seafloor; Fault C, Geist and Yoshioka, 1996) following the mechanism of tsunami earthquakes proposed by Fukao (1979).

5.5. Summary of Static Source Parameter Effects

Through the forgoing parametric analyses, the effect of individual static source parameters on local tsunami generation is established. Mean slip during rupture has the largest effect on vertical seafloor displacement and, hence, on the amplitude of the generated tsunami. Therefore, whereas the magnitude of far-field tsunamis is dependent on the total volume of water displaced (approximated by the logarithm of M_0), the severity of broadside run-up from local tsunamis is more dependent on the amplitude of the tsunami at the source, which, in turn, depends directly on the amount of slip. By comparison, variations in the geometric parameters of rupture (L , W , δ , h_0) have a slowly varying effect (within the parameter range considered) on seafloor displacement, especially for large earthquakes. The analyses also indicate that, for a given earthquake magnitude, shallow subduction zone earthquakes are comparatively efficient at generating local tsunamis because of the positive influence that shallowness of rupture (z_1), moderate dip, and large W (in comparison to near-vertical faults) has on tsunami generation. Finally, oblique slip along dipping faults results in a composite seafloor displacement pattern that leads to the generation of initially oblique secondary wavefronts, in addition to the strike-normal propagating primary wavefronts generated by the dip-slip component of dislocation. During propagation, these secondary wavefronts are partially refracted toward shore and focused, in addition to the raypath-independent Green's Law amplification.

6. EFFECT OF SPATIAL VARIATIONS IN EARTHQUAKE SOURCE PARAMETERS

In this section, the effect that spatial variations of source parameters (i.e., considered immediately after rupture) have on local tsunamis is examined. In Section 5, slip was determined to have the largest effect on tsunami generation, and so most of the discussion in this section will be on spatial variations in the amount of slip, which can vary by an order of magnitude for a given event. Spatial variations in faulting that arise from triggered and compound earthquakes are also discussed. Spatial variations in the geometric source parameters are not considered, because of their secondary influence on tsunami generation and the fault- and rupture-specific nature of these variations. Also, spatial variations of rake (λ) are not considered here, as would be the case for a partial-stress-release rupture and homogeneous pre-existing stress field (Cotton and Campillo, 1995). To determine the effect of spatial variations in source parameters in

seafloor displacement, numerical methods are used for both elastic dislocation and tsunami propagation, as described in Section 2.2. It should be noted, however, that Singh *et al.* (1994) have derived closed-form expressions for the displacement field due to predefined analytic slip functions along vertical faults.

6.1. Slip Variations

Variations in the slip field are considered both from a point of view of constraints from fracture mechanics and from direct inversion of seismic and tsunami waves. From fracture mechanics, the relationship between stress conditions and slip along an arbitrary planar fracture is given by singular integral equations, as reviewed by Dmowska and Rice (1986). For general solutions of the problem, numerical techniques are required. For cases in which uniform stress drop and crack geometry are specified *a priori*, analytic expressions can be derived (see, for example, Kostrov and Das, 1984; Dmowska and Rice, 1986). As indicated by Dmowska and Rice (1986), however, uniform stress-drop models are appropriate only for very smooth rupture propagation. Factors such as coupling between shear and normal stress in the case of shallow and surface rupture (e.g., Rudnicki and Wu, 1995) and heterogeneity of dynamic friction (e.g., Boatwright and Cocco, 1996) lead to nonuniform stress drop. One could also suppose that stresses are required to be finite at the rupture edge, imposing additional constraints on slip and stress drop-distributions (Freund and Barnett, 1976). Finally, dynamic and spatially variant stress changes (independent of physical heterogeneity) during rupture and between successive events result in a self-organized diversity in slip and stress-drop distributions (e.g., see reviews by Rundle and Klein, 1995, and Main, 1996).

The inversion of seismograms can yield information on the spatial variation of moment release, as specifically described for subduction zone earthquakes by Kikuchi and Fukao (1987), Beck and Ruff (1989), and Ruff and Miller (1994). In general terms, the two components of slip resolved in the plane of the fault (ξ_1, ξ_2) can be independently variable (i.e., $D_i(\xi_j)$, $i, j = 1, 2$). The relationship between the seismic moment tensor and the distribution of slip is (Aki and Richards, 1980):

$$M_{pq} = \iint_{\Sigma} D_i \nu_j c_{ijpq} d\Sigma,$$

where ν_j is the unit normal to the fault plane and c_{ijpq} is the modulus tensor. For arbitrary and spatially-variant rake, the moment-density tensor is given by $m_{pq} = D_i \nu_j c_{ijpq}$ (Aki and Richards, 1980; Ruff, 1987). If the

rake angle is constrained to be spatially invariant, then one need consider only spatial variations in the absolute magnitude of slip ($D(\xi_i) \equiv \|D(\xi_i)\|$) such that

$$M_0 = \mu \iint_{\Sigma} D d\Sigma.$$

The static (time-integrated) moment density distribution ($m_{pq}(\xi_i)$) can be derived if the time history of rupture is somehow known, often requiring *a priori* knowledge of the source time function, rupture azimuth, and velocity (Beck and Ruff, 1989; Ruff and Miller, 1994). Furthermore, if the shear modulus can be determined (or, more often, assumed), the slip distribution ($D(\xi_i)$) can then be derived from the moment density distribution.

The inversion of seismic and tsunami waves from subduction zone events reveals a surprising diversity of slip and moment release distributions (Thatcher, 1990). Although identifying regions of high moment release with asperities is a general approach in the sense that the cause of high-strength (shear stress) regions is not necessarily given, the asperity interpretation is particularly suited to the degree that source processes can be resolved and parameterized from seismic data. Das and Aki (1977) consider different models with multiple asperities and barriers (depending on whether the strong regions are broken or not). The suite of models they describe provide a useful framework to explain the observed strong spatial variations of slip based on rupture mechanics.

6.1.1. Effect on Surface Displacement

In general, for a Somigliana dislocation with an arbitrary slip distribution ($D_i(\xi_1, \xi_2)$ Fig. 5), the static displacement field is given by (Rybicki, 1986)

$$u_m = \iint_{\Sigma} D_i v_j U_m^{ij} d\Sigma.$$

Rybicki (1986) defines the six Green's functions U_m^{ij} based on the static Green's tensor for an elastic medium (G_m^i):

$$U_m^{ij} = U_m^{ji} = \lambda \delta_{ij} G_m^{n..n} + \mu [G_m^{i..j} + G_m^{j..i}].$$

Because G_m^i has been determined analytically for only a few simple slip distributions and fault geometries (e.g., Wang and Wu, 1983; Singh et al., 1994), numerical methods are often employed (e.g., Chinnery and Petrak, 1968; Freund and Barnett, 1976; Yang and Toksöz, 1981).

The analysis of Freund and Barnett (1976), which precludes stress singularities at the rupture front, can be applied to analyze the effect of

slip variation in the dip direction (ξ_1) for a subduction zone thrust event. Shown in Fig. 20 are predefined, normalized slip distributions for different values of the skewness parameter (q). The resulting vertical displacement profiles for these distributions, as well as the displacement profile from an integrated, equivalent uniform slip dislocation, are shown in Fig. 21. For all values of q , the amplitude of vertical displacement is greater than for the case of uniform slip. In particular, a slip distribution skewed up-dip (e.g., $q = 0.3$) results in a substantially larger peak vertical surface displacement (Fig. 21). (In contrast, the changes in the horizontal displacement are more subtle: Freund and Barnett, 1976.) From fracture theory, Rudnicki and Wu (1995) demonstrate that the dip-directed slip distribution will, in fact, be skewed toward the surface as the up-dip depth of rupture decreases. Observationally, Satake (1993) also demonstrates, from the joint inversion of tsunami and geodetic data, an up-dip increase in coseismic slip in the shallow region of the accretionary wedge for the 1944 Tonankai and 1946 Nankaido earthquakes. In addition, Hartzell and Langer (1993) determine a dip-directed slip distribution for the 1974 Peru earthquake that calls for large amount of slip up-dip from the hypocenter, near the seafloor, as does Linde and Silver (1989) for the 1960 great Chilean earthquake and Satake (1994a) and Ihmlé (1996a,b) for the 1992 Nicaragua tsunami earthquake. The observed slip distributions for these earthquakes are consistent with rupture at or near the seafloor. Slip consistent with the mechanics of dip-slip rupture is discussed further in Section 8.3.

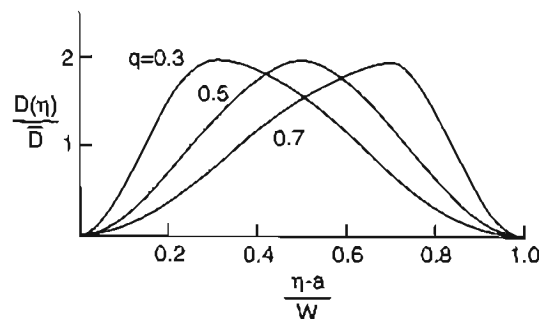


FIG. 20. Prescribed slip functions used by Freund and Barnett (1976). Slip (D) is normalized with respect to average slip (\bar{D}). The abscissa is the dip-parallel distance from the surface (η -coordinate). q represents the skewness parameter controlling the shape of the slip distribution. (Freund and Barnett, 1976; reproduced with permission from *Bull. Seism. Soc. Am.*, © 1976 Seismological Society of America).

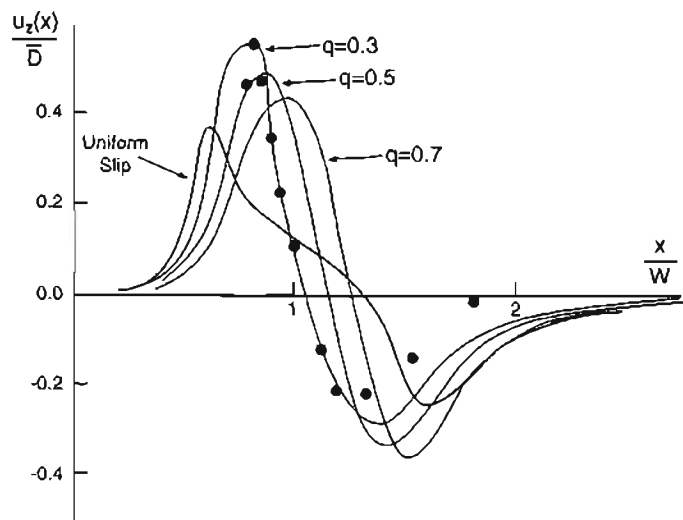


FIG. 21. Comparison of vertical surface displacement (u_z) along a strike-perpendicular profile for different skewness parameters (see Fig. 20). Note that vertical displacement is concentrated toward the center of the rupture zone for each case of variable slip distribution, compared to the vertical surface displacement from uniform slip. Dots represent measured vertical displacement from the 1964 Alaska earthquake. (Freund and Barnett, 1976; reproduced with permission from *Bull. Seism. Soc. Am.*, © 1976 Seismological Society of America)

Aside from variations in slip in the dip direction, along-strike variations in slip and surface displacement also need to be considered for local tsunami propagation models. Even for shallow events, the spatial resolution of slip variations determined from inversion of seismic observations is sufficient to describe the vertical surface displacement field. That is, small length-scale variations beyond the resolution of seismic data do not appreciably affect the locally observed tsunami. Increasing the source depth decreases the spatial wavelength of the surface displacement associated with slip variations. To illustrate this, the slip distribution of the October 3, 1974, Peru earthquake ($M_w = 8.0$) determined by Beck and Ruff (1989) is examined in relation to surface displacement and tsunami generation. Figure 22a shows the slip distribution along the fault plane derived by Beck and Ruff (1989) from the moment density distribution and assuming $W = 40$ km and $\mu = 5 \times 10^{10} \text{ N} \cdot \text{m}^{-2}$. The along-strike slip distribution is characterized by two regions of high slip approximately 50 km to the northwest and 70 km to the southeast of the epicenter, qualitatively similar to slip distribution derived by Hartzell and Langer (1993). The vertical seafloor displacement for the slip distribution shown in

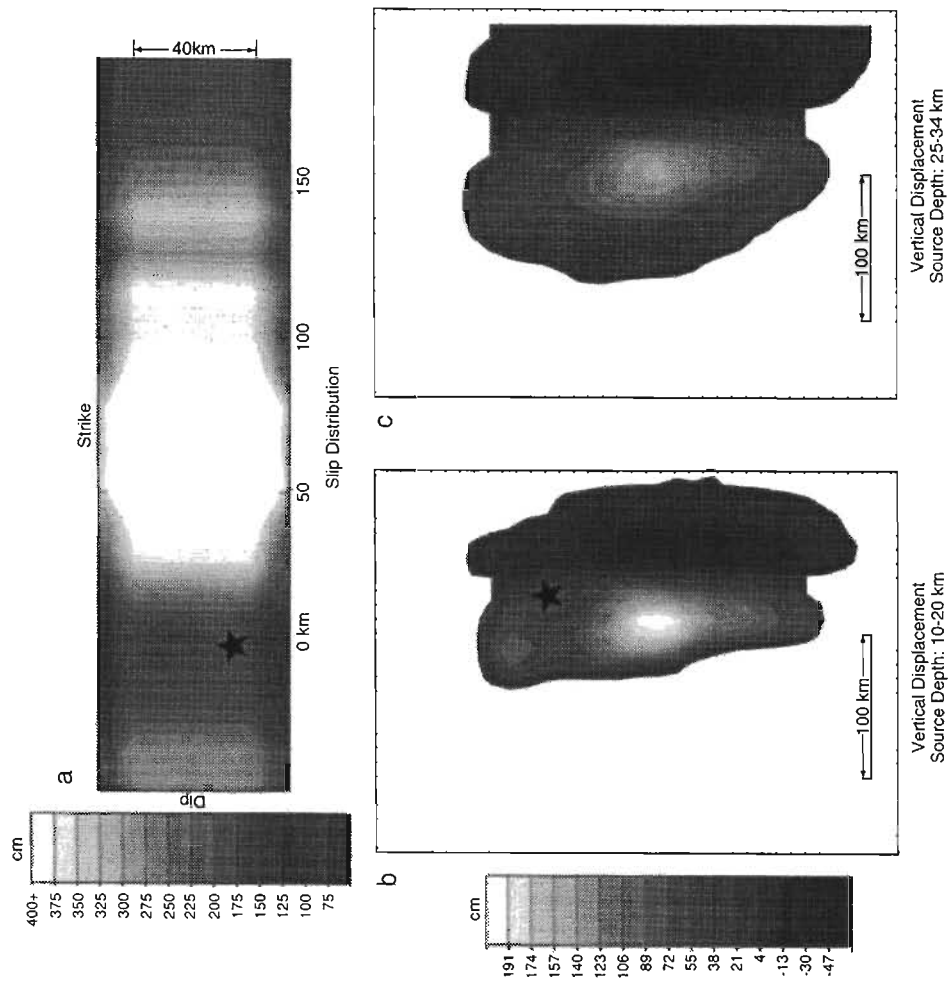


FIG. 22. (a) Slip distribution along the fault plane for the October 3, 1974, Peru earthquake determined from teleseismic observations (Beck and Ruff, 1989). Maximum slip is 7 m. For display purposes, slip greater than 4 m is not contoured, although the full range of slip was used in the displacement calculations. Dip-directed slip distribution is smoothed at ends of the rupture but are otherwise uniform. The star represents the approximate location of the hypocenter. (b) and (c) Map views of surface displacement calculated from three-dimensional finite element models for two different cases: (b) source depth 10–20 km (the source depth determined by Beck and Ruff, 1989) and (c) a hypothetical case in which the source depth is 25–34 km, to illustrate that displacement variations are attenuated with increasing source depth.

Fig. 22a is calculated using the three-dimensional finite-element model of Yoshioka *et al.* (1989). For a shallow source depth (Fig. 22b) approximately that determined by Beck and Ruff (1989), the vertical seafloor displacement is characterized by two regions of uplift correlating with the location of the two regions of high slip. If the source depth is increased, the variation in seafloor displacement is less pronounced for the same slip distribution (Fig. 22c).

6.1.2. *Effect on Local Tsunamis*

From Freund and Barnett's (1976) model (Fig. 21), the increase in amplitude of vertical displacement in the dip direction is caused by the concentration of slip toward the center of the rupture zone. This results in a larger tsunami than predicted by uniform slip. Moreover, run-up will also increase, not only from the larger amplitude but also from an attendant increase in the steepness of the leading wave (Fig. 9). This strongly suggests that conventional tsunami propagation models that are based on a uniform slip distribution underestimate the amplitude of seafloor displacement and the run-up from the resulting local tsunami that is generated.

The along-strike variations in the initial tsunami (such as derived from the vertical displacement field shown in Fig. 22) are generally attenuated by radial spreading during tsunami propagation. For propagation across the continental margin, however, focusing of the refracted components of the tsunami, as described in Section 5.3, preserves the wavefront-parallel changes in amplitude. In reference again to the October 3, 1974, Peru earthquake, the tsunami that results from the variable slip distribution is calculated at 500 s after generation using a finite-difference approximation to the linear-long-wave equations (right side, Fig. 23a). In general, the variation in tsunami amplitude has been attenuated for the basinward-propagating tsunami. The amplitude variation of the local, landward propagating tsunami, however, reflects the variation in slip at the source.

The tsunami derived from the detailed source process (Fig. 22a) can also be compared to a tsunami derived from the more conventional approach of using the analytical expression of surface displacement for average slip over a finite rectangular region (Volterra dislocation). Seafloor displacement for the 1974 Peru earthquake shown in Fig. 23b (left side) was derived from the analytical expressions of Okada (1985) by assuming uniform slip equal to the average slip for the earthquake (3 m) determined by Beck and Ruff (1989). Comparing the resulting local tsunamis (right side of Fig. 23a and b), it is evident that the overall maximum tsunami amplitude is underestimated for a uniform slip distribution, whereas the

length of shoreline that is significantly impacted by the tsunami is slightly overestimated.

6.2. Triggered and Compound Earthquakes

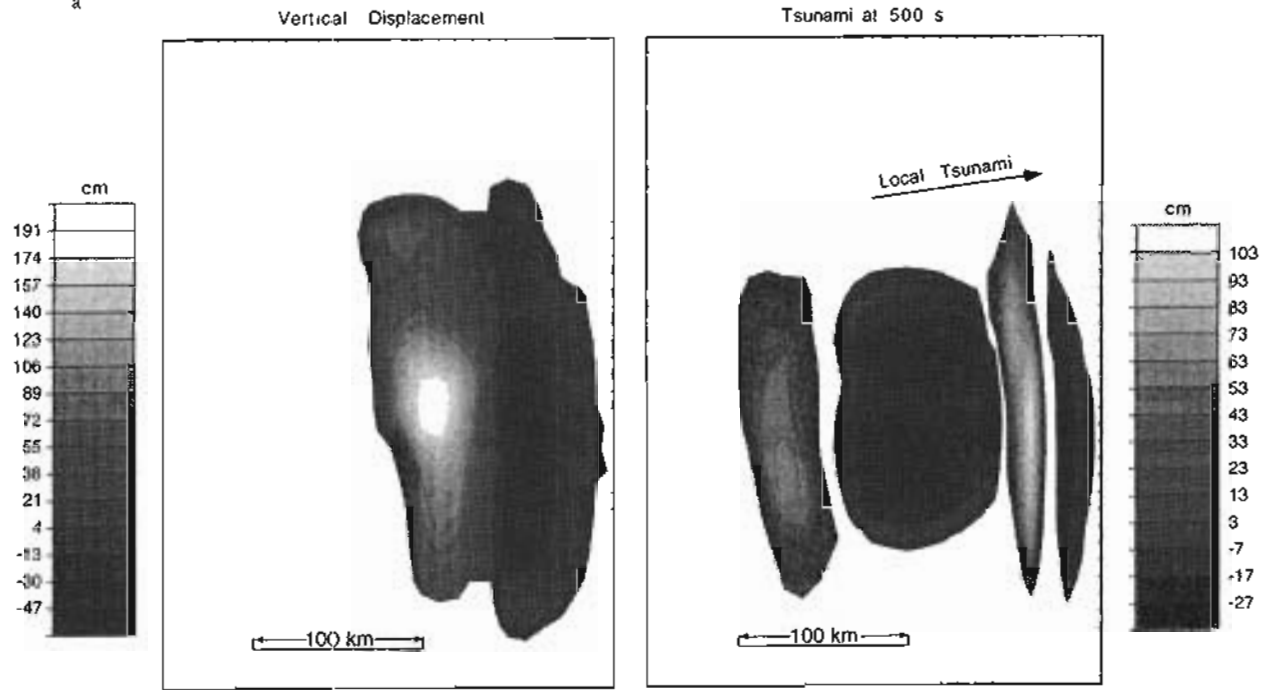
Triggering of earthquakes that occur shortly after a main event has been quantified by the change in the Coulomb failure stress (e.g., Harris and Simpson, 1992; Reasenber and Simpson, 1992; Stein *et al.*, 1992; Kagan, 1994). The change in Coulomb failure stress (σ_f) is given by

$$\Delta\sigma_f = \Delta\tau_s - \mu_f(\Delta\sigma_n - \Delta P),$$

where τ_s and σ_n are the shear and normal stress acting along the fault, respectively, μ_f is the static coefficient of friction, and P is the pore fluid pressure. Calculation of $\Delta\sigma_f$ is dependent on the preferred orientation of faulting, which can be determined from field studies, or, assuming that small faults occur with all possible orientations, on that orientation optimally oriented for failure. Regions off the master fault where $\Delta\sigma_f > 0$ are regions where separate events (aftershocks) are likely to be triggered. An interesting example of triggered earthquakes in relation to tsunami hazards is the case of offshore earthquakes in southern California triggered by large San Andreas events. Deng and Sykes (1996) demonstrate that the tsunamigenic 1812 M 7.1 Santa Barbara earthquake may have been triggered by an earthquake on the San Andreas fault 13 days earlier (the 1812 M_w 7.5 Wrightwood earthquake). In a subduction zone setting, an increase in $\Delta\sigma_f$ is noted by Geist and Yoshioka (1996) for landward-dipping faults at shallower depths than the main rupture on the interplate thrust. Occasionally, doublet or multiple earthquakes occur within a short enough time interval to result in interference during propagation. This is especially pertinent when reflection is considered within a semiclosed basin, as with the 1956 Southern Aegean tsunami (Yalciner *et al.*, 1995).

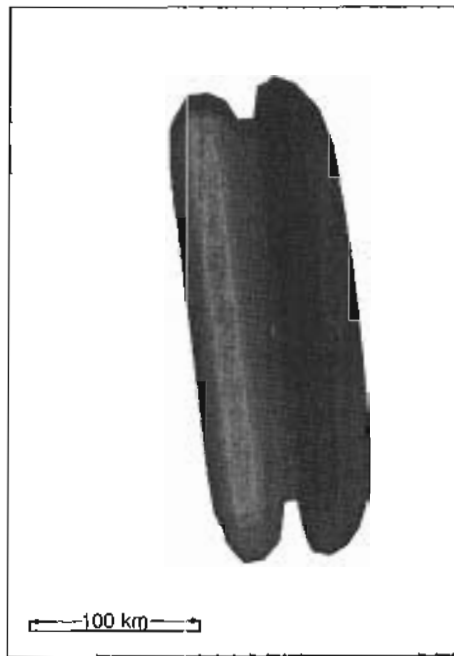
FIG. 23. Surface displacement (left) and tsunami amplitude at 500 s after generation (right) for two different source models of the October 3, 1974, Peru earthquake. For each case, the tsunami was calculated using a finite difference approximation to the linear long-wave equation. A local tsunami propagating eastward (to the right) is amplified and reduced in wavelength during shoaling. (a) Seafloor displacement and tsunami associated with slip distribution shown in Fig. 22a. Seafloor displacement field calculated from elastic-finite element model (Yoshioka *et al.*, 1989). (b) Seafloor displacement and tsunami for uniform slip. Seafloor displacement calculated from analytical expressions of Okada (1985), assuming uniform slip model equal to the average slip for the event (3 m). Note the higher maximum tsunami amplitude for the variable slip model (a).

a

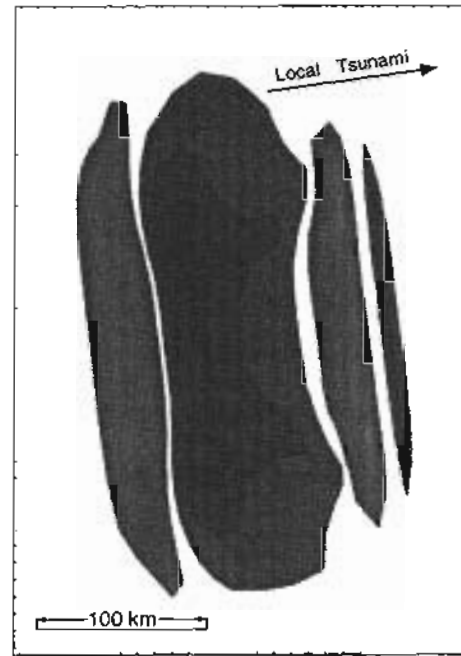


b

Vertical Displacement



Tsunami at 500 s



Often, though, the tsunamis derived from the master and triggered events can be considered separately in terms of their propagation effects.

Compound events that occur on faults of different dips can have a significant effect on the initial tsunami waveform. The seafloor displacement from compound events can be viewed as the superposition for displacement fields from individual events (Satake, 1994b). One possible compound event, as described by Fukao (1979), would be rupture extending from the low-angle subduction thrust to a steeply dipping splay approaching the seafloor. Secondary slip along an upward-branching splay may have been associated with the 1964 Great Alaska earthquake (Shuto, 1991; Shuto *et al.*, 1995). The effect that this type of compound event has on vertical seafloor displacement is shown in Fig. 24. Although narrower in extent, the part of rupture occurring on the shallow, steeply dipping splay (Fig. 24b) greatly increases the vertical displacement over dislocation along gently dipping thrust (Fig. 24a). Offshore compound earthquakes such as

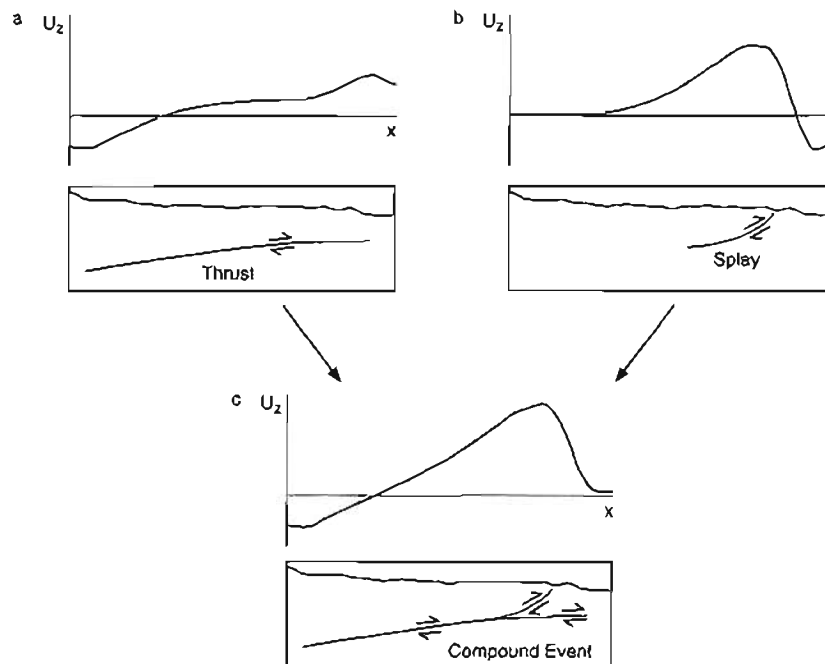


FIG. 24. Effect that a compound event involving a shallow, steeply dipping splay has on vertical seafloor displacement (following the model of Fukao, 1979). (a) Displacement from low-angle thrust. (b) Displacement from splay. (c) Summation of (a) and (b) to yield displacement from compound event.

shown in Fig. 24c are difficult to identify and likely represent an infrequent phenomenon, although onshore evidence exists of rupture on similar-type structures (Berberian, 1982). A compound tsunamigenic event is proposed for the 1983 Nihonkai-Chubu (Japan Sea) earthquake (Shuto *et al.*, 1995), in which slip may have occurred on a fault antithetic to the main rupture zone.

7. EFFECT OF TEMPORAL VARIATIONS IN EARTHQUAKE SOURCE PARAMETERS

Because the propagation velocity of tsunamis is low in comparison to the rupture velocity, the time history of rupture propagation, in most cases, has little effect on the tsunami in comparison to an assumed instantaneous source (e.g., Yamashita and Sato, 1974; Kajiura, 1981; Kowalik and Whitmore, 1991). In contrast, seismic body waves are directly dependent on the time history of rupture specified in terms of the moment-rate function $\dot{M}(t) = \mu[\partial(A(t)D(t))/\partial t]$ (Lay and Wallace, 1995). Satake (1987) also notes, with regard to the tsunami inversion, that the temporal sampling of tsunamis at tide gauge stations is typically 1 min, insufficient to resolve time scales less than the source-process time of most earthquakes. However, tsunami earthquakes, in particular, often are slow earthquakes, and the temporal source processes can ostensibly affect the local tsunami. In this section the effect of a finite source-process time is investigated, specifically the effect of rise time and rupture propagation. The effect of rupture direction (bilateral and unilateral rupture) and the temporal dependence of the vertical displacement field on tsunami generation is also considered in this section.

7.1. Rise Time

The far-field source-time function of an earthquake can be ideally described as the convolution of two boxcar functions (Fig. 25): one representing the rise time of the earthquake (τ_r) and the other representing the rupture duration ($\tau_c = L/v_r$), where v_r is the rupture speed for the one-dimensional Haskell fault model (Haskell, 1964; Lay and Wallace, 1995). Using this model, the slip function at a particular point on the fault plane is given by (Aki and Richards, 1980)

$$D(t) = \begin{cases} 0 & t < 0 \\ D_1 t / \tau_r & 0 < t < \tau_r \\ D_1 & t > \tau_r \end{cases}$$

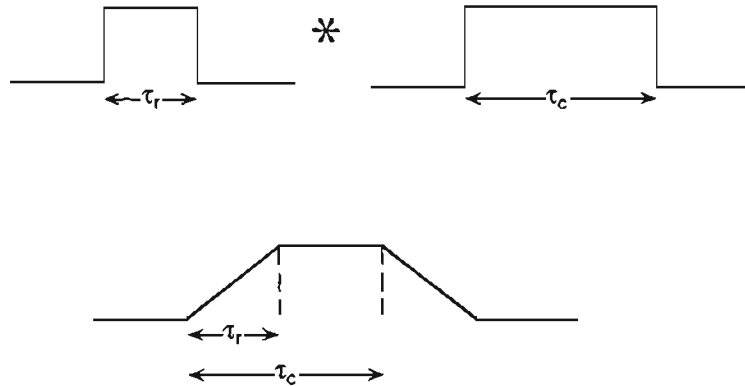


FIG. 25. Convolution model for far-field representation of the source-time function. τ_r and τ_c are the rise time and rupture duration, respectively. (Lay and Wallace, 1995; reproduced with permission from *Modern Global Seismology*, © 1995 Academic Press).

where D_1 is the final displacement. An alternative to this ramp function is an exponential function of the form (Ben-Menahem and Toksöz, 1963; Kanamori, 1972):

$$D(t) = \begin{cases} 0 & t < 0 \\ D_1(1 - e^{-t/\tau_r}) & t > 0 \end{cases}$$

In either case, the average dislocation velocity (\dot{D}) for a point on the fault plane is D_1/τ_r . Beeler and Tullis (1996) demonstrate that τ_r is dependent on the specific constitutive parameters of fault friction and that the observation of short rise times relative to the duration of rupture is a result of the negative velocity dependence of crack strength (see also dynamic rupture models of Heaton, 1990; Rydelek and Sacks, 1996; Beroza and Mikumo, 1996).

A useful measure of the effect finite rise time has on the tsunami during generation is the dimensionless number (I term it as t^*) defined by Hammack (1973) as $t^* = 2\tau_r\sqrt{gh}/\lambda_0$, where λ_0 is the dominant wavelength of the seafloor displacement profile. For $t^* \ll 1$, displacement of the seafloor can be considered instantaneous (in terms of tsunami generation) and the tsunami waveform will be similar to the seafloor displacement profile. For very short rise times, a significant amount of energy will be transferred from seafloor displacement to compressional waves within the water column (Kajiura, 1970). The other extreme, which is rarely realized for earthquakes but may be important for submarine slide-generated tsunamis, is where $t^* \gg 1$. For these creeping motions, the initial

tsunami profile mimics the time history of displacement rather than the actual seafloor displacement profile and has a much lower overall amplitude (Hammack, 1973).

Even for the case where $t^* \ll 1$, τ_r has a measurable effect on tsunami amplitude. Similar to the parametric analysis presented in Section 5, the effect that rise time has on the near-shore tsunami waveform is examined, with the results shown in Fig. 26. For this analysis, dip-directed rupture propagation is not modeled such that the time-history of the vertical displacement field is uniformly controlled by the exponential ramp function given previously. A broad range of rise times (or, more precisely, source-deformation times) are examined ($\tau_r = 1-100$ s, where $t^* \approx 0.003-0.3$). In modeling these source effects, the time step in the finite difference calculations is necessarily decreased from the minimum time-step necessary to model tsunami propagation conventionally. Note that the difference between Fig. 26 and figures presented previously (e.g., Fig. 10) is that the magnitudes of the maximum and minima are not normalized for

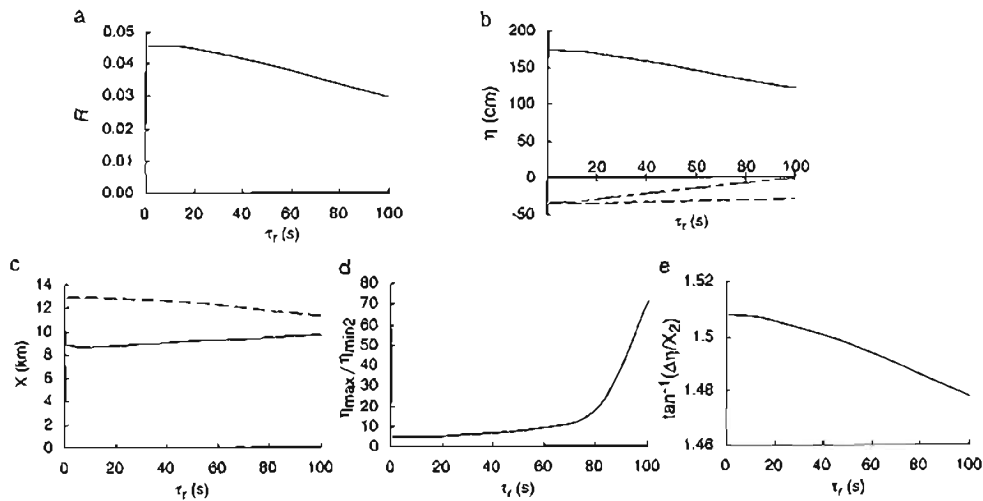


FIG. 26. Effect of varying the rise time on local run-up and characteristic parameters of the propagated waveform (see Fig. 8). Other source parameters of the earthquake held constant. Tsunami amplitude at the 50-m water depth calculated from numerical approximation to the Peregrine (1967) equations for propagation across a continental margin-type bathymetry. (a) Normalized maximum run-up calculated from an N-wave approximation to the propagated tsunami waveforms. Run-up parameters described in Fig. 10a. (b) Amplitude of local maximum and minima normalized with respect to the average amount of slip during rupture. Solid line is η_{max} ; short-dashed line is η_{min1} ; long-dashed line is η_{min2} . (c) Distance from central maximum to local minima. Solid line is X_1 , dashed line is X_2 . (d) Ratio of amplitude of central maximum to leading minimum. (e) Leading-wave steepness.

this specific propagation case and that the separation between extrema is less and the wave steepness is greater due to the effects of shoaling.

The rise time of the majority of subduction zone earthquakes is less than 20 s; thus, little effect is predicted for the separation distance, amplitude ratio, and wave steepness of the tsunami (Fig. 26c, d, e, respectively). For this range of rise times between 1 and 20 s, there is a slight decrease in the maximum tsunami amplitude with increasing rise time, owing to changes in the short-period components of the waveform (Fig. 26b; Kajiura, 1970; Yamashita and Sato, 1974). There is a more measurable effect on the tsunami waveform for rise times greater than 20 s. Owing to a decrease in extrema amplitude and leading-wave steepness with increasing rise time, there is an overall gradual decrease in run-up with increasing rise time (Fig. 26a). The effect that rise time and other time-varying characteristics of rupture have on the tsunami are moderately amplified with increasing water depth at the source. Spatial variation in the rise time during rupture (Madariaga, 1976; Hartzell and Langer, 1993) is not expected to have a significant effect on tsunami generation.

Although long rise-time events are rare and studies of recent tsunami earthquakes do not necessarily indicate anomalous rise times, two of the most significant tsunami earthquakes in history have a "source-deformation time constant" that approaches 100 s: the 1896 Sanriku and 1946 Aleutian earthquakes (Kanamori, 1972). Beroza and Jordan (1990) and Li and Nabelek (1996) discuss techniques to identify slow and even "silent" earthquakes that do not emit teleseismically detectable high-frequency seismic energy.

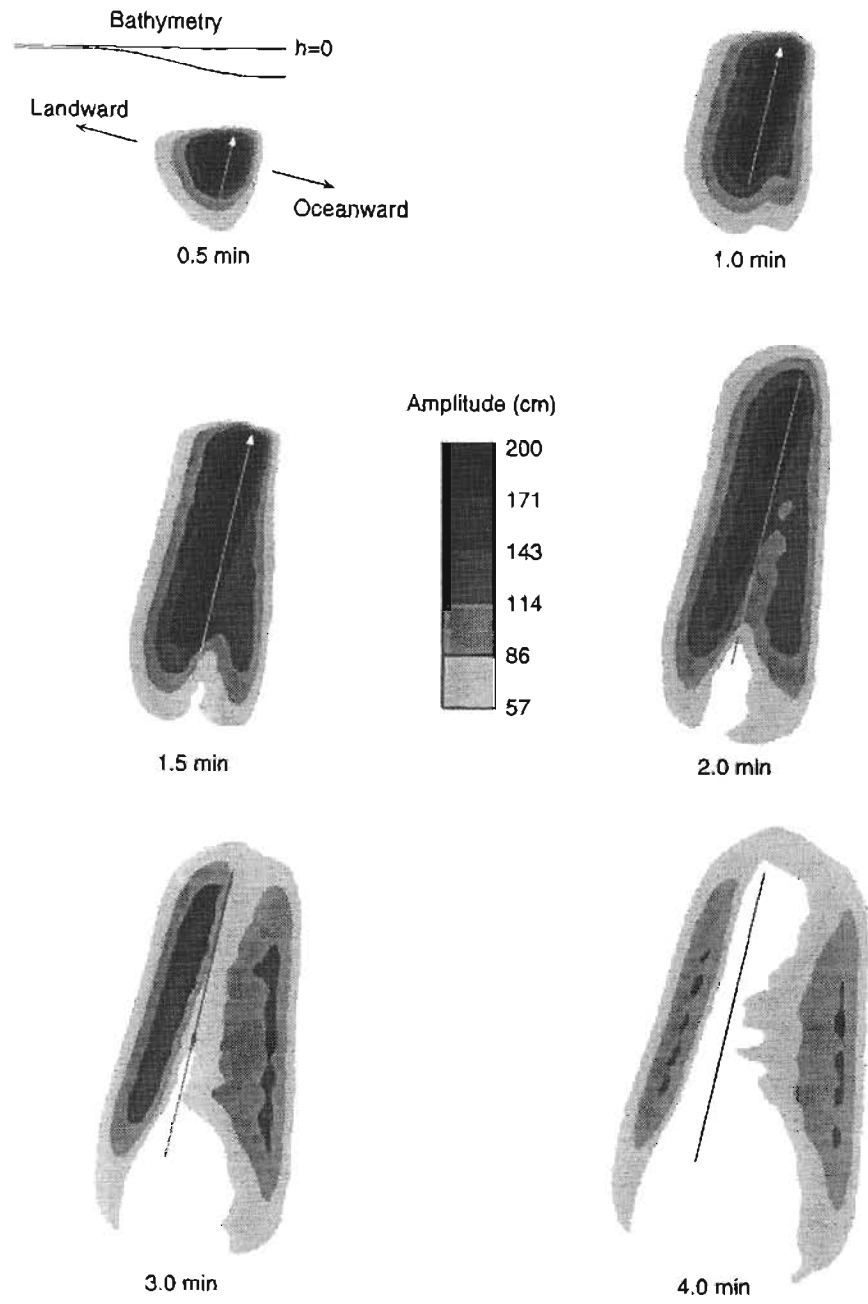
7.2. Rupture Velocity

The other characteristic time of earthquake rupture is rupture duration: ($\tau_c = L/v_c$). Rupture velocity is dynamically limited, as pointed out by, among others, Das (1981) and Dmowska and Rice (1986). Because the terminal velocity is generally different for Mode II and Mode III ruptures, an equidimensionally expanding rupture will have a different terminal rupture velocity in the dip direction than in the strike direction (Das, 1981; Dmowska and Rice, 1986). There are conditions, however, in which rupture velocity can exceed shear wave speed or stay well below its terminal limit (Andrews, 1976). For rupture in the presence of poorly consolidated sediments (specifically, for shallow subduction zone thrust faulting), the rupture speed is often limited to low values, as in the case of the 1992 Nicaragua tsunami earthquake ($v_r = 1.0\text{--}1.5$ km/s, Kikuchi and Kanamori,

1995). In general, anomalously slow earthquakes (e.g., Kanamori and Stewart, 1979) have been explained by the fracture of an asperity in an otherwise stress-free fault (Das and Kostrov, 1986) and as a result of low-dynamic-stress-drop events (Yamashita, 1980). Rupture propagation models indicate that, in the absence of barriers, rupture typically starts slowly and accelerates to its terminal velocity (Das and Aki, 1977; Dmowska and Rice, 1986). Otherwise, for models that incorporate barriers and asperities, propagation of the rupture front can be erratic.

The effect that along-strike rupture propagation has on tsunami generation is to skew the wavefront away from a parallel orientation with fault strike and to increase directivity in the direction of propagation. Tsunami wavefields related to along-strike rupture propagation are computed using a Haskell-type source model, again not including the effect of dip-directed rupture propagation. For the case of unilateral rupture propagation shown in Fig. 27, a slow rupture speed (1 km/s) is used to show the effects more clearly. The rotation in the wavefront is more evident in the oceanward-propagating tsunami, because of the higher tsunami propagation speed. Directivity-related amplitude variations along the wavefront apparent during initiation are attenuated as the tsunami leaves the source area, although in general the directivity in the direction of rupture propagation is evident. (Incidentally, the beaming perpendicular to strike due to finite fault length, as described by Yamashita and Sato, 1974, and Ward, 1982, is also evident in Fig. 27). Shown in Fig. 28 is the peak phase of the tsunami after 3 min for two different rupture speeds. Increasing the rupture speed decreases the amount the wavefront is rotated and decreases the directivity effects.

Observations indicate that the point of rupture initiation can be located anywhere within the final rupture area, though the majority of subduction earthquakes initiate near the deepest extent of rupture (Das and Scholz, 1983). Two idealized modes of rupture, unilateral and bilateral, are compared in relation to the effect on the tsunami during generation in Fig. 29. The tsunamis are plotted 2 min. after rupture initiation and, again, only the peak phase is shown, for clarity. The two modes of rupture are also compared to a commonly assumed time-independent rupture along strike. As illustrated in Fig. 29, during tsunami generation there is a significant effect on the amplitude field and directivity, depending on the assumed mode of rupture. For bilateral rupture, the directivity effect is apparent toward both ends of the rupture zone. During the early propagation of the tsunami, the amplitude and directivity effects are attenuated as shown in Fig. 27.



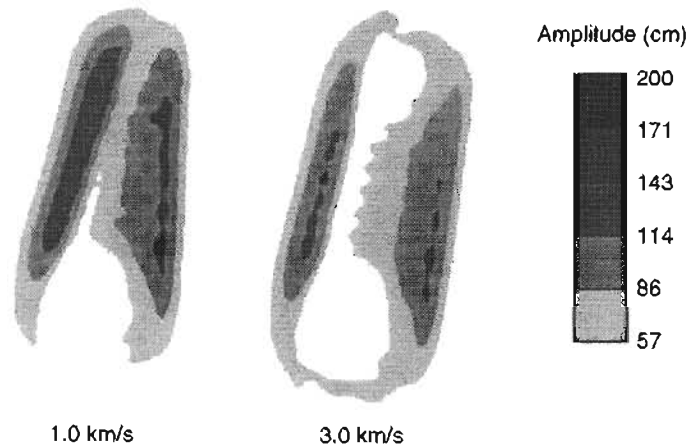


FIG. 28. Unilateral rupture propagation for two different rupture speeds: 1 km/s and 3 km/s. Peak phase of tsunami is shown at 3 min after rupture initiation. Bathymetry as in Fig. 27.

7.3. Dynamic Overshoot of Vertical Displacements

Forward modeling of near-field, strong-motion waveforms by Bouchon (1980) demonstrate a dynamic overshoot in the vertical displacement field related to up-dip rupture propagation for a thrust fault. If low-velocity sedimentary layers near the surface are included in the strong-motion calculations, the overshoot attains an oscillatory character. Because calculating the complete strong ground motion wavefield is beyond the scope of this study (see a review by Spudich and Hartzell, 1985), we simulate the effect of the dynamic overshoot by an underdamped oscillation (Fig. 30). That is, the exponential ramp function that models the time history of the displacement field is modified as follows:

$$u_z(x, t) = u_z(x) [1 - e^{-t/\tau} \cos(\omega_0 t)],$$

FIG. 27. Effect of along-strike rupture propagation (Haskell model) on tsunami generation. Tsunami waveform during generation is shown for unilateral rupture propagation at 1 km/s. Rupture is completed by 2 minutes. For simplicity, only the peak phase of the tsunami waveform is shown. Rupture occurs at the base of the continental slope such that the oceanward-propagating tsunami (faster) is directed to the right and the landward-propagating tsunami (slower) is directed to the left. (See bathymetric profile in upper left-hand corner.) White arrow designates the location of the up-dip extent of the rupture zone and direction of rupture. Recall that tsunami amplitude is reduced by approximately half as the oppositely propagating components leave the source region (cf. Fig. 3).

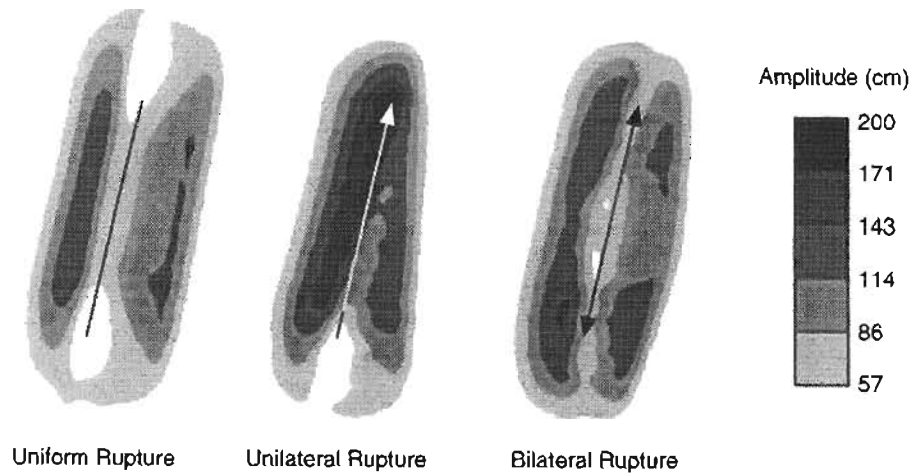


FIG. 29. Peak phase of tsunami at 2 min. after rupture initiation for unilateral and bilateral rupture compared to no assumed temporal dependence of along-strike rupture propagation (uniform rupture). Bathymetry as in Fig. 27.

where ω_0 is the *ad hoc* damping frequency that is dependent on τ_r . Because the overshoot occurs over a short period of time relative to the propagation of the tsunami, the change in the tsunami waveform soon after initiation is slight, as shown in Fig. 30.

8. LOCAL EFFECTS OF TSUNAMI EARTHQUAKES

The importance of studying tsunami earthquakes has been underscored in recent years, owing to the destruction that can result from anomalous tsunamis generated by these earthquakes (Satake and Imamura, 1995). As originally considered by Kanamori (1972), tsunami earthquakes are those events that generate anomalous tsunamis relative to their surface wave magnitude (M_s , measured at a period of 20 s). Specifically, Kanamori (1972) noted that for tsunami earthquakes, the effective moment (as a function of frequency) increases substantially with decreasing frequency, whereas for ordinary earthquakes, the effective moment is approximately constant with respect to frequency. Tsunami earthquakes are therefore often defined by a disparity between M_s and M_w (Kanamori and Kikuchi, 1993). The magnitude scale M_s , based on both near- and far-field tsunami data (Abe, 1979, 1995) is a good measure of the scalar seismic moment of the earthquake and the overall far-field energy of the resulting tsunami.

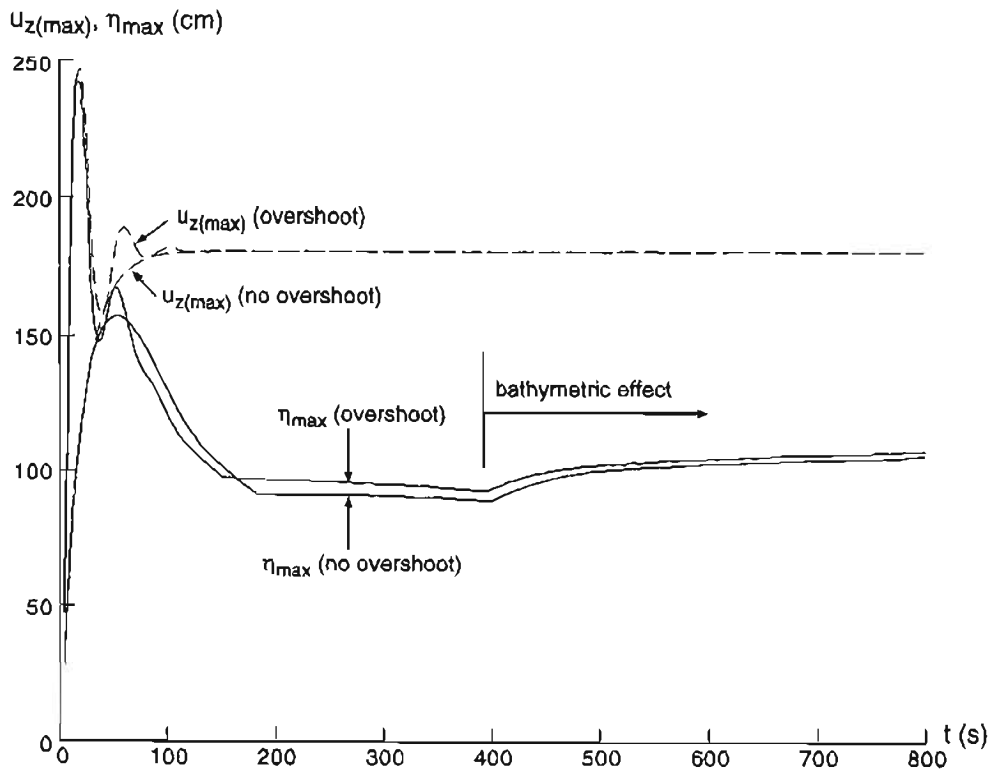


FIG. 30. Effect of dynamic overshoot of vertical displacement on maximum tsunami amplitude. Dynamic overshoot indicated by numerical ground motion models (Bouchon, 1980) and simulated for this figure using an underdamped oscillation ($u_{z(\max)}$ overshoot). Although during rupture the maximum tsunami amplitude mimics the time history of ground motion, soon after the tsunami leaves the source region the dynamic effects are negligible (cf. Fig. 3).

Studies by Okal (1988) and Pelayo and Wiens (1992) also note that, in most cases, tsunami amplitude is linearly proportional to the logarithm of the seismic moment, if directivity effects are accounted for. Recent efforts to improve tsunami warning systems, therefore, are focused on obtaining rapid estimates of M_w , rather than relying on surface-wave magnitudes. Specific techniques to achieve this are discussed by Okal and Talandier (1986), Talandier and Okal (1989), Okal (1993), Schindelé *et al.* (1995), and Tsuboi *et al.* (1995).

Even relative to the seismic moment, anomalously high far-field tsunami excitation can occur, owing to partial moment release in the low-shear-

modulus sedimentary layers and, consequently, to a significant increase in slip during rupture (Okal, 1988; Pelayo and Wiens, 1992). As indicated in this chapter, because local tsunamis are poorly represented by a point source, critical source parameters that characterize rupture over a finite area need to be considered in predicting the effects on local tsunami amplitude and run-up. Partial seismic moment release in shallow, low-shear-modulus layers is particularly important when examining the local effects of tsunami earthquakes, because local broadside run-up is more sensitive to the amplitude and shape of the initial waveform than to the total volume of water displaced. In this section, recent results from the seismic source characterization of tsunami earthquakes are reviewed and the mechanics of shallow thrust faulting in relation to the local tsunami problem are discussed.

8.1. Characteristics of Tsunami Earthquakes

Most, if not all, tsunami earthquakes occur along the shallow part of the interplate thrust or décollement near the trench. Many of the unique source parameters of tsunami earthquakes (Table 3) can be explained as a result of rupture in this setting. It is important to realize, however, that tsunami earthquakes are defined by the relative amplitude of the tsunami wave with respect to the amplitude of short-period seismic waves. Tsunami earthquakes do not necessarily indicate a particular mechanism or tectonic setting.

The most remarked-upon characteristic of tsunami earthquakes is the long rupture duration (τ_c) and, hence, the slow rupture velocity (e.g., Pelayo and Wiens, 1992; Kanamori and Kikuchi, 1993). Pelayo and Wiens (1992) indicate that the rupture velocity of most tsunami earthquakes is approximately 1.0 km/s, compared to approximately 2.5–3.5 km/s for normal subduction zone earthquakes. Because rupture velocity is most likely limited by the shear wave speed, the characteristic low rupture velocity of tsunami earthquakes can be explained by rupture in slow-accreted or subducted sediment near the trench (Kanamori and Kikuchi, 1993). However, Ihmlé (1996a) notes that the sedimentary rocks surrounding the fault zone may be of normal wave shear-wave speed at a few kilometers of burial and that the low rupture velocity of tsunami earthquakes may be due to the unique frictional properties along the fault. Although the rupture velocity and source duration do not greatly affect tsunami excitation other than by directivity changes (Fig. 29), the slow rupture velocity does directly affect the excitation of short-period seismic waves. Pelayo and Wiens (1992) demonstrate that because of slower seismic wave speeds, saturation of the surface-wave magnitude scale oc-

curs at $M_s = 7.3$, compared to $M_s = 8.0$ for ordinary subduction zone earthquakes.

The characteristic geometric source parameters of tsunami earthquakes, namely, shallow source depth and shallow fault dip, have contrasting effects on the local tsunami waveform. For large earthquakes, reduction in the source depth increases tsunami amplitude and attendant run-up (Fig. 10), whereas reduction of the fault dip at low values results in a decrease in tsunami amplitude and run-up (Fig. 12). The shallow source depth and fault dip do present difficulty in accurately estimating the seismic moment and mechanism of an event, as described by Pelayo and Wiens (1992).

Perhaps the most significant characteristic of tsunami earthquakes in relation to the excitation of local tsunamis is the anomalously high slip values. As shown in Fig. 31, the average amount of slip is considerably greater than the average slip of other tsunamigenic earthquakes of comparable magnitude. Anomalous average slip values are most likely a result of

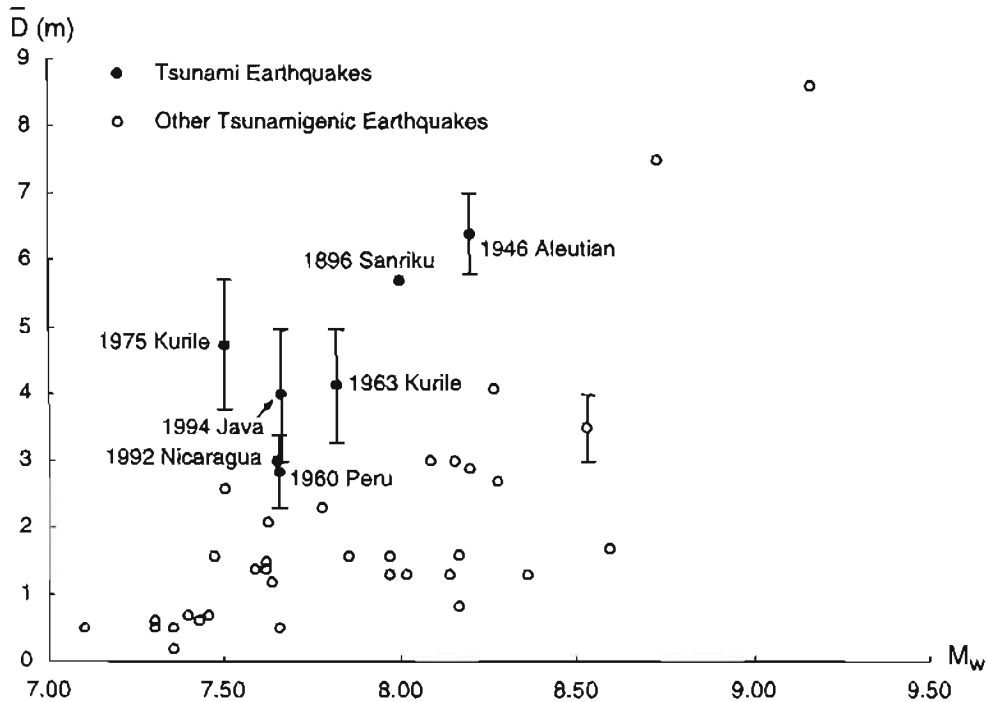


FIG. 31. Moment magnitude (M_w) versus average slip for tsunami and other tsunamigenic earthquakes. References for slip and seismic moment determination given in Tables 2 and 3. Error bars shown only for those events in which error was specified in the references.

TABLE 3 SOURCE PARAMETERS FOR TSUNAMI EARTHQUAKES

Region	Date	M_s	M_0 (10^{20} Nm)	M_w	Dip	Depth (km)	Length (km)	Width (km)	Rupture duration(s)	Average slip (m)	Reference
Sanriku	6/15/1896	7.2	12	8.0	20°	17	210	50		5.7	Tanioka and Satake (1996b)
Aleutian	4/1/46	7.4	23	8.2	6°		95	80	100–150	6.4	Johnson and Satake (in press)
Peru	11/20/60	6.8	3.4	7.6	6°	9	100	50	130	2.3–3.4	Pelayo and Wiens (1990)
Kurile	10/20/63	6.9	6.0	7.8	7°	9	110	45	85	3.3–5.0	Pelayo and Wiens (1992)
Kurile	6/10/75	7.0	2.0	7.5	8°	5	100	60	60	3.8–5.7	Pelayo and Wiens (1992)
Nicaragua	9/2/92	7.2	3.4	7.7	10°	10	160	50	100	3.0	Satake (1994a)
Java	6/2/94	7.2	3.5	7.7	15°	15			90	3.24	Tanioka and Satake (1996a)

Note: See also Fig. 31. Source parameters for other tsunamigenic earthquakes are shown in Table 2.

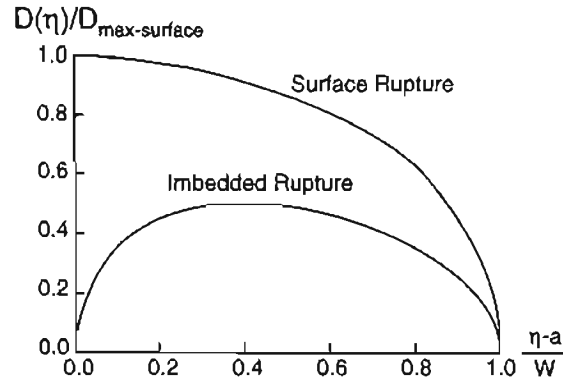


FIG. 32. Dip-directed slip distribution for an example of shallow-imbedded rupture and surface rupture. Horizontal axis is distance from the up-dip edge of rupture ($\eta = a$) normalized with respect to rupture width (cf., Fig. 20). Slip distribution calculated using the crack model of Dmowska and Kostrov (1973), in which $\delta = 15^\circ$, $\mu_f = 0.01$, and $W = 70$ km. For imbedded rupture, $z_1 = 1$ km.

both rupture within low-shear-modulus layers and rupture of the seafloor (Fig. 32). Because for local tsunamis there is a greater than linear scaling of tsunami run-up with slip, the high average slip associated with tsunami earthquakes alone can account for the anomalous excitation of local tsunamis.

8.2. Results from Broadband Analysis of Recent Tsunami Earthquakes

As noted by Kikuchi and Kanamori (1995), the 1992 Nicaragua earthquake was the first tsunami earthquake amenable to analysis of data collected by the global network of broadband seismographs. The last significant tsunami earthquake prior to 1992 was the 1975 Kurile event ($M_s = 7.0$ and $M_w = 7.5$, Pelayo and Wiens, 1992). (Though the 1983 Japan Sea event generated a sizable tsunami, this event was not designated a tsunami earthquake, based on a magnitude determination of $M_s = 7.7$ and $M_w = 7.9$ by Satake, 1985.) Analysis of both tsunami and high-run-up tsunamigenic earthquakes since then (1992 Flores, 1993 Hokkaido, and 1994 Java events) yields important results regarding the kinematics of these earthquakes.

8.2.1. Stress Drop

Pelayo and Wiens (1992) indicate that tsunami earthquakes do not exhibit abnormally low static stress drops (< 2 MPa), using a stress

drop–seismic moment relation for the older events. For the 1992 Nicaragua tsunami earthquake, Ihmlé (1996a) estimates a static stress drop of 3.0–7.0 MPa, whereas Ide *et al.* (1993) and Kikuchi and Kanamori (1995) estimate a static stress drop of 0.25–0.39 MPa and 1.1 MPa, respectively. These seemingly contradictory estimates for the stress drop of this event present difficulties in evaluating whether or not tsunami earthquakes are in fact unusually low-stress-drop events. Estimating the static stress drop from the dislocation and rupture velocities ($\Delta\sigma \approx \mu\dot{D}/v_r$, Boatwright, 1984) is also inconclusive, owing to characteristically low values for both μ and v_r . For the 1994 Java earthquake, the stress drop is most likely less than 1.0 MPa, using source dimensions approximated by the zone of aftershocks (Tsuji *et al.*, 1995) and results from Tanioka and Satake (1996a). In contrast to the shallow-interplate-thrust events, the stress drop for the recent high-run-up, back-arc events are significantly higher: 3.0–5.6 MPa for the 1992 Flores event (Beckers and Lay, 1995) and 0.3–3.4 for the 1993 Hokkaido event (using the source parameters of subfaults described by Satake and Tanioka, 1995).

8.2.2. Source-Time Function

There is also some disagreement as to whether the 1992 Nicaragua tsunami earthquake is characterized by distinct subevents (Ide *et al.*, 1993; Velasco *et al.*, 1994; Ihmlé, 1996a,b) or smooth rupture (Kikuchi and Kanamori, 1995), as indicated by the source-time function. In all studies of the 1992 Nicaragua event, asymmetric bilateral rupture is evident. For the analyses that indicate distinct subevents, rupture appears to be characterized by one or two subevents 20–80 km northwest of the epicenter and a prominent subevent 120–160 km southeast of the epicenter, with an intervening region of low seismic moment density. Rupture occurring in distinct subevents is also proposed for the 1992 Flores earthquake (Imamura *et al.*, 1995), the 1993 Hokkaido earthquake (Satake and Tanioka, 1995; Tanioka *et al.*, 1995; Mendoza and Fukuyama, 1996), and many other earthquakes, from the inversion of tsunami, geodetic, and seismic waveform data. For the 1992 Flores event, Beckers and Lay (1995) suggest up-dip and bilateral propagation. The rise time of the 1992 Nicaragua earthquake is estimated to be 40 s, 6–13 s, and 10–18 s by Ide *et al.* (1993), Kikuchi and Kanamori (1995), and Ihmlé (1996a), respectively. The unambiguous difference between the rise time and rupture duration (100–120 s) suggests evidence for wave-mediated rupture arrest (Heaton, 1990) or rupture occurring on discrete and interacting patches (e.g., Rydelek and Sacks, 1996).

8.2.3. Slip Distribution

To determine the slip distribution from the moment-density distribution inverted from seismic waveforms, a specific fault width is often assumed *a priori*. The assumed fault width from analysis of seismic waves is frequently larger than the width necessary to model the tsunami data. For example, a 70-km fault width is used by Ihmlé (1996a) in analyzing the 1992 Nicaragua event, whereas Satake (1994a) indicates that 40 km is necessary to explain the tide gauge data for that event. Similarly, a 60-km fault width is used in the seismic analysis by Beckers and Lay (1995) for the 1992 Flores event, whereas Imamura *et al.* (1995) use a fault width of 25 km to model the tsunami. This seemingly consistent discrepancy in fault width between the seismic and tsunami models can be at least partially accounted for if mechanics-based slip distributions (Section 8.3) are used for the tsunami modeling, rather than presupposing uniform (average) slip.

For models that resolve distinct subevents, along-strike variations in slip are as much as an order of magnitude. Analysis of both seismic and tsunami waves indicates heterogeneous slip distribution for recent tsunamigenic events: the 1992 Nicaragua event (Ihmlé, 1996a), the 1992 Flores event (Beckers and Lay, 1995), and the 1993 Hokkaido event (Takahashi *et al.*, 1995; Satake and Tanioka, 1995; Tanioka *et al.*, 1995; Mendoza and Fukuyama, 1996). For slow earthquakes, Yamashita (1980) indicates that small variations in the initial stress or frictional behavior of the fault can lead to significant rupture heterogeneity, resulting in earthquakes with “multiple components”.

8.3. Mechanics of Shallow Thrust Faults Related to Local Tsunamis

Geist and Dmowska (in preparation) demonstrate that dip-directed distributed slip based on the mechanics of shallow thrust faulting has a significant effect on the waveform of the local tsunami. Dmowska and Kostrov (1973) and Rudnicki and Wu (1995) investigated the mechanics on dip-slip faulting and note that the normal stress acting on the fault is affected for surface and near-surface rupture, hence modifying the characteristic elliptical slip distribution derived from crack models. For example, a comparison of the slip distribution associated with a very shallow ($z_1 = 1.0$ km) imbedded fault and a surface fault is shown in Fig. 32, based on the results of Dmowska and Kostrov (1973) and Rudnicki and Wu (1995). The average slip increases twofold with surface faulting, explaining the observation that tsunami earthquakes occurring on the décollement near the trench have higher slip (Fig. 31). However, there is a less than twofold difference in the vertical surface displacement profiles shown in

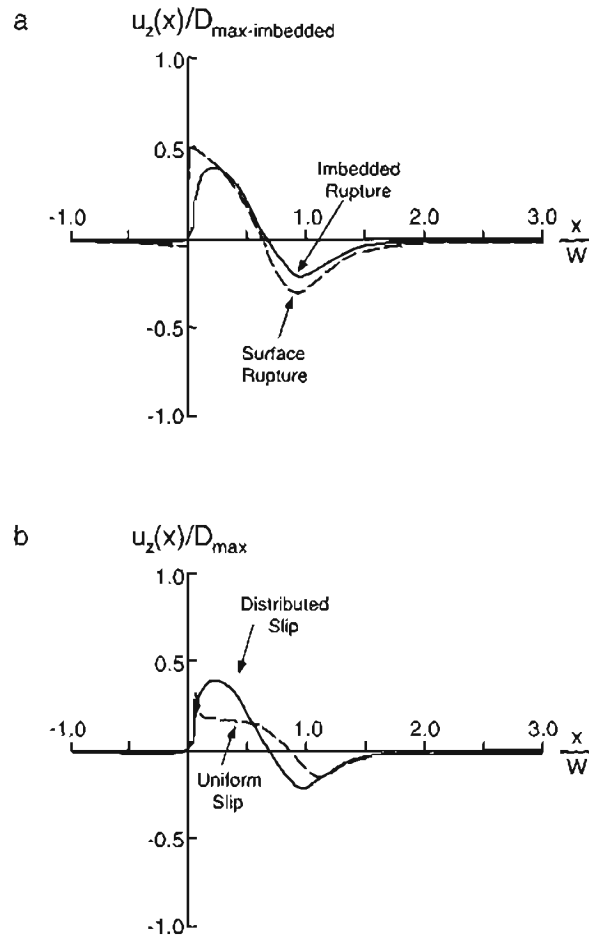


FIG. 33. Comparison of surface displacement profiles for faulting parameters given in Fig. 32. (a) Vertical displacement from shallow imbedded rupture and surface rupture (corresponding slip distribution shown in Fig. 32). (b) Vertical displacement from shallow imbedded rupture (slip distribution shown in Fig. 32) and equivalent uniform slip (equal to the average of the imbedded rupture slip distribution). Vertical displacement normalized with respect to the maximum slip of the imbedded slip distribution. Horizontal distance axis normalized with respect to rupture width. Surface displacement for non-uniform slip calculated using a numerical method described by Freund and Barnett (1976). Surface displacement for uniform slip calculated using the method of Savage and Hastie (1966).

Fig. 33a for the two slip distributions. Shown in Fig. 33b is the surface displacement profile for shallow faulting, assuming uniform slip equal to the average slip of the distribution shown in Fig. 32 (cf., Fig. 21). In general, assuming uniform slip critically underestimates the amplitude and leading-wave steepness of the initial tsunami for imbedded rupture. These results emphasize the fact that accurate slip distributions need to be incorporated into simulation models for local tsunamis. Using a uniform (average) slip distribution is prone to yielding inaccurate results for local tsunamis, especially for shallow events.

8.4. Outstanding Problems

The outstanding unresolved aspects of these earthquakes is explaining why they nucleate at shallow depths and determining the instability conditions for which tsunami earthquakes can occur. Typically, the seismic front designates the seaward extent of the seismogenic zone (Fig. 4; Yoshii, 1979; Byrne et al., 1988). Generally, the sediment near the toe of the accretionary wedge in the region seaward of the seismic front is underconsolidated and does not support spontaneous rupture. Specifically, poorly consolidated sediments are velocity strengthening such that the rate parameter $a - b$ (Dieterich, 1992) is positive and rupture is stably inhibited (Marone and Scholz, 1988; Scholz, 1990). In addition, Vrolijk (1990) and Hyndman and Wang (1993, 1995) have suggested that the seismic front may coincide with the dehydration of smectite and the corresponding mineralogic transition to illite at 110–150°C. Smectite is thought to be the weakest component in subduction zones because of the lubricating effect of water bound between individual phyllosilicate layers (Vrolijk, 1990). The constitutive behavior of faulting within accretionary complexes, however, awaits further sliding experiments specifically designed for clay-bearing fault zones and host rocks. Higher levels of pore pressure at the fault zone decrease the effective normal stress and the shear stress at which Coulomb failure occurs. Instability itself, however, appears to be dependent on frictional dilatancy during rupture, as discussed by Lockner and Byerlee (1994) and Sleep (1995). For fault zones that dilate dynamically during the early stages of rupture, there will be a negative change in pore pressure, stabilizing rupture. Much of what is known about frictional controls on rupture instability is, therefore, seemingly inconsistent with tsunami earthquake rupture within the shallow accretionary wedge.

The conditions for the occurrence of tsunami earthquakes seaward of the ambient seismic front must then involve anomalous and possibly transient properties of the fault zone. Ihmlé (1996a,b) suggests that the frictional properties of the fault zone were the cause of the slow rupture of

both the 1992 Nicaragua event and a previous event (April 3, 1990, $M_w = 6.8$) in the same region. From the perspective of fracture mechanics (Das and Scholz, 1981), rupture propagation for typical earthquakes begins when the stress intensity factor (k) at a crack tip reaches a critical value (K_0). Rupture propagation then accelerates up to a limiting velocity at which $k = K_c$. If however, rupture propagates into a region where $k < K_0$ (requiring fault zone heterogeneity), a slow earthquake would result (Das and Scholz, 1981). Therefore, tsunami earthquake rupture may initiate at depth in a region of instability (velocity-weakening frictional behavior, $k > K_0$) and, consistent with observations, expand up-dip by some as-yet-unresolved dynamic process. The specific frictional constitutive properties that explain the dynamic process of tsunami earthquake rupture in the shallow, near-trench part of the subduction is an important subject for future research.

9. CASE HISTORY: 1992 NICARAGUA EARTHQUAKE AND TSUNAMI

The relative effect of individual source parameters on local tsunamis is summarized by examining the tsunami derived from the 1992 Nicaragua tsunami earthquake (Fig. 34). Modern broadband seismic records of this event have facilitated the determination of the spatial and temporal source process of this event (Section 8.2). Discussion of how individual source parameters relate to tsunami generation and run-up for this event is limited, in large extent, to those parameters that directly influence the local tsunami.

9.1. Geometric and Physical Parameters

The unique location of tsunami earthquakes, such as the 1992 Nicaragua event, along the up-dip extent of the interplate thrust affects the excitation and propagation of the ensuing tsunami. First, the greater water depth at the source area increases the tsunami amplification given by Green's Law over that for a tsunami generated along the continental shelf. However, because the down-dip extent of rupture for the 1992 Nicaragua event is far from the coast, tsunami run-up is not exacerbated by coseismic subsidence as may occur with typical interplate thrust events (Fig. 2). Second, although the fault zone width is poorly constrained by inversion of seismic waves (50–100 km assumed in these studies), tsunami studies (Satake, 1994a; Piatanesi *et al.*, 1996) indicate a narrow (40–50-km) rupture zone under the condition of uniform slip. For a given amount of average slip, reduc-

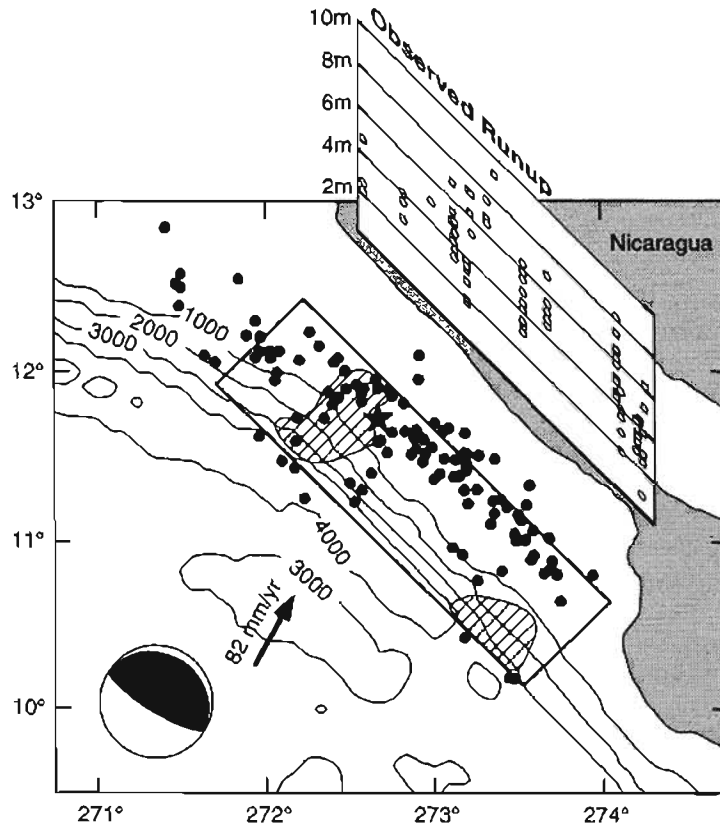


FIG. 34. 1992 M_w 7.7 Nicaragua tsunami earthquake and run-up. Aftershock distribution (solid circles) for three months after main shock and source area considered by Ihlmlé (1996a) shown by rectangle. Shaded areas represent regions of high moment release determined by Ihlmlé (1996a). Mechanism of earthquake shown in lower left corner. Cocos-Caribbean relative plate motion vector (arrow) from DeMets *et al.* (1990). Run-up from field surveys by Abe *et al.* (1993) (open circles) and Baptista *et al.* (1993) (open squares). Note broadside correlation between high moment release at the source and high run-up at the coast. (Ihlmlé, 1996a; modified from *Geophys. Res. Lett.*, © 1996 American Geophysical Union).

tion in the rupture width from that of typical interplate thrust events of comparable magnitude decreases the amount of vertical displacement of the seafloor and the amplitude of the generated tsunami (Fig. 11). Likewise, the shallow dip of the fault plane (16° , Ide *et al.*, 1993; Kikuchi and Kanamori, 1995) corresponds to a reduction in the amplitude of the initial tsunami waveform relative to steeper-dip faults (Fig. 12). It should also be emphasized, however, that these negative effects associated with the geo-

metrical source parameters of tsunami earthquakes are minor in comparison to the positive effect from the high amount of slip associated with these events (Section 9.3).

9.2. Temporal Progression of Rupture

The rise time estimated for the 1992 Nicaragua event by Kikuchi and Kanamori (1995) and Ihmlé (1996a) is less than 20 s and, thus, does not significantly affect local tsunami excitation in comparison to events with shorter rise times. For a rise time of 40 s, as estimated by Ide *et al.* (1993), however, there may be a comparative decrease in the tsunami amplitude as the tsunami leaves the source area (Fig. 26). Most studies agree that the 1992 Nicaragua event involved asymmetric bilateral rupture. Refraction of the local tsunami during shoaling decreases the shoreline-parallel delay in the tsunami arrival time from the comparative delay at the source (i.e., reduction of the amount of wavefront rotation incurred from along-strike rupture propagation). The greater rupture propagation distance to the southeast suggests that directivity effects would have been enhanced in that direction. A directivity analysis by Ihmlé (1996b) also indicates a SE-propagating long-duration component. This directivity effect, in combination with geometric attenuation effects, may explain the relatively larger far-field amplitude (peak-to-trough) recorded offshore Ecuador (0.26–1.12 m) as compared to the amplitude recorded offshore Mexico (0.13–0.16 m) (Ide *et al.*, 1993).

9.3. Magnitude and Distribution of Slip

Estimates of the amount of slip averaged over the rupture area from the seismic moment of the event are dependent on the assumed rupture width. Seismic estimates of average slip range from 0.5 m (Ide *et al.*, 1993) to 1.3 m (Kikuchi and Kanamori, 1995). In contrast, larger amounts of average slip are required to explain the tsunami data (Satake, 1994a; Piatanesi *et al.*, 1996) and, hence, require a narrow fault width and lower shear modulus to match the estimate of seismic moment for the event. The discrepancy between the tsunami and seismic models can to a great extent be resolved if one considers a nonuniform slip distribution from fracture mechanics (Section 8.3). Because vertical deformation is concentrated toward the center of the rupture zone for nonuniform slip distributions, the initial tsunami amplitude is higher in comparison to uniform slip models for the same average amount of slip (Fig. 32). Slip distributions preferred by both Satake (1994a) and Ihmlé (1996a,b) call for higher slip

trenchward of the epicenter, consistent with slip distributions arising from surface rupture (Fig. 31). Realistic slip distributions are important in accurately estimating the local tsunami amplitude, especially for tsunami earthquakes such as the 1992 Nicaragua event.

There is a good agreement between the along-strike variation of slip determined from a least squares fit to the tsunami run-up data (Piatanesi et al., 1996) and the along-strike variation in moment density from inversion of Rayleigh waves (Ihmlé, 1996a). Both studies indicate a high amount of slip to the southeast and moderate slip near the epicenter, with intervening regions of lower slip. Radial spreading smoothes these along-strike variations for the basinward-propagating tsunami. However, as discussed in Section 6.1, the slip variations at the source are largely preserved for the local tsunami, as evident in the variation of run-up along the coast (Fig. 34).

10. CONCLUSIONS

In this study, the relationship between individual earthquake source parameters and tsunami generation has been established. Furthermore, inferences about the effect source parameters ultimately have on local run-up are made possible by the formulation of run-up laws, in particular, the generalized N-wave run-up law of Tadepalli and Synolakis (1994a). The magnitude of the effect on vertical seafloor displacement varies among source parameters, but an upper limit of the maximum seafloor displacement is commonly evident. This upper limit arises from either (1) bounds on the value individual parameters can attain (termed here as *parameter bounding*) or (2) bounds on the effect individual parameters have on seafloor displacement (termed *effect bounding*). An example of parameter bounding is rupture width in which the maximum tsunami amplitude is realized for earthquakes that rupture the entire schizosphere (Fig. 11). An example of effect bounding is dip of the fault plane in which the relative maximum in tsunami run-up is realized for fault dips common in subduction zone settings (approximately 20° – 30° , Fig. 12).

Among the source parameters studied, the magnitude of slip and the spatial variations of slip have a dominant effect on the excitation of local tsunamis. Because the relationship between average slip and seafloor displacement is linear, seafloor displacement is not effect bounded with respect to slip variations. In addition, if slip scales with the length of the rupture zone, slip is parameter bounded only for very long fault lengths (Das, 1988; Yin and Rogers, 1996). If, however, slip scales with the width

of the fault zone, then slip would be parameter bounded (as width is). Although other source parameters may be of secondary importance, their effects can be compounded, leading to significant changes in the generated tsunami. For example, shallow rupture on a gently dipping fault will generate a larger tsunami, compared to deeper rupture on a steeply dipping fault. For this reason, forward modeling of tsunamis is critically dependent on the accuracy of seismologically determined source parameters.

Although the effects of spatial and temporal variations of source parameters were not exhaustively studied, in general, spatial variations seem to have a much greater effect on the tsunami wavefield than do temporal changes. This is easily explained by the fact that, in most cases, the tsunami wave propagation speed is substantially lower than the rupture speed of an earthquake (Satake, 1987). Any substantial changes in the wavefield owing to time-dependent processes such as rupture propagation are further diminished during shoaling of the local tsunami. The effect of long source process times associated with tsunami earthquakes is more important in terms of accurately estimating the seismic moment of the earthquake from seismograms, as indicated by Kanamori (1972).

The hazard from impending local tsunamis can also be addressed from the perspective provided by this source parameter study. As discussed by Geist and Yoshioka (1996), examining the comparative effect of earthquake source parameters relates primarily to estimating the severity of local tsunamis. Aside from bathymetric variations, it is apparent that maximum slip during rupture controls the maximum run-up of the ensuing tsunami, as is evident from the 1992 Nicaragua tsunami (Satake, 1994a; Piatanesi *et al.*, 1996). The average tsunami amplitude associated with various-scenario earthquakes can be grossly estimated by using slip-scaling laws in which the average slip is related to the dimensions of the model rupture zone. One must be careful, however, in using uniform-rupture models to estimate local tsunami hazards, for three reasons: (1) the average slip associated with tsunami earthquakes is greater than that suggested by slip-scaling laws; (2) dip-directed variations in slip and the circumstance of surface rupture strongly affect the initial tsunami waveform; and (3) the maximum tsunami amplitude is ultimately dependent on the maximum of a slip distribution that is observed to be remarkably heterogeneous for subduction zone events. Other components of hazard assessment, such as likelihood, location, and extent, remain even more problematic to forecast. This recognition underscores the importance of efforts to provide real-time estimation of earthquake source parameters for the purpose of providing a rapid and accurate tsunami warning system.

ACKNOWLEDGMENTS

The author is indebted to Dr. Shoichi Yoshioka for providing the finite element program for calculating coseismic displacements. Constructive reviews of the manuscript by Drs. Carlos Mendoza, Renata Dmowska, Kenji Satake, George Carrier, and Bruce Jaffe are gratefully acknowledged. I also thank Anne Rosenthal for her support during the preparation of the manuscript.

APPENDIX

The expressions for vertical surface displacement (u_z) due to shear dislocation along a fault derived by Okada (1985) are given here. The geometry of the source is a rectangular rupture zone of dimensions (L, W) and dip (δ) imbedded in a homogeneous, elastic half-space. The down-dip extent of the rupture zone is at $z = -d$. The strike-slip (U_1) and dip-slip (U_2) components of dislocation in the area of the rupture are spatially invariable. The notation $f(\xi, \eta)$ represents

$$f(\xi, \eta) = f(x, p) - f(x, p - W) - f(x - L, p) + f(x - L, p - W). \quad (3)$$

For the strike-slip component, the vertical displacement normalized with respect to the slip is

$$\frac{u_z}{U_1} = -\frac{1}{2\pi} \left[\frac{\tilde{d}q}{R(R + \eta)} + \frac{q \sin \delta}{R + \eta} + I_4 \sin \delta \right], \quad (4)$$

where

$$\begin{cases} I_4 = \frac{\mu}{\lambda + \mu \cos \delta} \frac{1}{\delta} [\ln(R + \tilde{d}) - \sin \delta \ln(R + \eta)], & \cos \delta \neq 0 \\ I_4 = -\frac{\mu}{\lambda + \mu} \frac{q}{R + \tilde{d}}, & \cos \delta = 0. \end{cases} \quad (5)$$

For the dip-slip component,

$$\frac{u_z}{U_2} = -\frac{1}{2\pi} \left[\frac{\tilde{d}q}{R(R + \xi)} + \sin \delta \tan^{-1} \frac{\xi \eta}{qR} - I_3 \sin \delta \cos \delta \right], \quad (6)$$

where

$$\begin{cases} I_s = \frac{\mu}{\lambda + \mu} \frac{2}{\cos \delta} \tan^{-1} \left[\frac{\eta(X + q \cos \delta) + X(R + X) \sin \delta}{\xi(R + X) \cos \delta} \right], & \cos \delta \neq 0 \\ I_s = -\frac{\mu}{\lambda + 2.02\mu} \frac{\xi \sin \delta}{R + \bar{d}}, & \cos \delta = 0. \end{cases}$$

In all of these expressions,

$$\begin{cases} p = y \cos \delta + d \sin \delta \\ q = y \sin \delta - d \cos \delta \\ \bar{d} = \eta \sin \delta - q \cos \delta \\ R^2 = \xi^2 + \eta^2 + q^2 \\ X^2 = \xi^2 + q^2. \end{cases}$$

REFERENCES

- Abe, K. (1972). Mechanisms and tectonic implications of the 1966 and 1970 Peru earthquakes. *Phys. Earth Planet. Inter.* 5, 367-379.
- Abe, K. (1973). Tsunami and mechanisms of great earthquakes. *Phys. Earth Planet. Inter.* 7, 143-153.
- Abe, K. (1979). Size of great earthquakes of 1837-1974 inferred from tsunami data. *J. Geophys. Res.* 84, 1561-1568.
- Abe, K. (1995). Estimate of tsunami run-up heights from earthquake magnitudes. In "Tsunami: Progress in Prediction, Disaster Prevention and Warning" (Y. Tsuchiya and N. Shuto, eds), Kluwer Academic Publishers, Dordrecht, The Netherlands, pp. 21-35.
- Abe, K., and Ishii, H. (1980). Propagation of tsunami on a linear slope between two flat regions. Part II reflection and transmission. *J. Phys. Earth* 28, 543-552.
- Abe, Ku., Abe, Ka., Tsuji, Y., Imamura, F., Katao, H., Iio, Y., Satake, K., Bourgeois, J., Noguera, E., and Estrada, F. (1993). Field survey of the Nicaragua earthquake and tsunami of September 2, 1992. *Bull. Earthq. Res. Inst.* 68, 23-70.
- Aida, I. (1969). Numerical experiments for the tsunami propagation—the 1964 Niigata tsunami and the 1968 Tokachi-Oki tsunami. *Bull. Earthq. Res. Inst.* 47, 673-700.
- Aida, I. (1978). Reliability of a tsunami source model derived from fault parameters. *J. Phys. Earth* 26, 57-73.
- Aida, I. (1983). Numerical simulation of historical tsunamis generated off the Tokai District in Central Japan. In "Tsunamis: Their Science and Engineering" (J. Iida and T. Iwasaki, eds.), Terra Science Pub. Co., Tokyo/Reidel, Dordrecht, pp. 277-291.
- Aki, K., and Richards, P. G. (1980). "Quantitative Seismology: Theory and Methods." W. H. Freeman and Co., San Francisco.
- Ando, M. (1975). Possibility of a major earthquake in the Tokai District, Japan, and its pre-estimated seismotectonic effects. *Tectonophysics* 25, 69-85.

- Ando, M. (1982). A fault model of the 1946 Nankaido earthquake derived from tsunami data. *Phys. Earth Planet. Inter.* **28**, 320-336.
- Andrews, D. J. (1976). Rupture velocity of plane strain shear cracks. *J. Geophys. Res.* **81**, 5679-5687.
- Antunes do Carmo, J. S., and Seabra-Santos, F. J. (1996). On breaking waves and wave-current interaction in shallow water: A 2DH finite element model. *Int. J. Num. Methods in Fluids* **22**, 429-444.
- Baptista, A. M., Priest, G. R., and Murty, T. S. (1993). Field survey of the 1992 Nicaragua tsunami. *Marine Geodesy* **16**, 169-203.
- Beck, S. L., and Christensen, D. H. (1991). Rupture process of the February 4, 1965, Rat Islands earthquake. *J. Geophys. Res.* **96**, 2205-2221.
- Beck, S., and Ruff, L. J. (1984). The rupture process of the great 1979 Colombia earthquake: evidence from the asperity model. *J. Geophys. Res.* **89**, 9281-9291.
- Beck, S. L., and Ruff, L. J. (1989). Great earthquakes and subduction along the Peru trench. *Phys. Earth Planet. Inter.* **57**, 199-224.
- Beckers, J., and Lay, T. (1995). Very broadband seismic analysis of the 1992 Flores, Indonesia, earthquake ($M_w = 7.9$). *J. Geophys. Res.* **100**, 18,179-18,193.
- Beeler, N. M., and Tullis, T. E. (1996). Self-healing slip pulses in dynamic rupture models due to velocity-dependent strength. *Bull. Seismol. Soc. Am.* **86**, 1130-1148.
- Ben-Menahem, A., and Rosenman, M. (1972). Amplitude patterns of tsunami waves from submarine earthquakes. *J. Geophys. Res.* **77**, 3097-3128.
- Ben-Menahem, A., and Toksöz, M. N. (1963). Source mechanism from spectra of long period surface waves. *J. Geophys. Res.* **68**, 5207-5222.
- Ben-Zion, Y., and Rice, J. R. (1995). Slip patterns and earthquake populations along different classes of faults in elastic solids. *J. Geophys. Res.* **100**, 12,959-12,983.
- Berberian, M. (1982). Aftershock tectonics of the 1978 Tabas-e-Golshan (Iran) earthquake sequence: a documented active 'thin- and thick-skinned tectonic' case. *Geophys. J. R. Astr. Soc.* **68**, 499-530.
- Beroza, G. C. (1995). Seismic source modeling. *Rev. Geophys. Supplement, U.S. Nat. Rep. Int. Union of Geodesy and Geophys.* **1991-1994**, 299-308.
- Beroza, G. C., and Jordan, T. H. (1990). Searching for slow and silent earthquakes using free oscillations. *J. Geophys. Res.* **95**, 2485-2510.
- Beroza, G. C., and Mikumo, T. (1996). Short slip duration in dynamic rupture in the presence of heterogeneous fault properties. *J. Geophys. Res.* **101**, 22,449-22,460.
- Bilham, R., and King, G. (1989). The morphology of strike-slip faults: examples from the San Andreas fault, California. *J. Geophys. Res.* **94**, 10,204-10,216.
- Boatwright, J. (1984). Seismic estimates of stress release. *J. Geophys. Res.* **89**, 6961-6968.
- Boatwright, J., and Cocco, M. (1996). Frictional constraints on crustal faulting. *J. Geophys. Res.* **101**, 13,895-13,909.
- Boore, D. M., and Dunbar, W. S. (1977). Effect of the free surface on calculated stress drops. *Bull. Seismol. Soc. Am.* **67**, 1661-1664.
- Bouchon, M. (1980). The motion of the ground during an earthquake 2. The case of a dip slip fault. *J. Geophys. Res.* **85**, 367-375.
- Boyd, T. M., Engdahl, E. R., and Spence, W. (1995). Seismic cycles along the Aleutian arc: Analysis of seismicity from 1957 through 1991. *J. Geophys. Res.* **100**, 621-644.
- Briggs, M. J., Synolakis, C. E., Harkins, G. S., and Hughes, S. T. (1995). Large scale three-dimensional laboratory measurements of tsunami inundation. In "Tsunami: Progress in Prediction, Disaster Prevention and Warning" (Y. Tsuchiya and N. Shuto, eds.), Kluwer Academic Publishers, Dordrecht, The Netherlands, pp. 129-149.

- Byrne, D. E., Davis, D. M., and Sykes, L. R. (1988). Loci and maximum size of thrust earthquakes and the mechanics of the shallow region of subduction zones. *Tectonics* 7, 833-857.
- Carrier, G. F. (1966). Gravity waves on water of variable depth. *J. Fluid Mech.* 24, 641-659.
- Carrier, G. F. (1971). The dynamics of tsunamis. In "Mathematical Problems in the Geophysical Sciences I: Geophysical Fluid Dynamics, Lectures in Applied Mathematics," v. 13 (W. H. Reid, ed.), American Mathematical Society, Providence, Rhode Island, pp. 157-187.
- Carrier, G. F. (1995). On-shelf tsunami generation and coastal propagation. In "Tsunami: Progress in Prediction, Disaster Prevention and Warning" (Y. Tsuchiya and N. Shuto, eds.), Kluwer Academic Publishers, Dordrecht, The Netherlands, pp. 1-20.
- Carrier, G. F., and Greenspan, H. P. (1958). Water waves of finite amplitude on a sloping beach. *J. Fluid Mech.* 17, 97-109.
- Carrier, G. F., and Noiseux, C. F. (1983). The reflection of obliquely incident tsunamis. *J. Fluid Mech.* 133, 147-160.
- Castagna, J. P., Batzle, M. L., and Eastwood, R. L. (1985). Relationships between compressional-wave and shear-wave velocities in clastic silicate rocks. *Geophysics* 50, 571-581.
- Chael, E. P., and Stewart, G. S. (1982). Recent large earthquakes along the Middle American trench and their implications for the subduction process. *J. Geophys. Res.* 87, 329-338.
- Chinnery, M. A. (1961). The deformation of the ground around surface faults. *Bull. Seismol. Soc. Am.* 51, 355-372.
- Chinnery, M. A., and Petrak, J. A. (1968). The dislocation fault model with variable discontinuity. *Tectonophysics* 5, 513-539.
- Chu, K. K., and Abe, T. (1983). Tsunami run-up and back-wash on a dry bed. In "Tsunamis: Their Science and Engineering" (J. Iida and T. Iwasaki, eds.), Terra Science Pub. Co., Tokyo/Reidel, Dordrecht, pp. 453-466.
- Cochard, A., and Madariaga, R. (1996). Complexity of seismicity due to highly rate-dependent friction. *J. Geophys. Res.* 101, 25,321-25,336.
- Comer, R. P. (1984). Tsunami generation: a comparison of traditional and normal mode approaches. *Geophys. J. R. Astron. Soc.* 77, 29-41.
- Cotton, F., and Campillo, M. (1995). Stability of rake during the 1992, Landers earthquake. An indication for a small stress release? *Geophys. Res. Lett.* 22, 1921-1924.
- Cowie, P. A., and Scholz, C. H. (1992a). Physical explanation for the displacement-length relationship of faults using a post-yield fracture mechanics model. *J. Struct. Geol.* 14, 1133-1148.
- Cowie, P. A., and Scholz, C. H. (1992b). Displacement-length scaling relationship for faults: data synthesis and discussion. *J. Struct. Geol.* 14, 1149-1156.
- Crouch, S. L., and Starfield, A. M. (1983). "Boundary Element Methods in Solid Mechanics." Allen and Unwin, Winchester, Massachusetts.
- Das, S. (1981). Three-dimensional rupture propagation and implications for the earthquake source mechanism. *Geophys. J. R. Astron. Soc.* 67, 375-393.
- Das, S. (1988). Relation between average slip and average stress drop for rectangular faults with multiple asperities. *Bull. Seismol. Soc. Am.* 78, 924-930.
- Das, S., and Aki, K. (1977). Fault plane with barriers: a versatile earthquake model. *J. Geophys. Res.* 82, 5648-5670.
- Das, S., and Kostrov, B. V. (1986). Fracture of a single asperity on a finite fault: a model for weak earthquakes? In "Earthquake Source Mechanics" (S. Das, J. Boatwright, and C. H. Scholz, eds.), *Geophysical Monograph* 37, pp. 91-96, Am. Geophys. Union, Washington, D.C.
-

- Das, S., and Scholz, C. H. (1981). Theory of time-dependent rupture in the earth. *J. Geophys. Res.* 86, 6039-6051.
- Das, S., and Scholz, C. H. (1983). Why large earthquakes do not nucleate at shallow depths. *Nature* 305, 621-623.
- Das, S., and Suhadolc, P. (1996). On the inverse problem for earthquake rupture: the Haskell-type source model. *J. Geophys. Res.* 101, 5725-5738.
- DeMets, C., Gordon, R. G., Argus, D. F., and Stein, S. (1990). Current plate motions. *Geophys. J. Int.* 101, 425-478.
- Deng, J., and Sykes, L. R. (1996). Triggering of 1812 Santa Barbara earthquake by a great San Andreas shock: implications for future seismic hazards in southern California. *Geophys. Res. Lett.* 23, 1155-1158.
- Dieterich, J. H. (1992). Earthquake nucleation on faults with rate- and state-dependent strength. *Tectonophysics* 211, 115-134.
- Dmowska, R. and Kostrov, B. V. (1973). A shearing crack in a semi-space under plane strain conditions. *Archives Mechanics* 25, 421-440.
- Dmowska, R., and Lovison, L. C. (1988). Intermediate term seismic precursors for some coupled subduction zones. *Pageoph.* 126, 643-664.
- Dmowska, R., and Rice, J. R. (1986). Fracture theory and its seismological applications. In "Continuum Theories in Solid Earth Physics" (R. Teisseyre, ed.), Elsevier, Amsterdam, pp. 187-255.
- Dmowska, R., Zheng, G., and Rice, J. R. (1996). Seismicity and deformation at convergent margins due to heterogeneous coupling. *J. Geophys. Res.* 101, 3015-3029.
- Ebel, J. E. (1980). Source processes of the 1965 New Hebrides Islands earthquakes inferred from teleseismic waveforms. *Geophys. J. R. Astr. Soc.* 63, 381-403.
- Freund, L. B. and Barnett, D. M. (1976). A two-dimensional analysis of surface deformation due to dip-slip faulting. *Bull. Seism. Soc. Am.* 66, 667-675.
- Fukao, Y. (1979). Tsunami earthquakes and subduction processes near deep-sea trenches. *J. Geophys. Res.* 84, 2303-2314.
- Fukao, Y., and Furumoto, M. (1985). Hierarchy in earthquake size distribution. *Phys. Earth Planet. Inter.* 37, 149-168.
- Fuller, J. D., and Mysak, L. A. (1977). Edge waves in the presence of an irregular coastline. *J. Phys. Oceanogr.* 7, 846-855.
- Furumoto, A. S. (1991). Source parameters of destructive tsunamis. *Science of Tsunami Hazards* 9, 95-113.
- Geist, E. L., and Dmowska, R. (in prep.). Local tsunamis and continuously distributed slip at the source.
- Geist, E. L., and Scholl, D. W. (1992). Application of continuum models to deformation of the Aleutian island arc. *J. Geophys. Res.* 97, 4953-4967.
- Geist, E. L., and Yoshioka, S. (1996). Source parameters controlling the generation and propagation of potential local tsunamis along the Cascadia margin. *Natural Hazards* 13, 151-177.
- Gonzalez, F. I., Bernard, E. N., and Satake, K. (1995a). The Cape Mendocino tsunami, 25 April 1992. In "Tsunamis: Progress in Prediction, Disaster Prevention and Warning" (Y. Tsuchiya and N. Shuto, eds.), Kluwer Academic Publishers, Dordrecht, The Netherlands, pp. 151-158.
- Gonzalez, F. I., Satake, K., Boss, F., and Mojfeld, H. O. (1995b). Edge wave and non-trapped modes of the 25 April 1992 Cape Mendocino tsunami. *Pageoph.* 144, 409-426.
- Goto, C., and Shuto, N. (1983). Numerical simulation of tsunami propagation and run-up. In "Tsunamis: Their Science and Engineering" (J. Iida and T. Iwasaki, eds.), Terra Science Pub. Co., Tokyo/Reidel, Dordrecht, pp. 439-451.

- Greenberg, D. A., Murty, T. S., and Ruffman, A. (1993). A numerical model for the Halifax Harbor tsunami due to the 1917 explosion. *Marine Geodesy* 16, 153–167.
- Gregory, A. R. (1976). Fluid saturation effects on dynamic elastic properties of sedimentary rocks. *Geophysics* 41, 895–921.
- Hammack, J. L. (1973). A note on tsunamis: their generation and propagation in an ocean of uniform depth. *J. Fluid Mech.* 60, 769–799.
- Harris, R. A., and Simpson, R. W. (1992). Changes in static stress on southern California faults after the 1992 Landers earthquake. *Nature* 360, 251–254.
- Hartzell, S., and Langer, C. (1993). Importance of model parameterization in finite fault inversions: application to the 1974 M_w 8.0 Peru earthquake. *J. Geophys. Res.* 98, 22,123–22,134.
- Hashimoto, M. (1982). Numerical modeling of the three-dimensional stress field in southwestern Japan. *Tectonophysics* 84, 247–266.
- Haskell, N. A. (1964). Total energy and energy spectral density of elastic wave radiation from propagating faults. *Bull. Seismol. Soc. Am.* 54, 1811–1841.
- Heaton, T. H. (1990). Evidence for and implications of self-healing pulses of slip in earthquake rupture. *Phys. Earth. Planet. Inter.* 64, 1–20.
- Hwang, L., and Divoky, D. (1970). Tsunami generation. *J. Geophys. Res.* 75, 6802–6817.
- Hwang, L. J., and Kanamori, H. (1986). Source parameters of the May 7, 1986 Andreanof Islands earthquake. *Geophys. Res. Lett.* 13, 1426–1429.
- Hyndman, R. D., and Wang, K. (1993). Thermal constraints on the zone of major thrust earthquake failure: The Cascadia subduction zone. *J. Geophys. Res.* 98, 2039–2060.
- Hyndman, R. D., and Wang, K. (1995). The rupture zone of Cascadia great earthquake from current deformation and the thermal regime. *J. Geophys. Res.* 100, 22,133–22,154.
- Ide, S., Imamura, F., Yoshida, Y., and Abe, K. (1993). Source characteristics of the Nicaraguan tsunami earthquakes of September 2, 1992. *Geophys. Res. Lett.* 20, 863–866.
- Ihmlé, P. F. (1996a). Monte Carlo slip inversion in the frequency domain: Application to the 1992 Nicaragua slow earthquake. *Geophys. Res. Lett.* 23, 913–916.
- Ihmlé, P. F. (1996b). Frequency-dependent relocation of the 1992 Nicaragua slow earthquake: an empirical Green's function approach. *Geophys. J. Int.* 127, 75–85.
- Imamura, F., Gica, E., Takahashi, To., and Shuto, N. (1995). Numerical simulation of the 1992 Flores tsunami: interpretation of tsunami phenomena in northeastern Flores Island and damage at Babi Island. *Pageoph.* 144, 555–568.
- Ishii, H., and Abe, K. (1980). Propagation of tsunami on a linear slope between two flat regions. Part I edge wave. *J. Phys. Earth* 28, 531–541.
- Jarrard, R. D. (1986). Relations among subduction parameters. *Rev. Geophys.* 24, 217–284.
- Johnson, J. M., and Satake, K. (1993). Source parameters of the 1957 Aleutian earthquake from tsunami waveforms. *Geophys. Res. Lett.* 20, 1487–1490.
- Johnson, J. M., and Satake, K. (1994). Rupture extent of the 1938 Alaskan earthquake as inferred from tsunami waveforms. *Geophys. Res. Lett.* 21, 733–736.
- Johnson, J. M., and Satake, K. (1997). Estimation of seismic moment and slip distribution of the 1 April 1946 Aleutian tsunami earthquake. *J. Geophys. Res.* 102, 11,765–11,774.
- Johnson, J. M., Satake, K., Holdahl, S. R., and Sauber, J. (1996). The 1964 Prince William Sound earthquake: Joint inversion of tsunami and geodetic data. *J. Geophys. Res.* 101, 523–532.
- Jones, C. H., and Wesnousky, S. G. (1992). Variations in strength and slip rate along the San Andreas fault system. *Science* 256, 83–86.

- Kagan, Y. Y. (1994). Incremental stress and earthquakes. *Geophys. J. Int.* **117**, 345-364.
- Kajiura, K. (1963). The leading wave of a tsunami. *Bull. Earthquake Res. Inst.* **41**, 535-571.
- Kajiura, K. (1970). Tsunami source, energy and the directivity of wave radiation. *Bull. Earthquake Res. Inst.* **48**, 835-869.
- Kajiura, K. (1981). Tsunami energy in relation to parameters of the earthquake fault model. *Bull. Earthquake Res. Inst.* **56**, 415-440.
- Kanamori, H. (1971). Focal mechanism of the Tokachi-Oki earthquake of May 16, 1968: contortion of the lithosphere at a junction of two trenches. *Tectonophysics* **12**, 1-13.
- Kanamori, H. (1972). Mechanism of tsunami earthquakes. *Phys. Earth Planet. Inter.* **6**, 346-359.
- Kanamori, H. (1977). The energy release in great earthquakes. *J. Geophys. Res.* **82**, 2981-2987.
- Kanamori, H. (1981). The nature of seismicity patterns before large earthquakes. In "Earthquake Prediction: An International Review" (D. Simpson and P. Richards, eds.), Maurice Ewing Series 4, Am. Geophys. Union, Washington, D.C., pp. 1-19.
- Kanamori, H., and Given, J. W. (1981). Use of long-period surface waves for fast determination of earthquake source parameters. *Phys. Earth Planet. Inter.* **27**, 8-31.
- Kanamori, H., and Kikuchi, M. (1993). The 1992 Nicaragua earthquake: a slow tsunami earthquake associated with subducted sediments. *Nature* **361**, 714-716.
- Kanamori, H., and Stewart, G. S. (1979). A slow earthquake. *Phys. Earth Planet. Inter.* **18**, 167-175.
- Keller, J. B., and Keller, H. B. (1964). "Water wave run-up on a beach." ONR Research Rep. Contract NONR-3828(00). Dept. of the Navy, Washington, D.C.
- Kikuchi, M., and Fukao, Y. (1987). Inversion of long-period P-wave from great earthquakes along subduction zones. *Tectonophysics* **144**, 231-247.
- Kikuchi, M., and Kanamori, H. (1995). Source characteristics of the 1992 Nicaragua tsunami earthquake inferred from teleseismic body waves. *Pageoph.* **144**, 441-454.
- Knopoff, L. (1958). Energy release in earthquakes. *Geophys. J.* **1**, 44-52.
- Kostrov, B. V., and Das, S. (1984). Evaluation of stress and displacement fields due to an elliptical plane shear crack. *Geophys. J. Royal Astr. Soc.* **77**, 915-933.
- Kowalik, Z., and Whitmore, P. M. (1991). An investigation of two tsunamis recorded at Adak, Alaska. *Science of Tsunami Hazards* **9**, 67-83.
- Lay, T., and Kanamori, H. (1980). Earthquake doublets in the Solomon Islands. *Phys. Earth Planet. Inter.* **2**, 283-304.
- Lay, T., and Wallace, T. C. (1995). "Modern Global Seismology." Academic Press, San Diego.
- Lay, T., Kanamori, H., and Ruff, L. (1982). The asperity model and the nature of large subduction zone earthquakes. *Earthquake Prediction Res.* **1**, 3-71.
- LeBlond, P. H., and Mysak, L. A. (1978). "Waves in the Ocean." Elsevier Oceanography Series, v. 20, Amsterdam.
- Li, X., and Nábelek, J. (1996). Detecting slow, long-duration slip of large earthquakes using very long-period orbital surface waves. *Geophys. J. Int.* **124**, 483-501.
- Linde, A. T., and Silver, P. G. (1989). Elevation changes and the Great 1960 Chilean earthquake: Support for aseismic slip. *Geophys. Res. Lett.* **16**, 1305-1308.
- Liu, P. L.-F., and Earickson, J. (1983). A numerical model for tsunami generation and propagation. In "Tsunamis: Their Science and Engineering" (J. Iida and T. Iwasaki, eds.), Terra Science Pub. Co., Tokyo/Reidel, Dordrecht, pp. 227-240.
- Liu, P. L.-F., Synolakis, C., and Yeh, H. H. (1991). Report on the international workshop on long-wave run-up. *J. Fluid Mech.* **229**, 675-688.
- Lockner, D. A., and Byerlee, J. D. (1994). Dilatancy in hydraulically isolated faults and the suppression of instability. *Geophys. Res. Lett.* **21**, 2353-2356.

- Lockridge, P. A., and Smith, R. H. (1984). "Tsunamis in the Pacific Basin. 1900-1983." Nat. Geophys. Data Center, NOAA.
- Ma, X. Q., and Kusznir, N. J. (1992). 3-D subsurface displacement and strain fields for faults and fault arrays in a layered elastic half-space. *Geophys. J. Int.* 111, 542-558.
- Ma, X. Q., and Kusznir, N. J. (1994). Effects of rigidity layering, gravity and stress relaxation on 3-D subsurface fault displacement fields. *Geophys. J. Int.* 118, 201-220.
- Madariaga, R. (1976). Dynamics of an expanding circular fault. *Bull. Seismol. Soc. Am.* 32, 305-330.
- Mader, C. L., and Curtis, G. (1991). Modeling Hilo, Hawaii tsunami inundation. *Sci. Tsunami Haz.* 9, 85-94.
- Main, I. (1996). Statistical physics, seismogenesis, and seismic hazard. *Rev. Geophys.* 34, 433-462.
- Malvern, L. E. (1969). "Introduction to the Mechanics of a Continuous Medium." Prentice-Hall, Englewood Cliffs, New Jersey.
- Marone, C., and Scholz, C. H. (1988). The depth of seismic faulting and the upper transition from stable to unstable slip regimes. *Geophys. Res. Lett.* 15, 621-624.
- McCaffrey, R. (1992). Oblique plate convergence, slip vectors and forearc deformation. *J. Geophys. Res.* 97, 8905-8915.
- McCaffrey, R. (1993). On the role of the upper plate in great subduction zone earthquakes. *J. Geophys. Res.* 98, 11,953-11,966.
- McHugh, S., and Johnston, M. (1977). Surface shear stress, strain, and shear displacement for screw dislocations in a vertical slab with shear modulus contrast. *Geophys. J. R. Astr. Soc.* 49, 715-722.
- Mei, C. C. (1983). "The Applied Dynamics of Ocean Surface Waves." Wiley, New York.
- Melosh, H. J., and Raefsky, A. (1981). A simple and efficient method for introducing faults into finite element computations. *Bull. Seismol. Soc. Am.* 71, 1391-1400.
- Melosh, H. J., and Williams, C. A., Jr. (1989). Mechanics of graben formation in crustal rocks: A finite element analysis. *J. Geophys. Res.* 94, 13,961-13,973.
- Mendoza, C. (1993). Coseismic slip of two large Mexican earthquakes from teleseismic body waveforms: Implications for asperity interaction in the Michoacan plate boundary segment. *J. Geophys. Res.* 98, 8197-8210.
- Mendoza, C. (1995). Finite-fault analysis of the 1979 March 14 Petatlan, Mexico, earthquake using teleseismic P waveforms. *Geophys. J. Int.* 121, 675-683.
- Mendoza, C., and Fukuyama, E. (1996). The July 12, 1993, Hokkaido-Nansei-Oki, Japan, earthquake: Coseismic slip pattern from strong-motion and teleseismic recordings. *J. Geophys. Res.* 101, 791-801.
- Mendoza, C., Hartzell, S., and Monfret, T. (1994). Wide-band analysis of the 3 March 1985 central Chile earthquake. *Bull. Seismol. Soc. Am.* 84, 269-283.
- Michael, A. J. (1990). Energy constraints on kinematic models of oblique faulting: Loma Prieta versus Parkfield-Coalinga. *Geophys. Res. Lett.* 17, 1453-1456.
- Momoi, T. (1964). Tsunami in the vicinity of a wave origin (I). *Bull. Earthquake Res. Inst.* 42, 133-146.
- Myers, E. P., and Baptista, A. M. (1995). Finite element modeling of the July 12, 1993 Hokkaido Nansei-Oki Tsunami. *Pageoph.* 144, 769-802.
- Nagano, O., Imamura, F., and Shuto, N. (1991). A numerical model for far-field tsunamis and its application to predict damages done to aquaculture. *Natural Hazards* 4, 235-255.
- Ng, M. K.-F., LeBlond, P. H., and Murty, T. S. (1990). Simulation of tsunamis from great earthquakes on the Cascadia subduction zone. *Science* 250, 1248-1251.

- Niewiadomski, J., and Rybicki, K. (1984). The stress field induced by antiplane shear cracks—Application to earthquake study. *Bull. Earthquake Res. Inst.*, Univ. Tokyo 59, 67–81.
- O'Connell, R. J., and Budiansky, B. (1977). Viscoelastic properties of fluid-saturated cracked solids. *J. Geophys. Res.* 82, 5719–5735.
- Okada, Y. (1985). Surface deformation due to shear and tensile faults in a half-space. *Bull. Seismol. Soc. Am.* 75, 1135–1154.
- Okada, Y. (1992). Internal deformation due to shear and tensile faults in a half-space. *Bull. Seismol. Soc. Am.* 82, 1018–1040.
- Okal, E. A. (1982). Mode-wave equivalence and other asymptotic problems in tsunami theory. *Phys. Earth Planet. Inter.* 30, 1–11.
- Okal, E. A. (1988). Seismic parameters controlling far-field tsunami amplitudes: a review. *Natural Hazards* 1, 67–96.
- Okal, E. A. (1993). Predicting large tsunamis. *Nature* 361, 686–687.
- Okal, E. A., and Romanowicz, B. A. (1994). On the variation of *b*-values with earthquake size. *Phys. Earth Planet. Inter.* 87, 55–76.
- Okal, E. A., and Talandier, J. (1986). T-wave duration, magnitudes and seismic moment of an earthquake—application to tsunami warning. *J. Phys. Earth* 34, 19–42.
- Pacheco, J. F., and Sykes, L. R. (1992). Seismic moment catalog of large shallow earthquakes, 1900 to 1989. *Bull. Seismol. Soc. Am.* 82, 1306–1349.
- Pacheco, J. F., Sykes, L. R., and Scholz, C. H. (1993). Nature of seismic coupling along simple plate boundaries of the subduction type. *J. Geophys. Res.* 98, 14,133–14,159.
- Pelayo, A. M., and Wiens, D. A. (1990). The November 20, 1960 Peru tsunami earthquake: Source mechanism of a slow event. *Geophys. Res. Lett.* 17, 661–664.
- Pelayo, A. M., and Wiens, D. A. (1992). Tsunami earthquakes: slow thrust-faulting events in the accretionary wedge. *J. Geophys. Res.* 97, 15,321–15,337.
- Pelinovsky, E. N., and Mazova, R. Kh. (1992). Exact analytical solutions of nonlinear problems of tsunami wave run-up on slopes with different profiles. *Natural Hazards* 6, 227–249.
- Peraire, J., Zienkiewicz, O. C., and Morgan, K. (1986). Shallow water problems: a general explicit formulation. *Int. J. Num. Methods in Engineering* 22, 547–574.
- Peregrine, D. H. (1967). Long waves on a beach. *J. Fluid Mech.* 27, 815–827.
- Piatanesi, A., Tinti, S., and Gavagni, I. (1996). The slip distribution of the 1992 Nicaragua earthquake from tsunami run-up data. *Geophys. Res. Lett.* 23, 37–40.
- Pollitz, F. F. (1996). Coseismic deformation from earthquake faulting on a layered spherical earth. *Geophys. J. Int.* 125, 1–14.
- Reasenber, P. A., and Simpson, R. W. (1992). Response of regional seismicity to the static stress change produced by the Loma Prieta earthquake. *Science* 255, 1687–1690.
- Rice, J. R., and Ben-Zion, Y. (1996). Slip complexity in earthquake fault models. *Proc. Nat. Acad. Sci., USA* 93, 3811–3818.
- Romanowicz, B., and Rundle, J. B. (1993). On scaling relations for large earthquakes. *Bull. Seism. Soc. Am.* 83, 1294–1297.
- Rudnicki, J. W. and Wu, M. (1995). Mechanics of dip-slip faulting in an elastic half-space. *J. Geophys. Res.* 100, 22,173–22,186.
- Ruff, L. J. (1987). Tomographic imaging of seismic sources. In “Seismic Tomography” (G. Nolet, ed.), D. Reidel, Dordrecht, pp. 339–366.
- Ruff, L. J. (1992). Asperity distributions and large earthquake occurrence in subduction zones. *Tectonophysics* 211, 61–83.
- Ruff, L. J., and Kanamori, H. (1983). Seismic coupling and uncoupling at subduction zones. *Tectonophysics* 99, 99–117.

- Ruff, L. J., and Miller, A. D. (1994). Rupture process of large earthquakes in the northern Mexico subduction zone. *Pageoph.* 142, 101-171.
- Rundle, J. B., and Klein, W. (1995). New ideas about physics of earthquakes. *Rev. Geophys. Supplement*, U.S. Nat. Rep. Int. Union of Geodesy and Geophys. 1991-1994, 283-286.
- Rybicki, K. (1978). Static deformation of a laterally inhomogeneous half-space by a two-dimensional strike-slip fault. *J. Phys. Earth* 26, 351-366.
- Rybicki, K. (1986). Dislocations and their geophysical application. In "Continuum Theories in Solid Earth Physics" (R. Teisseyre, ed.), Elsevier, Amsterdam, pp. 18-186.
- Rydelek, P. A., and Sacks, I. S. (1996). Earthquake slip rise time and rupture propagation: numerical results of the quantum earthquake model. *Bull. Seismol. Soc. Am.* 86, 567-574.
- Satake, K. (1985). The mechanism of the 1983 Japan Sea earthquake as inferred from long-period surface waves and tsunamis. *Phys. Earth Planet. Inter.* 37, 249-260.
- Satake, K. (1987). Inversion of tsunami waveforms for the estimation of a fault heterogeneity: Method and numerical experiments. *J. Phys. Earth* 35, 241-254.
- Satake, K. (1989). Inversion of tsunami waveforms for the estimation of heterogeneous fault motion of large submarine earthquakes: The 1968 Tokachi-Oki and the 1983 Japan Sea earthquakes. *J. Geophys. Res.* 94, 5627-5636.
- Satake, K. (1993). Depth distribution of coseismic slip along the Nankai trough, Japan, from joint inversion of geodetic and tsunami data. *J. Geophys. Res.* 98, 4553-4565.
- Satake, K. (1994a). Mechanism of the 1992 Nicaragua tsunami earthquake. *Geophys. Res. Lett.* 21, 2519-2522.
- Satake, K. (1994b). Earthquake scenario study with regional tsunami model. In "Tsunami Inundation Model Study of Eureka and Crescent City" (E. Bernard, C. Mader, G. Curtis, and K. Satake), NOAA Tech. Memorandum ERL PMEL-103, Seattle, Washington, pp. 43-65.
- Satake, K. (1995). Linear and nonlinear computations of the 1992 Nicaragua earthquake tsunami. *Pageoph.* 144, 455-470.
- Satake, K., and Imamura, F. (1995). Introduction to "Tsunamis: 1992-94". *Pageoph.* 144, 373-379.
- Satake, K., and Kanamori, H. (1991). Use of tsunami waveforms for earthquake source study. *Natural Hazards* 4, 193-208.
- Satake, K., and Shimazaki, K. (1987). Computation of tsunami waveforms by a superposition of normal modes. *J. Phys. Earth* 35, 409-414.
- Satake, K., and Shimazaki, K. (1988). Free oscillation of the Japan Sea excited by earthquakes -II. Modal approach and synthetic tsunamis. *Geophys. J.* 93, 457-463.
- Satake, K., and Tanioka, Y. (1995). Tsunami generation of the 1993 Hokkaido Nansei-Oki earthquake. *Pageoph.* 144, 803-821.
- Sato, S. (1996). Numerical simulation of the propagation of the 1993 southwest Hokkaido earthquake tsunami around Okushiri Island. *Sci. Tsunami Haz.* 14, 119-134.
- Savage, J. C. (1987). Effect of crustal layering upon dislocation modeling. *J. Geophys. Res.* 92, 10,595-10,600.
- Savage, J. C., and Hastie, L. M. (1966). Surface deformation associated with dip-slip faulting. *J. Geophys. Res.* 71, 4897-4904.
- Schindelé, F., Reymond, D., Gaucher, E., and Okal, E. A. (1995). Analysis and automatic processing in near-field of eight 1992-1994 tsunamigenic earthquakes: Improvements towards real-time tsunami warning. *Pageoph.* 144, 381-408.
- Scholz, C. H. (1982). Scaling laws for large earthquakes: consequences for physical models. *Bull. Seismol. Soc. Am.* 72, 1-14.

- Scholz, C. H. (1989). Mechanics of faulting. *Ann. Rev. Earth Planet. Sci.* 17, 309-334.
- Scholz, C. H. (1990). "The Mechanics of Earthquakes and Faulting." Cambridge Univ. Press, Cambridge, England.
- Scholz, C. H. (1994). A reappraisal of large earthquake scaling. *Bull. Seismol. Soc. Am.* 84, 215-218.
- Schwartz, D. P., and Coppersmith, K. J. (1984). Fault behavior and characteristic earthquakes: examples from the Wasatch and San Andreas fault zones. *J. Geophys. Res.* 89, 5681-5698.
- Sezawa, K., and Kahai, K. (1939). On shallow water waves transmitted in the direction parallel to a sea coast, with special reference to Love-waves in heterogeneous media. *Bull. Earthquake Res. Inst.* 17, 685-694.
- Shibata, M. (1983). One-dimensional dispersive deformation of tsunami with typical initial profiles on continental topographies. In "Tsunamis: Their Science and Engineering" (J. Iida and T. Iwasaki, eds.), Terra Science Pub. Co., Tokyo/Reidel, Dordrecht, pp. 241-250.
- Shimazaki, K. (1974). Nemuro-Oki earthquake of June 17, 1973: A lithospheric rebound at the upper half of interface. *Phys. Earth Planet. Inter.* 39, 314-327.
- Shimazaki, K. (1986). Small and large earthquakes: The effects of the thickness of seismogenic layer and the free surface. In "Earthquake Source Mechanics" (S. Das, J. Boatwright, and C. H. Scholz, eds.), *Geophysical Monograph* 37, Am. Geophys. Union, Washington, D.C., pp. 209-216.
- Shimazaki, K., and Nakata, T. (1980). Time-predictable recurrence model for large earthquakes. *Geophys. Res. Lett.* 7, 279-282.
- Shono, K., Mikumo, T., and Ishikawa, Y. (1976). Focal mechanisms of earthquake in Hyuga-nada and Ryukyu arc and their tectonic implications. *Prog. Abst. Seismol. Soc. Japan* 2, 71.
- Shuto, N. (1972). Standing wave in front of a sloping dike, Proc. 13th Conf. on Coastal Eng., ASCE, 1649-1647.
- Shuto, N. (1991). Numerical simulation of tsunamis—Its present and near future. *Natural Hazards* 4, 171-191.
- Shuto, N., Chida, K., and Imamura, F. (1995). Generation mechanism of the first wave of the 1983 Nihonkai-Chubu earthquake tsunami. In "Tsunami: Progress in Prediction, Disaster Prevention and Warning" (Y. Tsuchiya and N. Shuto, eds.), Kluwer Academic Publishers, Dordrecht, The Netherlands, pp. 37-54.
- Silver, P. G., and Jordan, T. H. (1983). Total moment spectra of fourteen large earthquakes. *J. Geophys. Res.* 88, 3273-3293.
- Singh, S. J., Punia, M., and Rani, S. (1994). Crustal deformation due to non-uniform slip along a long fault. *Geophys. J. Int.* 118, 411-427.
- Sleep, N. H. (1995). Ductile creep, compaction, and rate and state dependent friction within major fault zones. *J. Geophys. Res.* 100, 13,065-13,080.
- Spudich, P. A., and Hartzell, S. H. (1985). Predicting earthquake ground-motion time-histories. In "Evaluating Earthquake Hazards in the Los Angeles Region—An Earth-Science Perspective" (J. I. Ziony, ed.), U.S. Geol. Surv. Professional Paper 1360, pp. 249-261.
- Starr, A. T. (1928). Slip in a crystal and rupture in a solid due to shear. *Proc. Camb. Phil. Soc.* 24, 489-500.
- Stein, R. S., King, G. C. P., and Lin, J. (1992). Change in failure stress on the southern San Andreas fault system caused by the 1992 magnitude = 7.4 Landers earthquake. *Science* 258, 1328-1332.
- Stewart, G. S., and Cohn, S. N. (1979). The 1976 August 16, Mindanao, Philippine earthquake (Ms = 7.8): evidence for a subduction zone south of Mindanao. *Geophys. J. R. Astr. Soc.* 57, 51-65.
- Stoney, R. (1964). The propagation of tsunamis. *Geophys. J.* 8, 64-81.

- Swenson, J. L., and Beck, S. L. (1996). Historical 1942 Ecuador and 1942 Peru subduction earthquakes, and earthquake cycles along Colombia-Ecuador and Peru subduction segments. *Pageoph.* 146, 67-101.
- Synolakis, C. E. (1987). The run-up of solitary waves. *J. Fluid Mech.* 185, 523-545.
- Synolakis, C. E. (1991). Tsunami run-up on steep slopes: How good linear theory really is. *Natural Hazards* 4, 221-234.
- Synolakis, C. E., and Skjelbreia, J. E. (1993). Evolution of maximum amplitude of solitary waves on plane beaches. *J. Waterway, Port, Coastal, Ocean Engineering* 119, 323-342.
- Synolakis, C. E., Deb, M. K., and Skjelbreia, J. E. (1987). The anomalous behavior of the run-up of cnoidal waves. *Phys. Fluids* 31, 3-5.
- Tadepalli, S., and Synolakis, C. E. (1994a). The run-up of N-waves on sloping beaches. *Proc. R. Soc. Lond. A* 445, 99-112.
- Tadepalli, S., and Synolakis, C. E. (1994b). A generalized model profile for long wave run-up. *EOS, Transactions, American Geophysical Union* 74 (supplement), 358.
- Takahashi, To., Takahashi, Ta., Shuto, N., Imamura, F., and Ortiz, M. (1995). Source models for the 1993 Hokkaido Nansei-Oki earthquake tsunami. *Pageoph.* 144, 748-767.
- Talandier, J., and Okal, E. A. (1979). Human perception of T waves: the June 22, 1977 Tonga earthquake felt on Tahiti. *Bull. Seismol. Soc. Am.* 69, 1475-1486.
- Talandier, J., and Okal, E. A. (1989). An algorithm for automated tsunami warning in French Polynesia based on mantle magnitudes. *Bull. Seismol. Soc. Am.* 79, 1177-1193.
- Tanioka, Y., and Satake, K. (1996a). Tsunami generation by horizontal displacement of ocean bottom. *Geophys. Res. Lett.* 23, 861-864.
- Tanioka, Y., and Satake, K. (1996b). Fault parameters of the 1896 Sanriku tsunami earthquake estimated from tsunami numerical modeling. *Geophys. Res. Lett.* 23, 1549-1552.
- Tanioka, Y., Satake, K., and Ruff, L. (1995). Total analysis of the 1993 Hokkaido Nanei-Oki earthquake using seismic wave, tsunami, and geodetic data. *Geophys. Res. Lett.* 22, 9-12.
- Tanioka, Y., Ruff, L., and Satake, K. (1996). The Sanriku-Oki, Japan, earthquake of December 28, 1994 (M_w 7.7): Rupture of a different asperity from a previous earthquake. *Geophys. Res. Lett.* 23, 1465-1468.
- Thatcher, W. (1990). Order and diversity in the modes of circum-Pacific earthquake recurrence. *J. Geophys. Res.* 95, 2609-2623.
- Tinti, S., and Piatanesi, A. (1996). Numerical simulations of the tsunami induced by the 1627 earthquake affecting Gargano, southern Italy. *J. Geodynamics* 21, 141-160.
- Togashi, H. (1983). Shoreline wave height and land run-up height of tsunamis on uniformly sloping beaches. In "Tsunamis: Their Science and Engineering" (J. Iida and T. Iwasaki, eds.), Terra Science Pub. Co., Tokyo/Reidel, Dordrecht, pp. 495-509.
- Tse, S. T., and Rice, J. R. (1986). Crustal earthquake instability in relation to the depth variation of frictional slip properties. *J. Geophys. Res.* 91, 9452-9472.
- Tsuboi, S., Abe, K., Takano, K., and Yamanaka, Y. (1995). Rapid determination of M_w from broadband P waveforms. *Bull. Seismol. Soc. Am.* 85, 606-613.
- Tsuji, Y., Imamura, F., Matsutomi, H., Synolakis, C. E., Nanang, P. T., Jumadi, S., Harada, S., Han, S. S., Arai, K., and Cook, B. (1995). Field survey of the east Java earthquake and tsunami of June 3, 1994. *Pageoph.* 144, 839-854.
- Velasco, A. A., Ammon, C. J., Lay, T., and Zhang, J. (1994). Imaging a slow bilateral rupture with broadband seismic waves: the September 2, 1992 Nicaraguan tsunami earthquake. *Geophys. Res. Lett.* 21, 2629-2632.
- Vrolijk, P. (1990). On the mechanical role of smectite in subduction zones. *Geology* 18, 703-707.
- Wang, R., and Wu, H. L. (1983). Displacement and stress fields due to nonuniform slip along a strike slip fault. *Pageoph.* 121, 601-609.

- Ward, S. N. (1980). Relationships of tsunami generation and an earthquake source. *J. Phys. Earth* 28, 441-474.
- Ward, S. N. (1982). On tsunami nucleation II. An instantaneous modulated line source. *Phys. Earth Planet. Inter.* 27, 273-285.
- Wells, D. L., and Coppersmith, K. J. (1994). New empirical relationships among magnitude, rupture length, rupture width, rupture area, and surface displacement. *Bull. Seismol. Soc. Am.* 84, 974-1002.
- Wesnowsky, S. G. (1994). The Gutenberg-Richter or characteristic earthquake distribution, which is it? *Bull. Seismol. Soc. Am.* 84, 1940-1959.
- Whitmore, P. M. (1993). Expected tsunami amplitudes and currents along the North American coast for Cascadia subduction zone earthquakes. *Natural Hazards* 8, 59-73.
- Wu, T. Y. (1981). Long waves in ocean and coastal waters. *J. Engineering Mech. Div., ASCE* 107, 501-521.
- Yalciner, A. C., Kuran, U., Akyarli, A., and Imamura, F. (1995). An investigation of the propagation of tsunamis in the Aegean Sea by mathematical modeling. In "Tsunami: Progress in Prediction, Disaster Prevention and Warning" (Y. Tsuchiya and N. Shuto, eds.), Kluwer Academic Publishers, Dordrecht, The Netherlands, pp. 55-70.
- Yamashita, T. (1976). On the dynamical process of fault motion in the presence of friction and inhomogeneous initial stress, Part I. Rupture propagation. *J. Phys. Earth* 24, 417-444.
- Yamashita, T. (1980). Causes of slow earthquakes and multiple earthquakes. *J. Phys. Earth* 28, 169-190.
- Yamashita, T., and Sato, R. (1974). Generation of tsunami by a fault model. *J. Phys. Earth* 22, 415-440.
- Yang, M., and Toksöz, M. N. (1981). Time dependent deformation and stress relation after strike-slip earthquakes. *J. Geophys. Res.* 86, 2889-2901.
- Yeh, H. H. (1991). Tsunami bore run-up. *Natural Hazards* 4, 209-220.
- Yin, Z. M., and Rogers, G. C. (1996). Toward and physical understanding of earthquake scaling relations. *Pageoph.* 146, 661-675.
- Yoshii, T. (1979). A detailed cross-section of the deep seismic zone beneath northeastern Honshu, Japan. *Tectonophysics* 55, 349-360.
- Yoshioka, S., Hashimoto, M., and Hirahara, K. (1989). Displacement fields due to the 1946 Nankaido earthquake in a laterally inhomogeneous structure with the subducting Philippine Sea plate—a three-dimensional finite element approach. *Tectonophysics* 159, 121-136.
- Zhang, J., Davis, D. M., and Wong, T. (1993). The brittle-ductile transition in porous sedimentary rocks: geological implications for accretionary wedge aseismicity. *J. Struct. Geol.* 15, 819-830.
- Zienkiewicz, O. C., and Taylor, R. L. (1991). "The Finite Element Method," 4th ed. McGraw-Hill, London.
-